MECHANICS OF ADHESION AND FRICTION IN STICK INSECTS AND TREE FROGS

Dissertation zur Erlangung des
naturwissenschaftlichen Doktorgrades
der Bayerischen Julius-Maximilians-Universität
Würzburg

vorgelegt von

PATRICK HANS DRECHSLER
aus
Böblingen

Würzburg 2008

Eingereicht am:

Mitglieder der Promotionskommission:

Vorsitzender:
Gutachter: Dr. Walter Federle
Gutachter: Dr. Jon Barnes

Tag des Promotionskolloqiums:

Doktorurkunde ausgehändigt am:

PUBLICATIONS

Some ideas and figures have appeared previously in the following publications:

Drechsler, P. and Federle, W. (2005). Adhesion and friction in stick insect tarsal pads. *Comparative Biochemistry and Physiology*, 141A(3/Suppl.):S144.

Drechsler, P. and Federle, W. (2006). Biomechanics of smooth adhesive pads in insects: influence of tarsal secretion on attachment performance. *Journal of Comparative Physiology A Sensory Neural and Behavioral Physiology*, 192(11):1213–1222.

Federle, W., Barnes, W., Baumgartner, W., Drechsler, P., and Smith, J. (2006). Wet but not slippery: boundary friction in tree frog adhesive toe pads. *Journal of the Royal Society Interface*, 3(10):689–697.

CONTENTS

1 INTRODUCTION 1
- 1.1 Theories of adhesion and friction 1
  - 1.1.1 Theories of adhesion 2
  - 1.1.2 Theories of friction 7
  - 1.1.3 Theories of peeling 8
  - 1.1.4 Viscoelasticity 10
- 1.2 Biology of animal attachment 11
  - 1.2.1 Adhesion and locomotion 12
  - 1.2.2 Animal attachment structures 13
- 1.3 Biomechanics of smooth attachment pads 17
  - 1.3.1 Role of pad secretion 18
  - 1.3.2 Frictional anisotropy 20
  - 1.3.3 Mode of detachment 23

2 MATERIAL AND METHODS 27
- 2.1 Study animals 27
  - 2.1.1 Stick insects 27
  - 2.1.2 Tree frogs 27
- 2.2 Single pad force apparatus 29
- 2.3 Labview control program 31
- 2.4 Data analysis 31
- 2.5 Friction force measurements 32
  - 2.5.1 Anisotropy 32
  - 2.5.2 Amount of pad secretion 33
  - 2.5.3 Normal force 33
  - 2.5.4 Humidity 34
  - 2.5.5 Velocity 34
  - 2.5.6 Static friction 35
  - 2.5.7 Friction force measurements in tree frogs 35
- 2.6 Adhesion force measurements in stick insects 35
  - 2.6.1 Role of pad secretion 36
  - 2.6.2 Mode of detachment 38
- 2.7 Centrifuge apparatus 42
- 2.8 Statistics 44

3 RESULTS 47
- 3.1 Friction force measurements in stick insects 47

3.1.1 Anisotropy 47
3.1.2 Role of pad secretion 51
3.1.3 Normal force 52
3.1.4 Humidity 53
3.1.5 Velocity 54
3.1.6 Static friction 55
3.2 Adhesion force measurements in stick insects 57
3.2.1 Role of pad secretion 57
3.2.2 Mode of detachment 61
3.3 Friction force measurements in tree frogs 81
3.3.1 Possible contribution of surface tension forces to shear stress in tree frogs 83

4 DISCUSSION 87
4.1 Frictional anisotropy 87
4.2 Role of pad secretion 88
4.2.1 Role of pad secretion for attachment to smooth and rough substrates 88
4.2.2 Role of pad secretion for friction forces 90
4.3 Mode of detachment 94

5 SUMMARY 99

6 ZUSAMMENFASSUNG 101

A APPENDIX 103
A.1 Material and methods 103
A.1.1 LABVIEW 103
A.1.2 MATLAB 106
A.2 Results 107
A.2.1 Adhesion single leg 107
A.2.2 Contact time and surface roughness 126
A.2.3 Scaling of whole body forces 127

BIBLIOGRAPHY 128

ACKNOWLEDGMENTS 145

CURRICULUM VITAE 149

ERKLÄRUNG 151

LIST OF FIGURES

Figure 1.1 Explanatory diagram of Hertz and JKR models. 3
Figure 1.2 Example of Hertz and JKR curves. 5
Figure 1.3 Explanatory diagram of wet adhesion model. 5
Figure 1.4 Stribeck diagram. 9
Figure 1.5 Explanatory diagram of peeling model. 10
Figure 1.6 Models of viscoelasticity (Kelvin-Voigt and Maxwell model). 11
Figure 1.7 Variety of insect adhesive organs. 14
Figure 1.8 Morphology of stick insect pretarsus (*Carausius morosus*). 14
Figure 1.9 Ultrastructure of transversal section of the arolium cuticle of *Carausius morosus*. 15
Figure 1.10 Scanning electron microscope image of stick insect arolium. 16
Figure 1.11 Morphology of tree frog toe pads. 17
Figure 1.12 Diagram of different amounts of secretion present between pad and substrate. 20
Figure 1.13 Diagram of friction forces. 21
Figure 1.14 Chain model showing the effect of proximal and distal movement on peeling angle. 22
Figure 2.1 Immobilization of stick insect tarsus. 28
Figure 2.2 Immobilization of tree frog. 28
Figure 2.3 Experimental setup for measuring adhesion and shear stress of insect adhesive pads. 31
Figure 2.4 Simplified diagram of movement pattern for consecutive pull-offs. 37
Figure 2.5 Calculation of work of adhesion using peeling model (perpendicular pull-off). 39
Figure 2.6 Calculation of work of adhesion using peeling model with circular contact area. 40
Figure 2.7 Centrifuge apparatus. 43

Figure 3.1 Anisotropy example curves of friction, area and shear stress for adhesive pads. 48
Figure 3.2 Anisotropy of friction, area and shear stress for immobilized adhesive pads. 49
Figure 3.3 Velocity and direction dependence during anisotropic friction measurements. 50
Figure 3.4 Shear stress measurement in single adhesive pads of *Carausius morosus* 52
Figure 3.5 Influence of normal force on friction force, contact area and shear stress. 53
Figure 3.6 Influence of humidity on shear stress. 54
Figure 3.7 Single pad friction force and shear stress at four different velocities with "accumulated" secretion. 55
Figure 3.8 Friction force during and 2 min after a slow sliding movement. 56
Figure 3.9 Comparison of remaining shear stress with little and accumulated secretion two minutes after movement had ended. 57
Figure 3.10 Consecutive, alternating pull-offs of *Carausius morosus* adhesive pads from glass and rough aluminium oxide substrates. 59
Figure 3.11 Effect of contact time and secretion on pull-off forces from a rough and a smooth epoxy surface. 60
Figure 3.12 Example of stick insect's single leg detachment measurement with different normal forces. 61
Figure 3.13 Results of stick insect's single pad detachment experiments analysing the influence of normal force and velocity. 63
Figure 3.14 Scaling of stick insect's single leg pull-off forces plotted against body mass. 71
Figure 3.15 Scaling of stick insect's single leg pull-off forces plotted against contact area A_{F_0}. 72
Figure 3.16 Scaling of stick insect's single leg pull-off forces plotted against contact area $A_{F_{max}}$. 73

Figure 3.17 Summary of stick insect's single leg scaling coefficients using OLS and SMA regressions. 74
Figure 3.18 Scaling results of stick insect whole body measurements (centrifuge technique). 80
Figure 3.19 Shear stress measurement in single toe pads of *Litoria caerulea* (example data and boxplots). 85
Figure 3.20 Example data set to estimate fluid height between frog toe pad and substratum using non-linear regression. 86
Figure 4.1 "Footloose" arolium moving in proximal and distal directions. 88
Figure 4.2 Schematic diagram illustrating the adhesion-enhancing role of insect pad secretion on a rough substrate. 90
Figure 4.3 Proposed viscoelastic detachment model. 95
Figure A.1 Flowchart diagram of LABVIEW control program. 104
Figure A.2 Front panel of LABVIEW control program. 105
Figure A.3 Interaction plot showing the main effects and two-way interactions of log transformed pull-off force versus normal force and detachment velocity. 115
Figure A.4 Interaction plot showing the main effects and two-way interactions of log transformed contact area A_{F_0} versus normal force and detachment velocity. 116
Figure A.5 Interaction plot showing the main effects and two-way interactions of log transformed contact area $A_{F_{max}}$ versus normal force and detachment velocity. 116
Figure A.6 Interaction plot showing the main effects and two-way interactions of log transformed force per contact area F_P/A_{F_0} versus normal force and detachment velocity. 117

Figure A.7 Interaction plot showing the main effects and two-way interactions of log transformed work of adhesion WOA1 versus normal force and detachment velocity. 117
Figure A.8 Interaction plot showing the main effects and two-way interactions of log transformed work of adhesion $WOA2_{mean}$ versus normal force and detachment velocity. 118
Figure A.9 Interaction plot showing the main effects and two-way interactions of log transformed work of adhesion $WOA2_{max}$ versus normal force and detachment velocity. 118

LIST OF TABLES

Table 1.1 Overview of adhesion models and their implications on scaling. 24
Table 3.1 Two-way within-subject ANOVA table testing the influence of surface roughness, secretion and contact time as well as their interaction. 58
Table 3.2 Summary of Two-way ANOVAs analysing the influence of normal force and velocity on dependent variables in stick insect's single leg detachment measurements. 62
Table 3.3 Scaling of stick insect's single adhesive pads pull-off force against body mass m using OLS regression. 65
Table 3.4 Scaling of stick insect's single adhesive pads pull-off force against contact area A_{F_0} using OLS regression. 66

Table 3.5 Scaling of stick insect's single adhesive pads pull-off force against contact area $A_{F_{max}}$ using OLS regression. 67
Table 3.6 Scaling of stick insect's single adhesive pads pull-off force against body mass m using SMA regression. 68
Table 3.7 Scaling of stick insect's single adhesive pads pull-off force against contact area A_{F_0} using SMA regression. 69
Table 3.8 Scaling of stick insect's single adhesive pads pull-off force against contact area $A_{F_{max}}$ using SMA regression. 70
Table 3.9 Test for common slope between different velocities during stick insect single leg measurements (F_P vs. m). 75
Table 3.10 Test for common slope between different velocities during stick insect single leg measurements (F_P vs. $A_{F_{max}}$). 76
Table 3.11 Test for common slope between different velocities during stick insect single leg measurements (F_P vs. $A_{F_{max}}$). 77
Table 3.12 Comparison of SMA regression slopes with predicted slopes for centrifuge data set. 78
Table 3.13 Test for common slope between stick insect single leg and whole body measurements. 81
Table 3.14 Descriptive statistics of friction experiments in tree frogs. 83
Table A.1 Shapiro-Wilks normality test for pull-off forces F_P. 108
Table A.2 Shapiro-Wilks normality test for contact area $A_{F_{max}}$. 108
Table A.3 Shapiro-Wilks normality test for force per area $F_P/A_{F_{max}}$. 108
Table A.4 Shapiro-Wilks normality test for work of adhesion WOA1. 109
Table A.5 Shapiro-Wilks normality test for work of adhesion $WOA2_{mean}$. 109
Table A.6 Shapiro-Wilks normality test for work of adhesion $WOA2_{max}$. 109

Table A.7 Bartlett Test of homogeneity of variances at five velocities on pull-off force. 110
Table A.8 Bartlett Test of homogeneity of variances at five velocities on contact area $A_{F_{max}}$. 110
Table A.9 Bartlett Test of homogeneity of variances at five velocities on force per area $F_P/A_{F_{max}}$. 110
Table A.10 Bartlett Test of homogeneity of variances at five velocities on work of adhesion WOA1. 110
Table A.11 Bartlett Test of homogeneity of variances at five velocities on work of adhesion $WOA2_{mean}$. 111
Table A.12 Bartlett Test of homogeneity of variances at five velocities on work of adhesion $WOA2_{max}$. 111
Table A.13 Two-way ANOVA table showing effects of normal force F_N and velocity v (as well as their interaction) on pull-off force F_P. 111
Table A.14 Two-way ANOVA table showing effects of normal force F_N and velocity v (as well as their interaction) on contact area $A_{F_{max}}$. 112
Table A.15 Two-way ANOVA table showing effects of normal force F_N and velocity v (as well as their interaction) on contact area at $A_{F=0}$. 112
Table A.16 Two-way ANOVA table showing effects of normal force F_N and velocity v (as well as their interaction) on force per area F_P/A_{F_0}. 112
Table A.17 Two-way ANOVA table showing effects of normal force F_N and velocity v (as well as their interaction) on work of adhesion WOA1. 113
Table A.18 Two-way ANOVA table showing effects of normal force F_N and velocity v (as well as their interaction) on work of adhesion $WOA2_{mean}$. 113

Table A.19 Two-way ANOVA table showing effects of normal force F_N and velocity v (as well as their interaction) on work of adhesion $WOA2_{max}$. 113
Table A.20 Two-way ANOVA table showing effects of normal force F_N and velocity v (after dropping the interaction term) on pull-off force F_P. 114
Table A.21 Two-way ANOVA table showing effects of normal force F_N and velocity v (after dropping the interaction term) on contact areas $A_{F_{max}}$. 114
Table A.22 Two-way ANOVA table showing effects of normal force F_N and velocity v (after dropping the interaction term) on contact area A_{F_0}. 114
Table A.23 Two-way ANOVA table showing effects of normal force F_N and velocity v (after dropping the interaction term) on pull-off force per area F_P/A_{F_0}. 114
Table A.24 Two-way ANOVA table showing effects of normal force F_N and velocity v (after dropping the interaction term) on work of adhesion WOA1. 115
Table A.25 One-way ANOVA table showing effect of normal force F_N on F_P at velocity $v = 10\,\mu m\,s^{-1}$. 119
Table A.26 One-way ANOVA table showing effect of normal force F_N on F_P at velocity $v = 50\,\mu m\,s^{-1}$. 119
Table A.27 One-way ANOVA table showing effect of normal force F_N on F_P at velocity $v = 100\,\mu m\,s^{-1}$. 119
Table A.28 One-way ANOVA table showing effect of normal force F_N on F_P at velocity $v = 500\,\mu m\,s^{-1}$. 119
Table A.29 One-way ANOVA table showing effect of normal force F_N on F_P at velocity $v = 5000\,\mu m\,s^{-1}$. 119

Table A.30 One-way ANOVA table showing effect of normal force F_N on $A_{F_{max}}$ at velocity $v = 10\,\mu m\,s^{-1}$. 120
Table A.31 One-way ANOVA table showing effect of normal force F_N on $A_{F_{max}}$ at velocity $v = 50\,\mu m\,s^{-1}$. 120
Table A.32 One-way ANOVA table showing effect of normal force F_N on $A_{F_{max}}$ at velocity $v = 100\,\mu m\,s^{-1}$. 120
Table A.33 One-way ANOVA table showing effect of normal force F_N on $A_{F_{max}}$ at velocity $v = 500\,\mu m\,s^{-1}$. 120
Table A.34 One-way ANOVA table showing effect of normal force F_N on $A_{F_{max}}$ at velocity $v = 5000\,\mu m\,s^{-1}$. 120
Table A.35 Tukey's HSD test showing effects of normal force F_N and velocity v on pull-off force F_P. 121
Table A.36 Tukey's HSD test showing effects of normal force F_N and velocity v on contact area $A_{F_{max}}$. 122
Table A.37 Tukey's HSD test showing effects of normal force F_N and velocity v on contact area A_{F_0}. 123
Table A.38 Tukey's HSD test showing effects of normal force F_N and velocity v on force per contact area F_P/A_{F_0}. 124
Table A.39 Tukey's HSD test showing effects of normal force F_N and velocity v on work of adhesion (WOA1). 125
Table A.40 Mean ($\overline{F_P}$) and standard deviation (SD) of all groups. 126
Table A.41 Shapiro-Wilks normality test. All groups were normally distributed. 126
Table A.42 Bartlett test of homogeneity of variances. Variances were tested between short and long contact times. All variances are homogeneous. 126

Table A.43 Descriptive statistics of stick insect's whole body force measurements (centrifuge technique). 127

LIST OF SYMBOLS

ANOVA	analysis of variance
A	contact area (m^2)
A_{F_0}	contact area during pull-off (m^2)
$A_{F_{max}}$	contact area at maximum load (m^2)
a_0	contact area at normal force $F_P = 0$ (m^2)
B	length of peeling edge (m)
b	adhesive strip width (m)
β_{SMA}	standardized major axis regression slope
$\hat{\beta}_{SMA}$	common standardized major axis regression slope
CI	confidence interval
E	Young's modulus of elasticity (Pa)
ϵ	strain (1)
η	viscosity (Pa s)
F_A	adhesion force (N)
F_N	normal force (N)
F_P	pull-off force (N)
F_F	friction force (N)
G	energy restitution rate (1)
γ_S	surface energy ($J\,m^{-2}$)

γ_{ST}	surface tension ($J\,m^{-2}$)
γ_{LV}	surface energy of liquid-vapor interface ($J\,m^{-2}$)
h	fluid film height (m)
K	bulk elastic modulus (Pa)
m	body mass (kg)
μ	friction coefficient (1)
ν	Poisson ratio (1)
p	vapor pressure (Pa)
R	radius of curvature (m)
R_a	average roughness (m)
SEM	scanning electron microscopy
SMA	standardized major axis
s	peeling or detachment distance (mm)
σ	stress (Pa)
TEM	transmission electron microscopy
t	time (s)
θ	peeling or contact angle (deg or rad)
v	velocity ($m\,s^{-1}$)
WOA	work of adhesion ($J\,m^{-2}$)
W	work of adhesion ($J\,m^{-2}$)
ω	angular velocity ($m\,s^{-1}$)
$\propto$	proportional to

1 INTRODUCTION

The structure and action of the Fly's foot have been so frequently treated of, and are so generally considered to be fully understood, that it may appear, at the first glance, as if nothing further could be done with so hackneyed a subject.

— *Tuffen West (West, 1862)*

Although our understanding of biological interactions is very broad from a chemical, ecological and neurological perspective, the purely mechanical "attachment" aspects have only begun to receive more attention during the last few decades. This is partly due to an improvement of available methods, but also in a growing interest in engineering sciences to "learn from nature" (often referred to as bionics or biomimetics). In particular advances in micro- and nanoscale manufacturing have given rise to the question on how nature solves problems arising with small scale production, such as friction, lubrication, wear and adhesion in miniaturized components, and if these solutions are portable to engineering (Bhushan, 2003; Geim et al., 2003; Sitti and Fearing, 2003; Abbott and Gaskell, 2007; del Campo et al., 2007; Creton and Gorb, 2007).

This study will try to shed some light on this subject by analysing attachment abilities of two model organisms: Stick insects and tree frogs. These animals were chosen because difference in size between the two organisms covers a wide range. On the other hand the growth of both animals is nearly shape constant (isometric). These factors facilitate comparisons not only within, but also between these species, allowing the application of generalized attachment models.

1.1 THEORIES OF ADHESION AND FRICTION

This section will introduce models of adhesion and friction as commonly used in engineering sciences today.

1.1.1 *Theories of adhesion*

Although occasionally used more broadly in the sense of "attachment" in literature, adhesion strictly refers to the force *perpendicular* to a surface. Adhesion is not a single process, but one which can be separated into three different but related actions: Jumping into contact, equilibrium and detachment (Kendall, 2001).

Models of adhesion can be divided into being either of the "dry" or "wet" type, depending on the presence of a fluid (such as animal secretion or condensed vapor) between the surfaces involved.

Each model description is concluded by its implication to scaling theory (see section 1.3.3).

1.1.1.1 *Work of adhesion*

Work of adhesion W is defined as work per area ($\mathrm{J\,m^{-2}}$) or force per length ($\mathrm{N\,m^{-1}}$). Ideally the adhesion energy gained by bringing two surfaces in contact (W_A: approaching work of adhesion) should equal the adhesion energy needed to separate them (W_R: receding work of adhesion). This is also reflected by the fact that work of adhesion is often described as an addition of the two surface energies (γ_S) involved:

$$W = 2\gamma_S \tag{1.1}$$

In contrast real loading-unloading cycles are characterized by energy loss (hysteresis):

$$W_R > W_A \tag{1.2}$$

This energy loss has been attributed to mechanical (viscoelastic or plastic deformations) and chemical hysteresis effects (Israelachvili, 1992a).

1.1.1.2 *Dry adhesion models (contact mechanics models)*

Dry adhesion models have in common that they do not require any kind of fluid between the two contacting surfaces. Therefore these models depend on less physical properties and are often used to describe biological attachment phenomena.

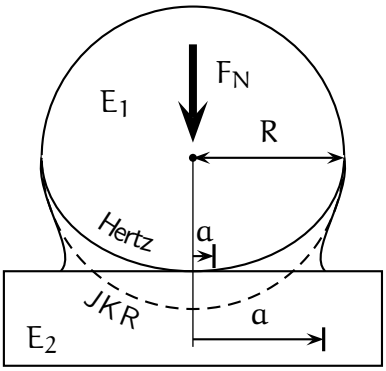

Figure 1.1: Explanatory diagram of Hertz and JKR models. Note that the bottom surface is simplified as a flat surface (instead of a sphere). a: contact radius, E_i, elasticity moduli, F_N: normal force, R: radius of curvature (Figure adopted from Israelachvili 1992a).

HERTZ MODEL Although this classical theory (Hertz, 1881) does *not* describe adhesion, it is mentioned here because it explains the deformation between *two elastic spheres* and forms the basis of many other adhesion theories. It describes the relation between contact radius a, radius of curvature R, normal force F_N and the bulk elastic modulus K (see Fig. 1.1):

$$a^3 = \frac{RF_N}{K} \tag{1.3}$$

The bulk elastic modulus K is defined as

$$\frac{1}{K} = \frac{3}{4}\left(\frac{1-\nu_1^2}{E_1} + \frac{1-\nu_2^2}{E_2}\right), \tag{1.4}$$

where ν_i are the Poisson ratios and E_i the modulus of elasticity (=Young's modulus) of the spheres.

Because the Hertz model does not account for adhesive contact without load, this model is also referred to as a nonadhesive contact theory: When no external forces perpendicular to the surface are present, the contact area equals zero. Therefore no pull-off can be defined in this model. Fogden and White (1990) introduced the "Generalized Hertz model" to include a fluid adhesive component (in form of vapor pressure) between surfaces.

JOHNSON-KENDALL-ROBERTS (JKR) MODEL This theory is an adhesive contact theory between *two elastic spheres* (Johnson

et al., 1971). It mainly differs from the Hertz theory in the fact that it includes a surface energy term, implying that an adhesion force is present between two surfaces even in the absence of external load. This theory *can* also include a fluid film between both spheres (i. e. condensed vapor). The contact radius a is defined as

$$a^3 = \frac{R}{K}\left(F_N + 3\pi RW + \sqrt{6\pi RWF_N + (3\pi RW)^2}\right), \qquad (1.5)$$

where F_N is force, W is work of adhesion and K is the bulk elastic modulus (Equ. 1.4). The radius of curvature R is defined as $R_1R_2/(R_1 + R_2)$. R_i are the radii of curvature of the two spheres.

Comparing the Hertz model with the JKR model reveals that contact radius is present even when no external force is applied (a_0) due to the adhesive component of the JKR theory:

$$a_0^3 = \frac{6\pi R^2W}{K} \qquad \text{or} \qquad a_0^3 = \frac{12\pi R^2\gamma_S}{K} \qquad (1.6)$$

For non-adhering surfaces (surface energy $\gamma_S = 0$) Equ. 1.5 can be reduced to the Hertz equation (Equ. 1.3).

The pull-off force F_P is defined as

$$F_P = -3\pi R\gamma_S. \qquad (1.7)$$

Note that pull-off force scales with a linear dimension ($F \propto L$). Fig. 1.1 illustrates the difference between Hertz and JKR model and Fig. 1.2 shows contact radius versus force diagram comparing both theories.

1.1.1.3 *Wet adhesion models*

Wet adhesion models have in common that the adhesion force relies on physical properties of the fluid between two surfaces. The presence of fluid discovered in many different animal attachment pads has made these theories popular recently (Federle et al., 2002; Barnes et al., 2006).

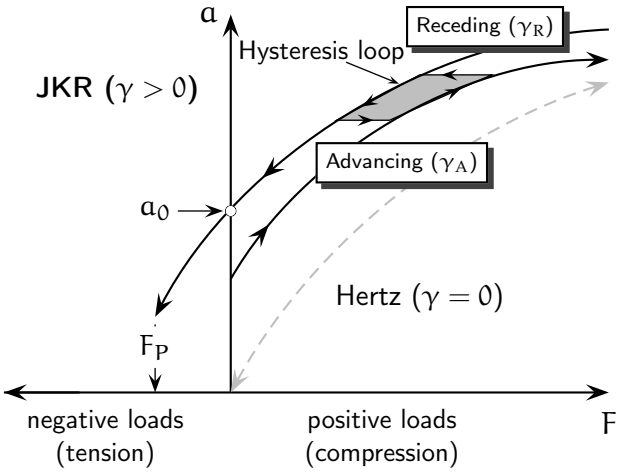

Figure 1.2: JKR curve displaying pull-off force F_P and contact radius a_0 (at $F = 0$). During the advancing/loading process surface energy γ_S has a different value (γ_A) then during the receding/unloading process (γ_R), resulting in an energy loss displayed by the hysteresis loop. The gray dashed line depicts the Hertz theory. Note that the contact area is zero when no force is applied in the Hertz model (Figure adopted from Israelachvili 1992a).

WET ADHESION MODEL The model of wet adhesion combines effects of surface tension and viscosity (Emerson and Diehl, 1980; Hanna and Barnes, 1991). It applies to *two flat, undeformable surfaces* where no peeling can occur during detachment (Fig. 1.3).

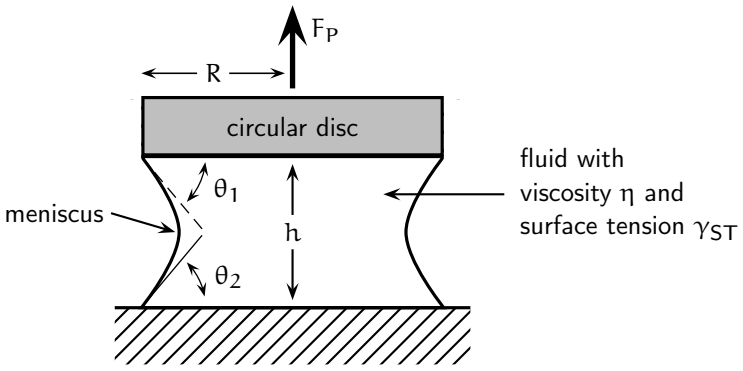

Figure 1.3: Explanatory diagram of wet adhesion model. F_P: pull-off force, θ_i: contact angle, η: viscosity, h: fluid film height, R: radius of contact area.

The viscosity term, also referred to as Stefan adhesion (Stefan, 1874), is

$$F_{\text{viscosity}} = \frac{3\pi R^4 \frac{dh}{dt}\eta}{2h^3}, \tag{1.8}$$

where R is radius of contact area, h is liquid film thickness, t is time of separation and η is viscosity. If velocity (dh/dt), fluid film height and viscosity are assumed constant, force will approximately scale with area squared ($F \propto L^4$).

The surface tension term, which is based on capillarity, is

$$F_{\text{surface tension}} = R^2\pi\frac{\gamma_{ST}(\cos\theta_1 + \cos\theta_2)}{h}, \tag{1.9}$$

where γ_{ST} is surface tension and θ_i are contact angles between the fluid and both surfaces. Assuming a completely wettable surface (contact angle of $\theta_i = 0°$), Equ. 1.9 can also be written as

$$F_{\text{surface tension}} = 2\gamma_{ST}A/h, \tag{1.10}$$

where $A = R^2\pi$. Since h is the liquid film thickness it can also be represented as $2R$. This gives

$$F_{\text{surface tension}} = \gamma_{ST}A/R. \tag{1.11}$$

If surface energy and fluid film height remain constant, the force resulting from surface tension will scale with area ($F \propto L^2$).

Combining these terms results in the wet adhesion model:

$$F_P = \underbrace{\frac{3\pi R^4 \frac{dh}{dt}\eta}{2h^3}}_{F_{\text{viscosity}}} + \underbrace{R^2\pi\frac{\gamma_{ST}(\cos\theta_1 + \cos\theta_2)}{h}}_{F_{\text{surface tension}}} \tag{1.12}$$

''ENHANCED'' WET ADHESION MODEL Francis and Horn (2001) have derived an "enhanced" wet adhesion model of a sphere to a flat surface for Newtonian fluids which also accommodates for viscosity effects resulting in pull-off force F_P being

$$F_P = 6\pi\eta R^2\left(\frac{dh}{dt}\frac{1}{h}\right), \tag{1.13}$$

with R being the sphere radius, h is the fluid film height and η being the viscosity of the Newtonian fluid ($h \ll R$). Note that pull-off force again scales with area ($F \propto L^2$).

1.1.2 *Theories of friction*

In contrast to adhesion, friction describes forces which are oriented *parallel* to surfaces. Early observations by Leonardo da Vinci, which were later confirmed by Amontons and Coulomb, showed that friction force F_F is proportional to normal force F_N and *independent* of "apparent" or macroscopic contact area A as well as velocity v (Dowson, 1998):

$$\mu = \frac{F_F}{F_N} = \text{constant (independent of } A \text{ and } v) \tag{1.14}$$

with μ denoting the friction coefficient.

Although these observations are valid for a large number of surfaces, Bowden and Tabor (1939, 1950) have demonstrated in a series of classic experiments that true (not projected) area of contact is proportional to the load pressing two solid surfaces together, whereby the true area of contact is mostly smaller than the projected area. This finding was attributed to surface roughness and elastic recovery of the substrates after removing the external load.

One has to distinguish two different friction processes: Static friction and kinetic friction. Whereas the former is defined as the force at the onset of sliding, the latter corresponds to the force required to keep a body in motion. In most cases sliding friction is smaller than static friction. This naturally leads to stick-slip motions ("stiction") at low velocities (Barquins et al., 1986; Gao and Kuhlmannwilsdorf, 1990; Persson, 1999). In most cases smooth kinetic sliding is preferred to stick-slip (with the exception of acoustics, such as bowing a violin or the sound production by stridulation in some insects).

Friction forces vary depending on their viscoelastic material properties (Grosch, 1963). In the case of materials with low elastic modulus, such as rubber, friction is comprised of an adhesive (surface) component and a hysteretic (bulk) component (Persson et al., 2005). On smooth substrates weak adhesive interactions such as Van der Waals forces can deform the soft rubber leading to nearly complete contact between the surfaces. Because the contact area between rubber and a rough surface will be smaller due to less effective area being in contact, the adhesive contribution to friction will also be smaller. Under these conditions the bulk properties prevail (Persson et al., 2005).

Due to the fact that a fluid is almost always present between two surfaces (for instance condensed vapor) a further classification is employed depending on the amount of fluid present: In case of a thick fluid layer ($\gtrsim$ 0.01 mm) *hydrodynamic friction* laws apply (Israelachvili, 1992a; Braun and Naumovets, 2006). These mainly focus on the bulk properties such as the viscosity of the liquid (Israelachvili, 1992a) and describe the common usage of the term "lubricant". In contrast, *boundary lubrication* describes friction forces in cases where the fluid layer is very thin, i. e. less than ten molecular layers (Homola et al., 1990; Israelachvili, 1992a,b; Bhushan et al., 1995; Israelachvili and Berman, 1995). The absence of fluid is considered as a special case of boundary lubrication. Fluid films intercalated between solids can become unstable and form dry contacts ("dewetting"; Brochard-Wyart and de Gennes, 1994; Martin et al., 2000). Currently, studies of boundary lubrication strongly rely on molecular dynamics simulations (reviews: Kendall, 2001; Persson, 2002; Gao et al., 2004; Braun and Naumovets, 2006). The regime in between hydrodynamic and boundary lubrication is referred to as *elasto-hydrodynamic lubrication*. It describes the situation where opposing surfaces are separated by a fluid but surface asperities are able to interact with each other. These surface asperities can deform elastically, which increases the contacting areas. The viscous component of the lubricant can hereby support the load between the surfaces. The different types of lubrication are often displayed using a Stribeck diagram (Fig. 1.4).

To summarize, friction force can depend on the following properties: (i) Contact area, (ii) normal force, (iii) material properties (surface roughness, elasticity) and (iv) fluid properties (viscosity, surface tension, fluid film height). Note that material and fluid properties can be rate-dependent.

1.1.3 *Theories of peeling (Mode of detachment)*

Opposed to classic fracture mechanics, which traditionally analyse crack propagation in rather brittle materials (Griffith, 1921), peeling describes a special case of fracture, namely the detachment phenomena of flexible strips of tape. Because of the wide range of peeling angles, peeling force can be comprised of a frictional as well as an adhesive contribution. The force required to perpendicularly peel a thin strip of tape from a surface was

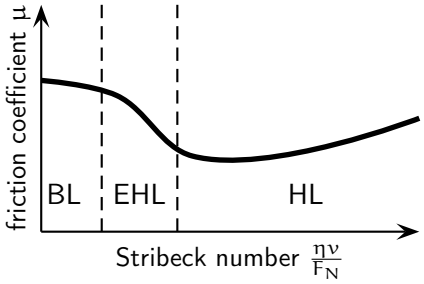

Figure 1.4: Stribeck diagram describing the different kinds of lubrication. BL: boundary lubrication, EHL: elastohydrodynamic lubrication, HL: hydrodynamic lubrication, F_N: load, η: viscosity, v: velocity, μ: friction coefficient.

first derived by Rivlin (1944) for elastic paint films: $F_{peel} = WB$ (F_{peel}: peeling force, W: work of adhesion, B: length of peeling edge). Because Rivlin's equation does not contain an area term, it relies solely on material properties and is independent of stress. Kendall (1971) later described peeling force as:

$$F_{peel} = \frac{B\gamma_S}{1 - \sin\theta} \tag{1.15}$$

where γ_S the surface energy of the solid and θ is the peeling angle (Fig. 1.5). Peeling force F_{peel} depends on velocity and preload (Barquins and Ciccotti, 1997). This is attributed to viscous processes of interfacial bonds (Gent and Petrich, 1969; Kendall, 1971). Newer models also include parameters such as the stiffness of the tape backing, geometry of the peel zone, fluid film height and viscosity (Piau et al., 2005; Pesika et al., 2007). An intuitive example of the influence of the tape backing is given by Federle (2006), describing the increased force needed to peel an elastic tape from a surface which has a rigid plate glued to its (non-sticky) back side.

Throughout these model enhancements, the linear scaling of peeling force remains unchanged ($F_{peel} \propto L$), unless the peel zone becomes larger than the area of contact. In this case peeling forces will scale with an area ($F_{peel} \propto L^2$).

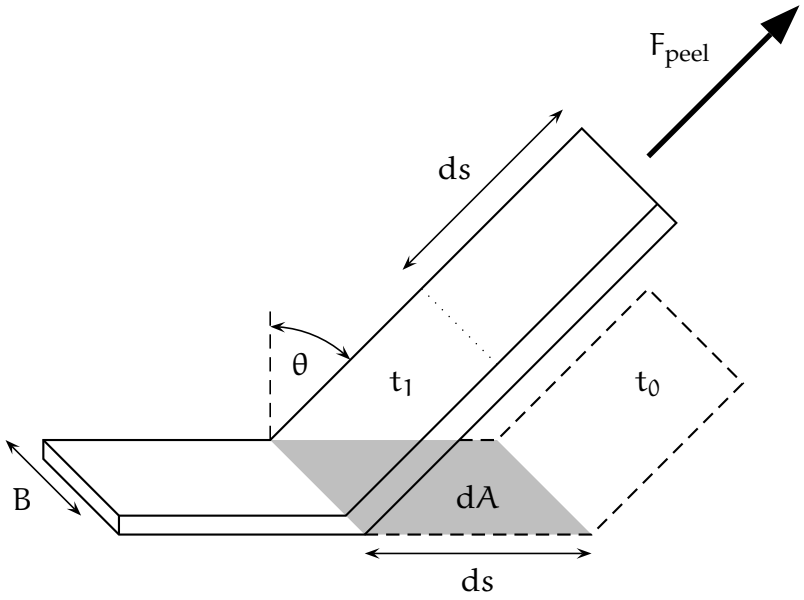

Figure 1.5: Explanatory diagram of peeling model. Peeling force F_{peel} is constant over time ($t_0 < t_1$). B is the length of the peeling edge, ds is the peeling distance, dA is the difference in contact area and θ being the peeling angle.

1.1.4 *Viscoelasticity*

All materials are to some extent viscoelastic (Vincent, 1990; Vogel, 2003; Zhang, 2005). Many elastic solids can be described by Hooke's law whereas many fluids behave as Newtonian fluids. However, viscoelastic materials do not follow these predictions alone. A combination of Hookean and Newtonian properties is often used to describe these kinds of materials. A commonly used model approach to viscoelastic materials is the use of springs describing the elastic (Hookean) behaviour and viscous (Newtonian) dashpots describing the fluid behaviour. Fig. 1.6 shows a dashpot and spring in parallel (Kelvin-Voigt model) and in series (Maxwell model) as well as their corresponding strain curves. Note that viscoelastic materials are time dependent. Relaxation time τ_r is the time needed for the stress to fall to 1/e times its initial value (Fig. 1.6). It is defined as the ratio of viscosity, μ, to Young's modulus of elasticity, E: $\tau_r = \mu/E$.

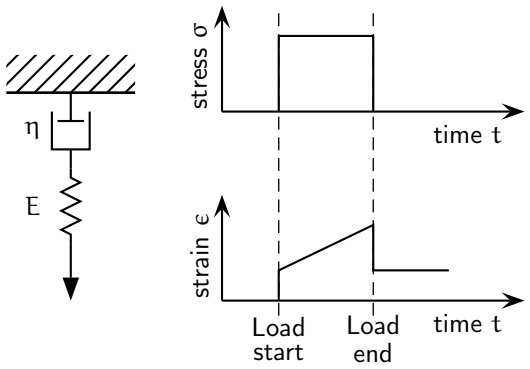

(a) Maxwell model

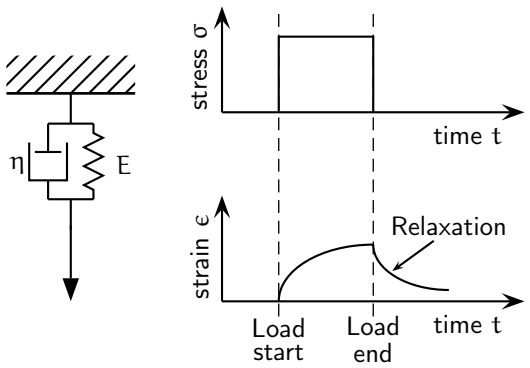

(b) Kelvin-Voigt model

Figure 1.6: Models of viscoelasticity. (a) The Maxwell model consists of a serial arrangement of a dashpot with viscosity η and a spring with elasticity E. When a load is suddenly implied (top plot in (a)) it will stretch the spring (bottom plot). While the load is maintained, the spring will keep its new length whereas the dashpot will gradually lengthen until the load is removed. (b) The Kelvin-Voigt model is a parallel configuration of a dashpot and a spring. The plot to the right again depicts the corresponding strain curve when a fixed load (stress) is first imposed and then removed. Note the relaxation curve after the load has been removed.

1.2 BIOLOGY OF ANIMAL ATTACHMENT

Animals in most ecosystems have to be able to attach to a multitude of different surfaces. Whereas marine and freshwater organisms have to cope with exposure to waves and water currents (limpets and mussels: Grenon and Walker, 1981; Yule and Walker, 1984; Waite et al., 2005), arboreal organisms have to prevent sudden detachment to stay in their ecological niche (weaver ants: Federle et al., 2001). But the ability to attach to

different surfaces is not restricted to such stationary functions: Many animals use their attachment capabilities to mate under rather non-stationary conditions like in mid air (blowfly: Walker et al., 1985) or under water (Great diving beetle: Nachtigall, 1974). Other animals use attachment mechanisms to capture prey (tongue pad in chameleons: Herrel et al., 2000; modified mouthparts in *Loricera* larvae (Carabidae) and *Stenus* species (Staphylinidae): Betz and Kölsch, 2004), to defend themselves (beetles (Staphylinidae): Dettner, 1993) or for transportation by phoresy or parasitism (Gorb, 2001). Last, but not least, the ability to attach to surfaces is used for locomotion.

1.2.1 *Adhesion and locomotion*

In the animal kingdom the term "locomotion" can range from being almost sessile, as found in many marine organisms like mussels, over the semi-sessile motions of snails, to very fast movements as present in many insects. Nature has come up with very effective permanent adhesives which are similar to engineering achievements, such as cement-like mussel adhesion (Waite et al., 2005). But this seems to contradict fast locomotion. Apparently, the conflict between secure adhesion and fast locomotion has been evolutionarily solved very efficiently by animals that move quickly such as insects and frogs.

As described in Federle and Endlein (2004), the control of animal adhesive contact can be accomplished at different hierarchical levels: *Body kinematics*, such as changes to posture and gait pattern, influence forces acting on the tarsi (Gorb, 2001). Second, variations in the angle in which the leg comes into contact with the ground can alter contact properties (*leg movement*; Federle et al., 2002; Niederegger and Gorb, 2003). Also, direct changes to the *(pre-)tarsal system* (for instance claws, adhesive pad) can influence the contact to the substratum (Federle et al., 2001). Finally, changes to the *adhesive system* itself, such as viscoelastic properties of the pad or the adhesive secretion, are likely candidates for controlling attachment abilities (Federle et al., 2002). In this thesis I will be focusing on the mechanisms of the latter two hierarchical levels as implied by stick insects and tree frogs.

1.2.2 *Animal attachment structures*

1.2.2.1 *Insect attachment structures*

In most insects the tarsus consists of tarsal claws and the actual attachment organ(s). Claws provide an effective attachment mechanism to rough substrates using friction and interlocking (Lees and Hardie, 1988; Betz, 2002; Dai et al., 2002). But for insects living on plants having a surface roughness smaller than the claw tip diameter, claws are often not able to interlock with these micro-rough surfaces (Federle et al., 1997; Betz, 2002; Dai et al., 2002). Many insects are able to circumvent this problem by using claws (Bruening, 2006; Federle and Bruening, 2006).

Although insects have evolved a large variety of different attachment structures (for an overview see Gorb and Beutel, 2001 and right side of Fig. 1.7), their adhesive organs can be categorized as being either "hairy" or "smooth" (left side of Fig. 1.7; Gorb and Beutel, 2001). Both designs are flexible cuticle structures which have in common that they are able to maximise their effective area of contact on different substrates (Gorb et al., 2000).

Additionally some insects possess further attachment structures at different parts of the leg, for example euplantulae in pretarsal segments in cockroaches, grasshoppers and stick insects (Fig. 1.8), fossula spongiosa between tibia and tarsus of assassin bugs (Reduviidae), claw pads of Ephemeroptera and balloon-shaped eversible pads of Thysanoptera (Gorb and Beutel, 2001; see bottom right side of Fig. 1.7).

In all insect tarsal pads reported on so far, adhesion is mediated by small volumes of fluid secreted into the contact zone, e. g. flies (Walker et al., 1985), bugs (Edwards and Tarkanian, 1970), and beetles (Ishii, 1987). Although the origin of the secretion and its method of transport to the gap between pad and substratum have been identified in some insects (Gorb, 1998; Beutel and Gorb, 2001), these details remain unclear for many other insect species. Recent findings show that insect pad secretion is an emulsion consisting of a hydrophilic and a hydrophobic phase (Gorb, 2001; Federle et al., 2002; Vötsch et al., 2002). However, the detailed nature of the two-phasic fluid is still unknown.

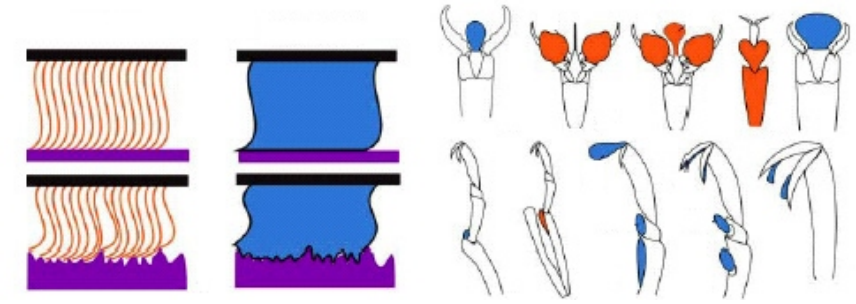

Figure 1.7: Variety of insect adhesive organs. The left side shows scheme of "hairy" and "smooth" attachment organs and their ability to attach to different surface structures. On the right different leg morphologies in insects are shown. "Hairy" attachment devices are indicated in red, "smooth" ones in blue. Figure adopted from Gorb and Beutel (2001).

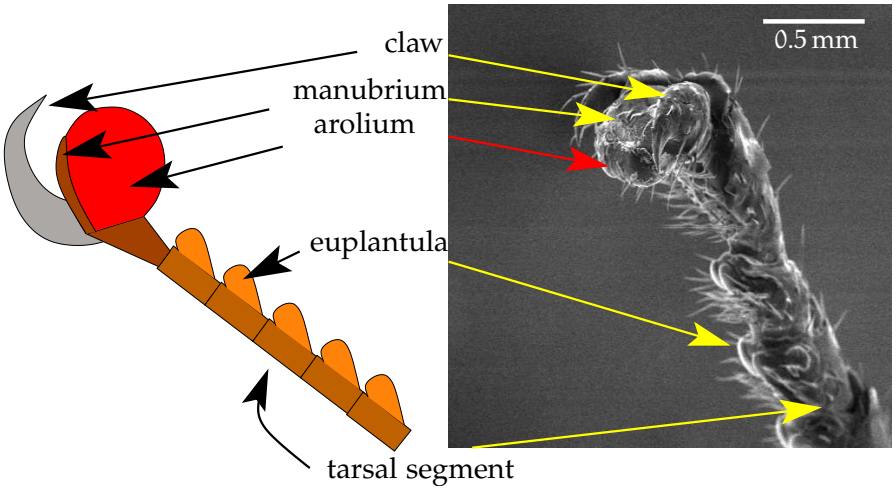

Figure 1.8: Morphology of stick insect pretarsus (*Carausius morosus*). Claws are used to attach to rough surfaces by mechanical interlocking. The arolium as well as euplantulae are both smooth adhesive structures which are implied during attachment to smooth substrates.

Hairy attachment structures are common in many insect orders such as flies (Walker et al., 1985), beetles (Ishii, 1987) and bugs (Edwards and Tarkanian, 1970). These structures are composed of cuticle protuberances of flexible adhesive hairs or setae (Gorb, 2001). Although the number (ranging from a few dozen to thousands), density and size of setae varies between insect groups and has been reported to be dependent on the size of the animal (Arzt et al., 2003), these findings have been questioned recently by Federle (2006).

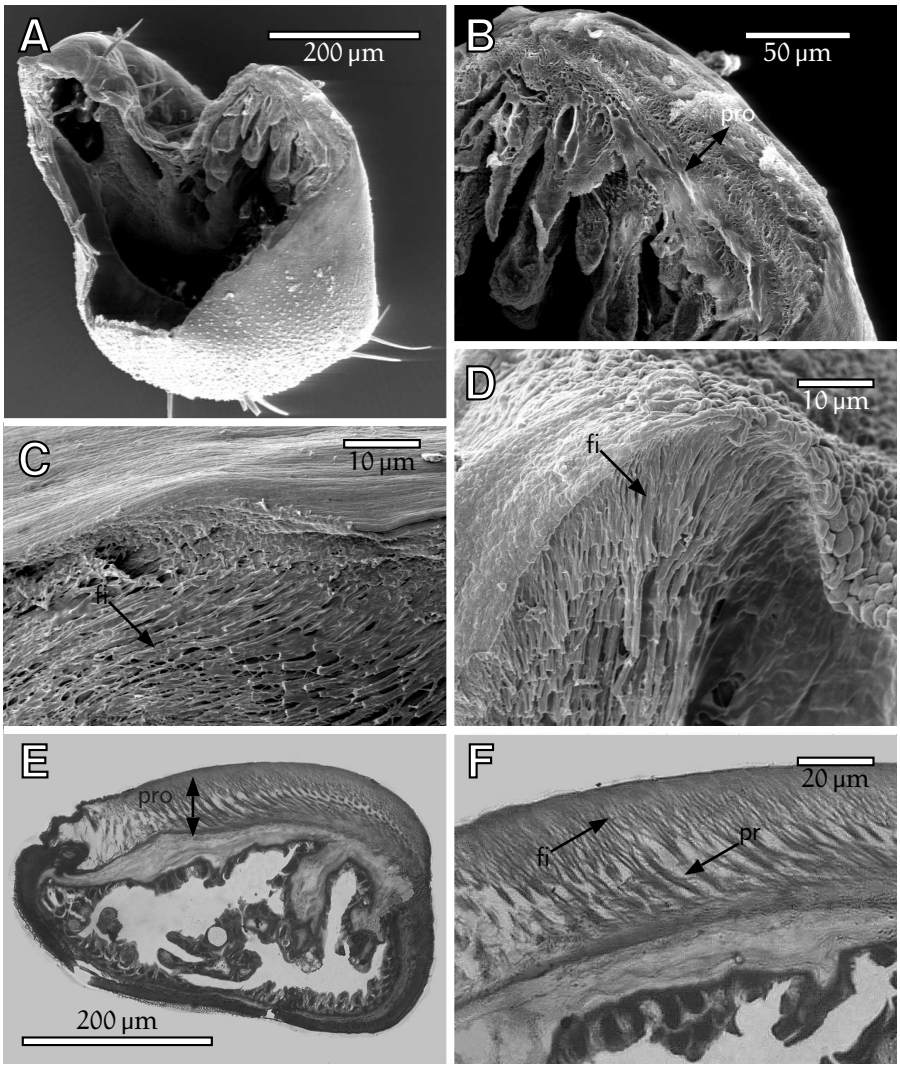

Figure 1.9: Ultrastructure of transversal section of the arolium cuticle of *Carausius morosus*. A–D: Freeze fracture scanning electron microscopy images. E and F: Light microscopy images of semi thin sections. fi: fine rods, pr: principal rodes, pro: procuticle.

Smooth adhesive pads are common in ants and bees, cockroaches, grasshoppers and stick insects (Gorb, 2001). Whereas the structures located on the ventral side of tarsal segments are called euplantula, those located at the distal end of the pretarsus are referred to as arolia[1] (Fig. 1.8). The arolium is a flexible, fluid filled, soft cuticle, sac-like structure. The functional morphology of arolia differs between insect groups. Whereas ants and bees are able to actively as well as passively extend

1 Note that smooth adhesive organs in flies are referred to as pulvilli.

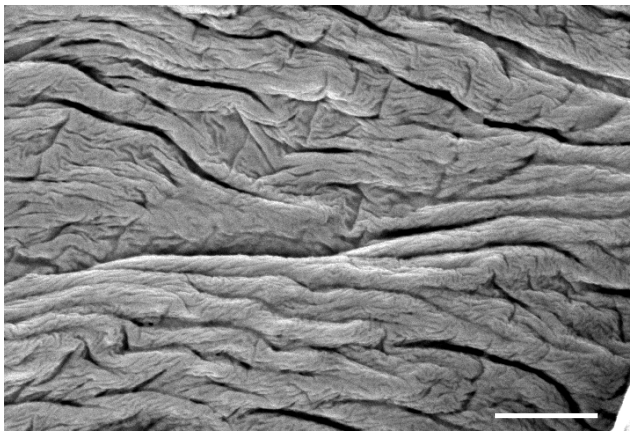

Figure 1.10: Scanning electron microscope (SEM) image of stick insect arolium surface. The vertical direction corresponds to proximal-distal direction. The scaling bar is 2µm long.

and retract their arolium (Snodgrass, 1956; Federle et al., 2000), most other insects' arolia only passively adopt to the surface roughness and acting load. This also applies to the stick insect's attachment organ used in this study. The arolium can be completely membranous or at least partly sclerotized. Its surface is smooth and its cuticle consists of rod-like chitin crystallites oriented perpendicular or at some angle to the surface (Fig. 1.9). The median empodium is composed of common layered cuticle and its surface is covered by acanthae (Beutel and Gorb, 2001). Smooth surface geometries differ between insect groups on the micrometer level. Gorb (2001) describes a variety of smooth systems ranging from hexagonal structures as found in grasshopper euplantulae (*Tettigonia*) to structures perpendicular to the longitudinal axis as found in wasp arolia (*Vespa crabro*). Fig. 1.8 and Fig. 1.9 give an overview of the stick insect's pretarsus morphology and its ultrastructure; Fig. 1.10 shows the structure of the stick insect's arolium surface architecture.

1.2.2.2 *Frog attachment structures*

Analogous in morphology and function to adhesive pads in some insects (Gorb et al., 2000; Beutel and Gorb, 2001), tree frog toe pads are soft and patterned with a regular hexagonal microstructure of approximately 10 µm diameter epidermal cells separated by approximately 1 µm wide channels. The flattened surface of each cell features a similar but much finer mi-

crostructure of approximately 0.1–0.4 µm diameter pegs which originate from hemidesmosomes (Ernst, 1973a; Welsch et al., 1974; Mizuhira, 2004; Fig. 1.11). The cellular and subcellular surface architecture differs significantly from that of all other epidermal cells of these frogs (Ernst, 1973a; Green, 1979). Tree frog adhesive pads are permanently wetted by mucus secreted from glands that open into the channels between epidermal cells (Ernst, 1973b).

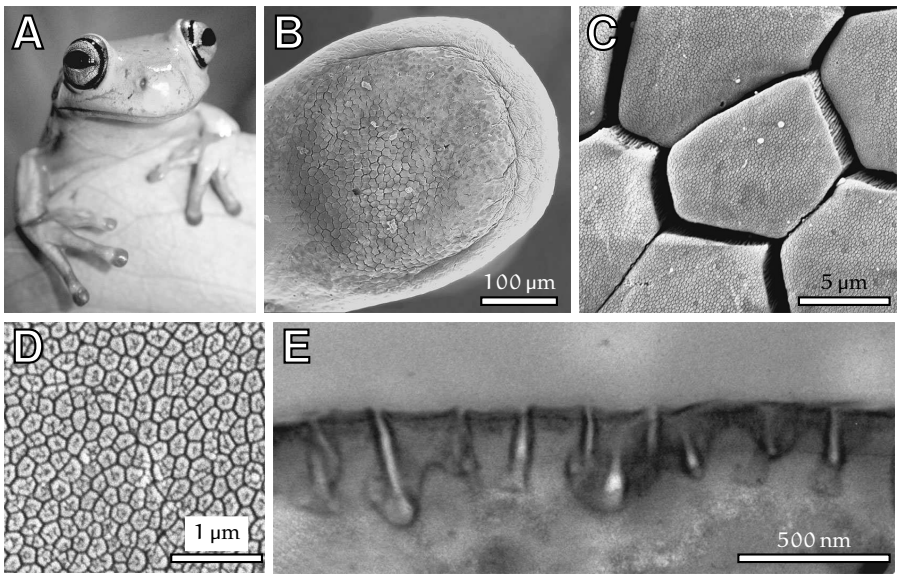

Figure 1.11: Morphology of tree frog toe pads. (A) White's tree frog (*Litoria caerulea*). (B–D) Scanning electron microscopy images of (B) toe pad, (C) epidermis with quasi hexagonal epithelial cells and (D) high power view of the surface of a single hexagonal cell showing peg-like projections. (E) Transmission electron microscopy of cross-section through cell surface. Fig. (A) kindly provided by T. Endlein.

1.3 BIOMECHANICS OF SMOOTH ATTACHMENT PADS

The capacity of many animals to attach to smooth surfaces has interested scientists for many centuries (i. e. Hooke, 1665; Blackwall, 1830; West, 1862; Dewitz, 1884; Jiao et al., 2000; Niederegger et al., 2002). Although some mechanisms such as mechanical interlocking, suction[2] and electrostatic forces have been

2 Exceptions occur in insects living underwater, such as the diving beetle *Dytiscus* (Aiken and Khan, 1992) and in disk-wing bats (Riskin and Fenton, 2001).

ruled out in most insects as possible attachment mechanisms in a classical paper by Stork (1980), many other mechanism have been put forward in the past decades.

The most discussed attachment mechanisms for smooth adhesive pads in insects and frogs seem to contradict each other in many theoretical aspects: Is the mechanism "wet" (wet adhesion model; Hanna and Barnes, 1991; Federle et al., 2002) or "dry" (intermolecular forces; Jiao et al., 2000)? Is this a static or dynamic process? Do attachment organs detach like rigid plates, therefore relying on the area of contact, or do they gradually peel (Federle et al., 2002; Niederegger and Gorb, 2003; Federle and Endlein, 2004)? These questions pose the main motivation for this thesis: What are the underlying mechanisms of attachment in smooth adhesive pads?

1.3.1 *Role of pad secretion*

The presence of a continuous fluid film in the contact zone of many animal attachment systems has led some previous authors to assume an adhesive, glue-like function for this liquid. Experimental support for the adhesion-enhancing role of insect foot pad secretion was reported in two studies which investigated the effect of removing the fluid (Edwards and Tarkanian, 1970; Dixon et al., 1990). A loss of adhesive function was observed after treating the pads with organic solvents (in *Rhodnius prolixus*: Edwards and Tarkanian, 1970) or silica gel (in *Aphis fabae*: Dixon et al., 1990). However, both treatments may have dehydrated the soft pad cuticle, which by itself can lead to reduced adhesion (Jiao et al., 2000; Niederegger and Gorb, 2006). Likewise, early research on frog adhesion led authors to assume a glue-like function of the mucus (Dewitz, 1884), but this was not confirmed by later experimental studies (Emerson and Diehl, 1980; Hanna and Barnes, 1991).

In contrast, more recent findings have given rise to the *wet adhesion model* in insects (Stork, 1980; Walker et al., 1985; Lees and Hardie, 1988; Langer et al., 2004) and frogs (Nachtigall, 1974; Emerson and Diehl, 1980; Green, 1981; Hanna and Barnes, 1991; Barnes, 1999; Barnes et al., 2002, 2006). Several lines of evidence have been provided to support this theory: Shear forces of attachment pads were found to be rate-dependent in weaver ants (Federle et al., 2004) and tree frogs (Hanna and Barnes, 1991);

furthermore in tree frogs there is a visible meniscus around the area of contact between the pad and the substrate and the sticking ability of frogs was reduced when toe pads were immersed in water (Emerson and Diehl, 1980). Recent work on the frog species *Colostethus trinitatis* (Barnes et al., 2002), however, showed that these freshwater frogs are capable of climbing on wet rock using their toe pads, even when water is flowing over the substrate.

These results pose a number of interesting questions, because a Newtonian fluid confined in between two substrates is expected to act as a *lubricant*, not as an adhesive, so that the pad should easily slide. Since the capacity to sustain adequate friction appears fundamental to animal locomotion and maneuverability (Radhakrishnan, 1998), the question arises if and how animals can generate sufficient static friction despite a fluid based adhesion mechanism.

Aside from the wet adhesion model, a variety of other physical models predict the forces due to the capillarity and viscosity of a fluid film between two solid adherends for different geometries (e. g. sphere on flat, flexible tape on flat; see Tbl. 1.1). For all geometries, adhesive forces are predicted to be *inversely* proportional to the amount of fluid present in the contact zone (i. e. to fluid film thickness). Similarly, the shear resistance of a fluid film decreases with its thickness. Thus, the physical models predict that animals should actually *maximize* forces by secreting less fluid. Obviously, it is still unclear whether animal "adhesive" secretion increases or reduces pad attachment forces. What is the function of this fluid?

The presence of a secretion could be explained by the fact that the size of true contact area on *rough* substrates is enlarged (Fig. 1.12). Due to the soft nature of insect and frog attachment pads, this effect might also be enhanced by increasing the load (=normal force). An increase of the amount of pad secretion as well as the applied load would enhance adhesive and friction forces.

However, it is still unclear whether attachment forces are mainly based on the fluid film as described above (i. e. capillarity and viscosity) or on a *direct interaction* between pad and substrate. The direct interaction between the adhesive pad and the substrate could be related to the contact of surface asperities with the pad across the adhesive liquid film (Roberts, 1971a) or

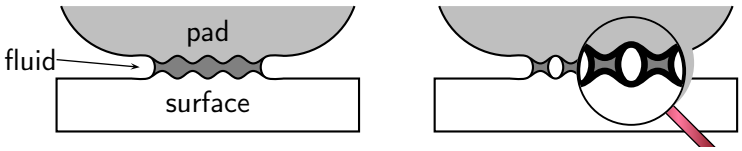

Figure 1.12: Diagram of different amounts of secretion present between pad and substrate: Accumulated (left side) and little (right side) secretion.

to the formation of "dry" contacts by dewetting of a metastable liquid film (Martin and Brochard-Wyart, 1998). Even if no direct contacts are formed, however, adhesive secretion (which is an emulsion) could behave like a solid due to non-Newtonian fluid properties. In fact, such a "yield stress" is a characteristic feature of many emulsions, especially if the volume fraction of the disperse phase is large (Tadros, 1994).

Here I investigate the biomechanics of smooth adhesive pads by focusing on the forces of single pretarsal pads in stick insects (*Carausius morosus*) and single toe pads of tree frogs (*Litoria caerulea*). This work differs from previous studies on insect shear forces (Gorb and Scherge, 2000; Federle et al., 2004) in that I tested sliding for large amplitudes of movement and directly measured shear stress (friction force per unit contact area) under different experimental conditions. With these experiments, the following questions are addressed: 1. Can insect and frog adhesive pads generate static friction? 2. How is the friction of insect adhesive pads influenced by load? 3. How does insect shear stress depend on sliding velocity? 4. How does the amount of fluid secretion influence adhesive and frictional forces?

1.3.2 *Frictional anisotropy*

Frictional anisotropy plays an important role in locomotion, since animals not only have to attach safely but at the same time must be able to detach quickly, which could be controlled by movement of the pad towards (proximal) or away from the body (distal). Animals hanging upside down from a smooth surface will experience a pulling force on each leg which is comprised of a friction component parallel to the surface and an adhesion component perpendicular to the surface. Friction

force, always having the opposite direction as movement direction, is directed away from the body. Opposed to this are situations were the animal is attaching to an incline: Here, the legs which are directed "downwards" will experience a friction force towards the body whereas the legs directed "upwards" experience a friction force away from the body (see right side of Fig. 1.13).

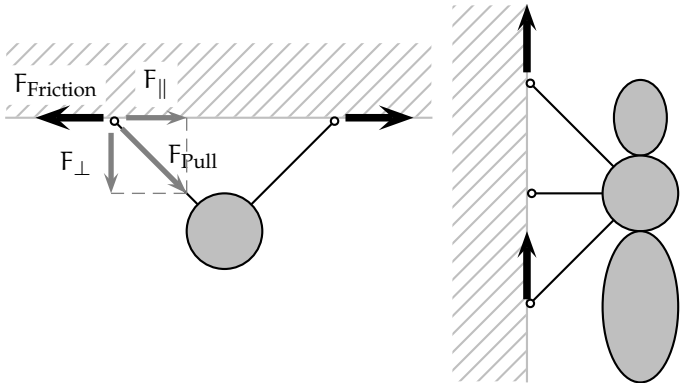

Figure 1.13: Diagram of friction forces of an insect hanging upside down from a smooth surface (left side) and an insect attaching to a 90° incline (right side). The left side also displays how pulling force F_{Pull} is composed of a vector parallel ($F_{||}$) and perpendicular ($F_{\perp}$) to the surface (dark gray arrows).

It has been reported that *adhesion* force in flies (Niederegger et al., 2002) and geckos (Autumn et al., 2000) is maximised by short proximal movements prior to perpendicular detachment. This also applies to stick insects (preliminary observation). The opposite was found in spiders: Here movements in distal direction increased the area of contact and the adhesive force (Niederegger and Gorb, 2006),

In contrast, studies on the anisotropy of *friction* have been inconsistent so far: Findings in bush crickets (*Tettigonia*; Gorb and Scherge, 2000) have shown increased friction forces in proximal direction. Contrarily, friction forces were larger in distal direction in spiders (bird spider *Aphonopelma seemanni* and hunting spider *Cupiennius salei*; Niederegger and Gorb, 2006). Following the argumentation of these authors, friction anisotropy in these animals arises from contact angles of hairy or rod-like structures losing elastic energy during movement toward the body. Niederegger and Gorb (2006) postulate that the attachment structures of spiders, which are made up of setae and

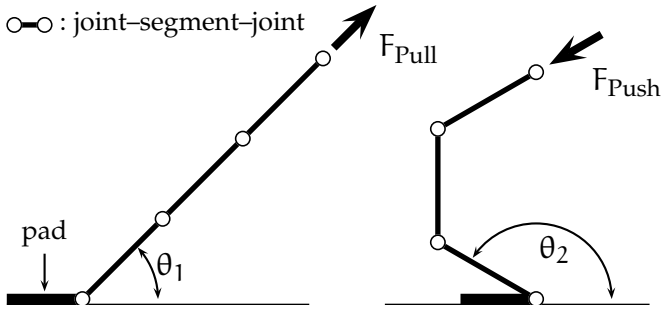

Figure 1.14: Chain model showing the effect of proximal (pulling towards the body; left side) and distal (pushing away from the body; right side) movement on peeling angle θ_i. Smaller peeling angles lead to larger peeling forces (see Equ. 1.15).

smaller spatulae, increase their true contact area in distal direction due to the arrangement of these structures.

Hill (1977) found the exact opposite behaviour in salticid spiders (*Phidippus audax*), namely that friction is maximised in proximal direction. The underlying mechanism is described as an interlocking of tenant setae with surface irregularities when legs are pulled towards the body. Detachment from the surface is accomplished by extending the leg in distal direction.

The aforementioned findings are not consistent with each other, leaving the question unanswered whether insects detach more easily by moving their adhesive pads in distal or in proximal direction. These discrepancies could be solely explained by changes in the size of contact area, even if there are no differences between friction force in proximal-distal direction. Furthermore, the insect tarsus consists of multiple joints which might behave like a chain, therefore increasing the peeling angle during distal movement which would lead to decreased attachment forces (see Fig. 1.14 and section 1.1.2).

I will therefore analyse friction force, contact area as well as shear stress of proximal and distal movements of the stick insect's tarsus under different experimental conditions. With these experiments I address the following questions: 1. Is friction anisotropy present in stick insect's adhesive pads? 2. Is this anisotropy controlled by friction forces or by size of contact area? 3. Does the flexible tarsus morphology influence anisotropy? 4. Can detachment be controlled by movement direction?

1.3.3 *Mode of detachment*

Animal adhesion has two conflicting goals: On the one hand animals have to be able to attach to a surface firmly, while on the other hand they must maintain their maneuverability by detaching quickly. Which mechanism(s) do animals utilise during detachment?

As discussed in the previous two sections, several mechanisms of adhesion involving a smooth attachment organ have been put forward to answer this question in the past, including contact mechanics models, wet adhesion model and peeling, clearly showing that no consensus has been reached. A possible source of this ambiguity arises from the usage of the term "adhesion". As stated in section 1.1.1, adhesion is a process composed of three different states: Jumping into contact, equilibrium and detachment. Aside from the aforementioned models focusing on different material properties of the adhesive system (pad vs. fluid properties), they also differ in the fact that some models describe a *static* event, corresponding to the equilibrium state, whereas others describe a *dynamic* event, representing the actual detachment process. As initially mentioned, the difference between static and dynamic detachment is not only of concern for theoretical considerations: Animals attaching to smooth surfaces profit from the ability to discern between involuntary events such as raindrops many times larger than the animal itself hitting a leaf they are attached to and voluntary (but still rapid) detachment during running. The question arises whether detachment force is rate dependent.

Although not mentioned explicitly, many attachment models rely on a viscoelastic property referred to as "history": Materials will behave differently, depending not only on the time, but also on the amount of external force which has been applied to the system before measuring detachment (Leckband and Israelachvili, 2001). Since viscoelastic materials are rate-dependent, the pad may behave like a rigid solid during abrupt detachment resulting in load-sharing (Bhushan, 2003). Is detachment force dependent on preload and the time of contact prior to detachment?

Different approaches have been pursued to shed light on these questions, ranging from purely theoretical models (Spolenak et al., 2004; Schargott et al., 2006), evaluating artificially

Table 1.1: Overview of adhesion models and their implications on scaling. F: detachment force, a: contact radius, R: radius of curvature, B: peeling length, h: fluid film height, θ_i: contact angle, γ_S: surface energy, η: viscosity, m: body mass.

	Mode of detachment				
	Peeling (stress concentration at the edge)			Sudden separation (load sharing)	
Model	Peeling tape	Sphere fluid flat, *static*	Sphere fluid flat, *dynamic (viscous)*	Rigid flat-fluid-flat, *static*	Rigid flat-fluid-flat, *dynamic (viscous)*
Theory	Kendall (1971)	JKR Johnson et al. (1971)	Francis and Horn (2001)	surface tension (capillarity): Hanna and Barnes (1991); Bhushan (2003)	viscosity (=Stefan adhesion): Hanna and Barnes (1991); Bhushan (2003); Stefan (1874)
Equation	$F = \frac{B\gamma_S}{1-\sin\theta}$	$F = -3\pi R\gamma_S$	$F = 6\pi\eta R^2\left(\frac{dh}{dt}\frac{1}{h}\right)$	$F = R^2\pi\frac{\gamma(\cos\theta_1+\cos\theta_2)}{h}$	$F = \frac{3\pi R^4\frac{dh}{dt}\eta}{2h^3}$
Rate-dependence considered in model	no	no	yes	no	yes
Scaling with pad radius of curvature, contact radius or peeling length	B	R	R^2	a^2	a^4
Scaling with body mass	$m^{1/3}$	$m^{1/3}$	$m^{2/3}$	$m^{2/3}$	$m^{4/3}$

modelled attachment devices (Arzt et al., 2003; Gorb et al., 2007) to experimental studies (e. g. Stork, 1980; Walker et al., 1985; Lees and Hardie, 1988; Gorb et al., 2000; Jiao et al., 2000). Yet another approach is the use of allometry, the science of the change in proportion of various parts of an organism as a consequence of growth. Analysing the detachment force of animals growing nearly isometrically[3], such as stick insects, seems to be ideal for these kind of studies. Therefore the relationship between pull-off force and body length, contact area or body mass under different conditions might help reveal an underlying mechanism. This relationship corresponds to the slope of log transformed force versus the log transformed body values (e. g. length, area or mass), the scaling coefficient. Large scaling coefficients (for instance force scaling with pad contact area or body mass) will increase the animals adhesive abilities whereas smaller scaling coefficients (force scaling with a length) will increase its mobility. Furthermore, from an isometric point of view, a small scaling coefficient presents a disadvantage for larger animals.

Theories predicting large scaling coefficients assume that two rigid plates are being separated perpendicularly. Although various studies have confirmed the presence of large scaling coefficients (Stork, 1980; Walker et al., 1985; Lees and Hardie, 1988), this does not seem to account for the soft, viscoelastic properties present in adhesive pads as described in Gorb et al. (2000). A soft, elastic sphere is more likely to detach by peeling from the substrate and hereby concentrating the force per area at the edge of the pad's contact area. This implies that force will not scale with the complete contact area, but only with its circumference, thus reducing the scaling coefficient considerably. In this case force scales with length, which is in unison with other contact mechanics models such as the JKR theory (Johnson et al., 1971).

A further question arising in this context is if animals are able to (actively or passively) control which mechanism is used during detachment depending on the circumstances, which can range from abrupt detachment events to actively maximising adhesive forces. It has been shown that ants and flies are able to detach by rolling their adhesive pad (Federle et al., 2002; Niederegger and Gorb, 2003; Federle and Endlein, 2004), hereby reducing their scaling coefficient. In contrast it is unclear whether

3 Isometric growth: No change to general body shape with growth.

insects can prevent peeling and therefore increase their scaling coefficient by virtue of viscoelastic properties influencing the pad contact area. Such viscoelastic alterations can include (1) increasing the stiffness of the adherend by increasing the load ($E = \sigma/\epsilon$, with E: modulus of elasticity σ: stress and ϵ: strain) or (2) the pad's radius of curvature to enhance the overall tension across contact area. Increasing adhesive forces could also be achieved by (3) actively or passively decreasing the peeling angle. Moreover, scaling coefficients can be increased when the system is predominated by viscosity effects (i. e. wet adhesion model, see Equ. 1.12). A further method to adapt the scaling coefficient, and therefore the mode of detachment, might arise if the pad material is viscoelastic. Slow detachments will then reveal smaller scaling coefficients than rapid detachments, because the pad will be dominated by either the elastic (slow detachment) or viscous (fast detachment) component of the pad material.

I have therefore performed measurements recording not only adhesion forces but also body lengths, contact areas and body masses in stick insects. In contrast to previous studies, these experiments were be performed with single leg measurements using different normal forces and velocities. Furthermore, experiments similar to Federle et al. (2000) measuring whole body detachment forces using a centrifuge technique were be conducted and compared to single leg forces. In contrast to the single leg force apparatus, insects were able to move freely while on the centrifuge surface, possibly revealing differences in the control of detachment. The questions posed in the context of mode of detachment were: 1. Does fast detachment differ from slow detachment? 2. Is detachment influenced by normal force? 3. Do single leg detachment forces scale differently for different pull-off velocities (due to viscoelasticity)? 4. Do whole body forces scale differently from single pad forces?

2 MATERIAL AND METHODS

2.1 STUDY ANIMALS

2.1.1 *Stick insects*

Adult stick insects (*Carausius morosus*) were taken from a laboratory colony. To measure adhesive and frictional forces of pretarsal pads ("arolia"), stick insects were enclosed, by taking advantage of their typical stick-like camouflage position, in a hollow square metal tube so that either front, middle or hind legs protruded from the end. Other protruding body parts (ipsilateral leg, abdomen, antennas) were prevented from touching the glass plate by plasticine. Precise control of normal forces as well as pull-off and sliding movements required the adhesive pad to be largely immobilized. This was done by attaching the dorsal side of the pretarsus to a piece of firm solder wire by applying melted paraffin wax (see Fig. 2.1a). In contrast, experiments dealing with direction dependence (section 2.5.1) were performed by leaving the pretarsus mobile (Fig. 2.1b).

The claws are hollow and fluid filled. To prevent them from touching the glass plate and contributing to the measured forces, the claw tips were clipped and sealed with paraffin wax. After each experiment the animals were weighed to the nearest mg and returned to the colony.

2.1.2 *Tree frogs*

Experiments were performed on three adult White's tree frogs (*Litoria caerulea*, average weight: 22 g). To measure attachment forces of tree frogs the animals were immobilized in a polystyrene petri dish (diameter: 86 mm, height: 17 mm) which was cushioned with plasticine for protection. Individual toes could be exposed through one of 30 holes drilled into the bottom of the petri dish (hole diameters: 7–10 mm). By moving the petri dish attached to a micromanipulator, the toe was brought into contact with a glass cover-slip mounted on a two-dimensional

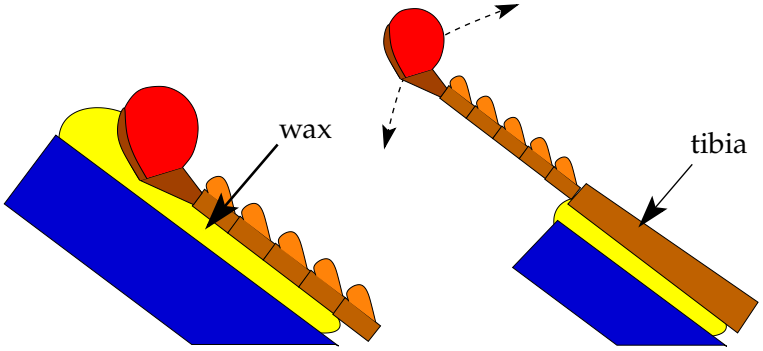

(a) immobilized arolium **(b)** "footloose" arolium

Figure 2.1: Immobilization of stick insect tarsus. (a) Potential movement of the pretarsus was circumvented by applying melted paraffin wax between the pretarsus (including the manubrium) and solder wire. This was the default method used for all experiments except anisotropy measurements. The latter experiment also included "footloose" measurements as displayed in (b): The influence of pretarsal movements was studied by immobilizing the tibia, leaving the pretarsus movable (see Fig. 1.8 for a morphological overview).

strain gauge force transducer (see Fig. 2.2). During the experiments the frog was kept moist with a humidifier by enclosing the experimental setup in a chamber of transparent plastic foil. Humidity was controlled by using an ultrasonic humidifier (Honeywell, BH-860 E). After each experiment the frogs were weighed to the nearest g and returned to the terrarium.

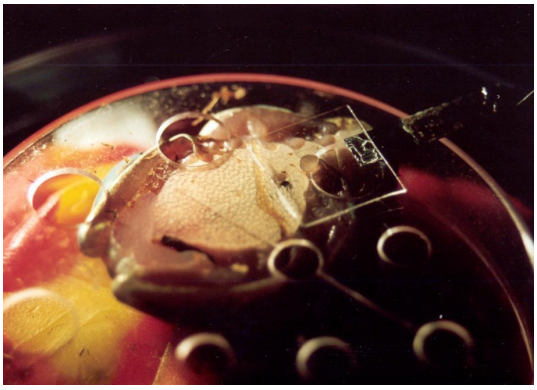

Figure 2.2: Immobilized tree frog (*Litoria caerulea*) in a petri dish with holes drilled in the bottom to expose individual toe pads which where brought in contact with the glass plate attached to the bending beam.

2.2 SINGLE PAD FORCE APPARATUS

An overview of the experimental setup is shown in Fig. 2.3. Forces were measured using a bending beam equipped with strain gauges. The scale of frictional and adhesive forces insect feet can achieve spans almost three orders of magnitude ranging from 10^{-6} N (µN) to 10^{-1} N. To meet these requirements a combination of different strain gauges were in use. Small adhesive forces were recorded using semi-conducters whereas foil strain gauges were used for large forces.

A glass coverslip (12 mm × 12 mm × 0.1 mm) was attached to the distal end of the bending beam. The insect foot was brought into contact with the bottom side of the glass coverslip. The adhesive contact area was measured from above under reflected light using a stereo microscope equipped with a coaxial illuminator (Wild M3C, Leica). This method yields high contrast images of the pad contact zone showing it as a dark area on a bright background (Federle et al., 2002) as illustrated in Fig. 2.3.

Contact areas were recorded at 10–100 frames per second using an externally triggered Redlake PCI 1000 B/W high speed video camera mounted on a stereo microscope. Video analysis was performed offline with custom made software using MATLAB (The Mathworks, USA; see section 2.4). Force input channels were amplified (ME-Meßsysteme, Henningsdorf, Germany) with an I/O board (PCI-6035E, National Instruments, USA) with a sampling frequency of 100 Hz.

To perform controlled movements the bending beam was mounted on a computer controlled three-dimensional DC positioning stage (M-126PD, C-843, Physik Instrumente, Germany). Motor movements, video trigger and force recording were synchronized by custom made software using LABVIEW (National Instruments, USA; see section 2.3). This software also maintained a constant normal force during friction experiments by small movements of the platform in the z-axis (feedback frequency: 10 Hz). Measurement of anisotropy (see section 2.5.1) were performed before the implementation of the feedback mechanism.

The following combination of force transducers and strain gauges were used:

- Pull-off experiments were performed using a one dimensional transducer consisting of two parallel bending beams

(20 mm × 5 mm × 0.1 mm; 6 mm between the beams) equipped with 350 Ω foil strain gauges (BLH, Heilbronn, Germany) in a full bridge configuration, and a strutting at the distal end to which the glass coverslip was attached. Depending on the lever arm, spring constant varied between 5 N m^{-1} and 50 N m^{-1}; resonance frequency was 71 Hz.

- Further pull-off experiments were performed using a one dimensional single beam equipped with 500 Ω semi conductor strain gauges in a full-bridge configuration.

- To measure friction and adhesion forces, a two dimensional bending beam was used (30 mm × 5 mm × 0.1 mm). To achieve an exact 90° rotation between the two axes of the transducer, the bending beam was folded three times. Half bridges of 350 Ω foil strain gauges (BLH, Heilbronn, Germany) were mounted on both sections of the bending beam for the measurement of normal forces and friction (Fig. 2.3).

- All experiments were conducted at temperatures between 21 °C and 28 °C.

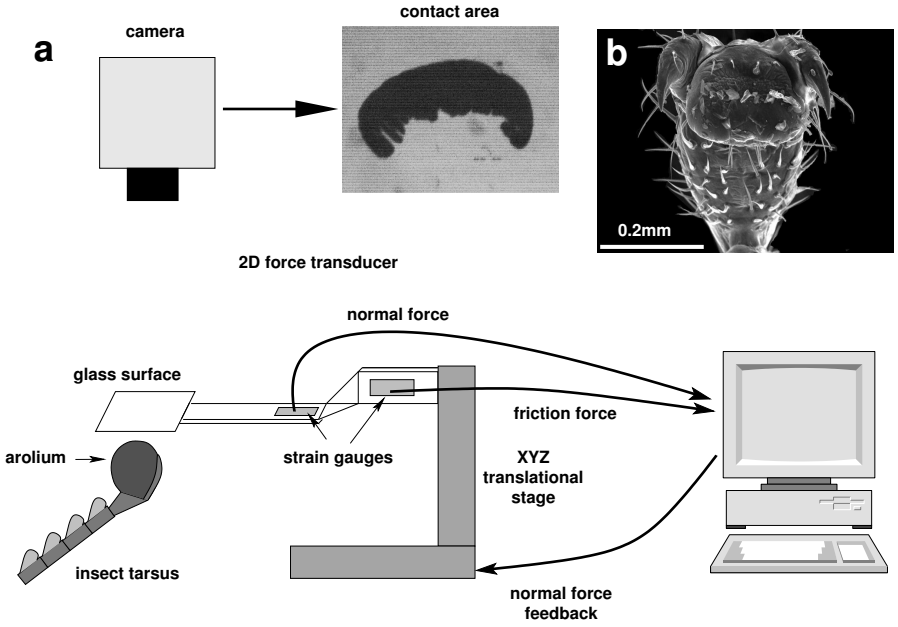

Figure 2.3: (a) Experimental setup for measuring adhesion and shear stress of insect adhesive pads. The arolium is brought into contact with a glass surface attached to a 2D bending beam force transducer for measuring friction and adhesion (i. e. normal forces). The bending beam is moved by a computer-controlled XYZ-translation stage. Forces in the normal direction can be adjusted via a feedback mechanism. Contact area is imaged from above using reflected light (see text for further details). (b) Scanning electron microscopy image of a stick insect pretarsus.

2.3 LABVIEW CONTROL PROGRAM

To synchronize motor control, video recording and data acquisition a custom-made software was implemented using LABVIEW. This program also enabled the use of a closed-loop feedback mechanism for controlling normal force during the experiments (for details see appendix section A.1.1). The minimum time for the feedback loop was 100 ms (10 Hz).

2.4 DATA ANALYSIS

Video as well as force analysis of the contact area was performed offline with custom made software in MATLAB. The code listed in the appendix (section A.1.2) illustrates the main calculation of the contact area for each individual frame.

2.5 FRICTION FORCE MEASUREMENTS

To measure friction, sliding movements of stick insect arolia were performed on the glass plate of the transducer. In all experiments, the transducer was moved in the distal direction, corresponding to a pull of the leg away from the body. As in adhesive pads of other insects, contact area and friction forces are maximal in this direction (bush crickets: Gorb and Scherge, 2000; flies: Niederegger et al., 2002; ants: Federle et al., 2001, Federle and Endlein, 2004). Due to the flexibility of the pad (even in the immobilized condition, see above), relatively large movement amplitudes (4–10 mm) were required to ensure that pads did not remain in stationary contact and friction reached a plateau when pads were sliding steadily (see Fig. 3.7a). During the slides, normal force was kept constant by using a force feedback loop. Shear stress was calculated as the ratio of friction force to the simultaneously measured contact area.

2.5.1 *Anisotropy*

Gorb and Scherge (2000) have described friction of smooth adhesive pads as being direction dependent[1]: Movements towards the body (proximal) showed lower static friction forces than movements directed away from the body (distal). Extending this analysis dynamic friction force as well as shear stress was measured by moving tarsal pads parallel to the surface while simultaneously measuring the corresponding contact area.

To differentiate between material properties of the adhesive pad and those of the pretarsus friction forces were measured under two conditions: (i) "Immobilized": The pretarsus was attached to the solder wire all the way to the manubrium with paraffin wax (see Fig. 2.1a); And (ii) "footloose": To simulate a more natural condition the leg was immobilized at the tibia, leaving the pretarsus freely movable around the tibia-tarsal joint (Fig. 2.1b).

For "immobilized" arolia six animals were tested with four velocities (50 µm s^{-1}, 100 µm s^{-1}, 250 µm s^{-1} and 500 µm s^{-1}) using an amplitude of 1 mm; for "footloose" arolia three animals were tested with five velocities (same as "immobilized" plus

1 Also see Niederegger and Gorb, 2006 for similar results for spiders.

1000 µm s^{-1}) and an amplitude of 2 mm. The proximal-distal movement was repeated five consecutive times ("immobilized" movements started with sliding in distal direction; "footloose" movements started with sliding in proximal direction; see Fig. 3.1). No feedback mechanism was applied.

2.5.2 *Amount of pad secretion*

To examine the influence of the amount of pad secretion between the arolium and the substrate during proximal sliding movements, two different conditions were compared (Fig. 1.12): (i) "Accumulated secretion": All slides were performed from the same starting point resulting in the attachment pad leaving behind more and more fluid on the surface. (ii) "Little secretion": Every repetition was performed on a "new" position, where the glass plate was still clean. Ten stick insects were tested under both conditions with seven repetitions. Sliding velocity was 500 µm s^{-1} covering an amplitude of 8 mm; normal force was set to 1 mN. Humidity was kept above 80 % using a humidifier (see below) to reduce possible effects due to evaporation of the hydrophilic part of the two-phase secretion (Federle et al., 2002). The maximum friction force of each slide and its corresponding contact area in the video recording were used for further analysis.

2.5.3 *Normal force*

The influence of normal force on sliding friction was tested by performing 4 mm sliding movements under four different feedback–controlled loads: 2 mN, 1 mN, 0.5 mN and −0.1 mN. As insect adhesive pads are viscoelastic (Gorb et al., 2000), there is a strong loading–unloading hysteresis and for a given force, contact areas are smaller during loading than during unloading. To be able to include a negative load in this experiment, and to make conditions comparable with each other, all pads were preloaded with 2 mN for 1 s before being set to the desired normal force by unloading. The effect of normal forces was tested both for "little" and "accumulated" secretion. The maximum friction force of each slide and corresponding contact area were used for further analysis. Ten pads were tested twice under ran-

domized orders of applied normal forces and pooled resulting in $N = 20$. Sliding velocity was $100\,\mu m\,s^{-1}$, covering a distance of 4 mm.

2.5.4 *Humidity*

Previous observations using interference reflection microscopy have shown that the hydrophilic component of the secretion is volatile (Federle et al., 2002). To investigate the effect of fluid evaporation on friction forces, I performed a series of trials to compare "accumulated" secretion forces under high ($> 80\,\%$) and low ($< 30\,\%$) humidity. Paired high-low humidity experiments were conducted with less than 2 minutes time in between both conditions. Humidity was increased by using an ultrasonic humidifier (Honeywell, BH-860 E) and enclosing the setup with transparent plastic foil. Five consecutive slides were performed with $500\,\mu m\,s^{-1}$ and 10 mm amplitude. Normal force was set to 1 mN. The first and the last slide of each series were evaluated as "little" and "accumulated" secretion, respectively. The maximum friction force of each slide and its corresponding contact area were used. Eleven pads from three animals were tested once under both humidities ($N = 12$).

2.5.5 *Velocity*

To examine the influence of different velocities four consecutive slides were performed with each slide conducted at a different velocity. The experiment was performed for "accumulated" secretion (see above). Velocities of $20\,\mu m\,s^{-1}$, $50\,\mu m\,s^{-1}$, $100\,\mu m\,s^{-1}$ and $250\,\mu m\,s^{-1}$ were used. The order of velocities was randomized to prevent possible effects of cuticle elasticity changes. Due to limitations of the recording time and the size of the glass plate used, different amplitudes had to be used for the four conditions ($v_{20,50,100}$: 4 mm, v_{250}: 10 mm). To make it possible to compare friction forces between the different velocities, forces were measured both after (i) an equal time of sliding (16 s) and (ii) after an equal sliding distance (4 mm). Both types of data were used separately for further analysis. Normal force was 1 mN and amplitude was 10 mm ($N = 14$).

2.5.6 *Static friction*

To evaluate if static friction is present in stick insects, I refrained from measuring the friction force during the onset of sliding (classical definition of static friction), because this force was velocity dependent (see Fig. 3.7a). Instead, I applied a sliding movement (80 % humidity, velocity 20 µm s^{-1} or 500 µm s^{-1}), after which the motor was stopped and the pad left in contact. I measured the remaining friction force of the pad two minutes after the end of the sliding movement. The velocity of the preceding sliding movement had no significant effect on remaining friction; data were therefore pooled.

2.5.7 *Friction force measurements in tree frogs*

Pad preload was adjusted manually to be approximately 1 mN. A closed feedback loop kept the normal load constant at 0.1 mN during the friction experiment. The glass surface was moved by 10 mm at a constant velocity of 500 µm s^{-1}. Shear forces were recorded (i) at the onset of pad sliding; (ii) during steady sliding (at the end of the movement); and (iii) 2 min after the movement had stopped (see Fig. 3.19a). To assess the possibility of very slow, residual sliding after the end of the motor movement, an exponential fit was calculated from measurements of the pad position during the 2 min after the motor had stopped. The glass surface was carefully cleaned with distilled water and acetone using lens paper after each trial to remove any mucus residues. An ultrasonic humidifier (Honeywell, BH-860 E) was used to perform the measurements at greater than 80 % air humidity (20 °C). To calculate shear stress (the ratio of shear force and contact area) the contact area of the toe pads during the force measurements was measured using reflected light video images (Federle and Endlein, 2004).

2.6 ADHESION FORCE MEASUREMENTS IN STICK INSECTS

Adhesion force measurements of stick insect's single attachment organs were performed using 1-D bending beams (section 2.6.1, 2.6.2.1). During each attachment/detachment (=loading/unloading) cycle the pad was brought into contact with the

glass plate using a feedback loop to establish a constant normal force. Contact time and attachment/detachment velocities were controlled using custom made software (see section 2.3). Results from these experiments were also used to analyse to role of pad secretion as well as mode of detachment.

In a second set of experiments adhesion forces of whole insects attaching freely to a centrifuge apparatus were measured to compare scaling effects between single pad and whole body attachment forces (section 2.7).

2.6.1 *Role of pad secretion, surface roughness & contact time*

To investigate the effect of pad fluid on adhesive forces, two experiments were performed. Both experiments consisted of consecutive pull-offs from different surfaces.

The first experiment was comprised of nine consecutive pull-offs (to deplete secretion) from smooth glass and from a rough surface (Aluminium oxide polishing paper, roughness average $R_a = 0.5\,\mu m$, Ultra Tec, USA). Pull-offs for each pad were performed perpendicular to the surface, alternately from the smooth and the rough substrate ($N = 10$). Approach and detach velocity was $500\,\mu m\,s^{-1}$. After the pad had been brought into contact, a short proximal movement was performed ($100\,\mu m$) followed by 2 s pause with normal force set to 1 mN to ensure good contact between the arolium and the substrate. To accelerate the depletion of pad fluid, the pad was brought into contact with laboratory filter paper before each pull-off for 2 s with a normal force of 1 mN. The data was analysed using Page's L-test.

In the second experiment smooth and rough surfaces were custom made from epoxy (Epoxidharz L, Härter L, R&G Faserverbundwerkstoffe GmbH, Waldenbuch, Germany) to eliminate possible differences in interface effects (such as polarity) between both surfaces. The average roughnesses of the smooth and rough surface were approximately $R_a = 0\,\mu m$ and $R_a = 16\,\mu m$, respectively.

The amount of secretion was controlled by dabbing the pad five consecutive times on the surface followed by a pull-off from a new position on the surface (no previous depletion: "little" secretion) or on the same position as the previous contacts ("accumulated" secretion). Approach and detach velocity as well as applied normal force were identical to the first ex-

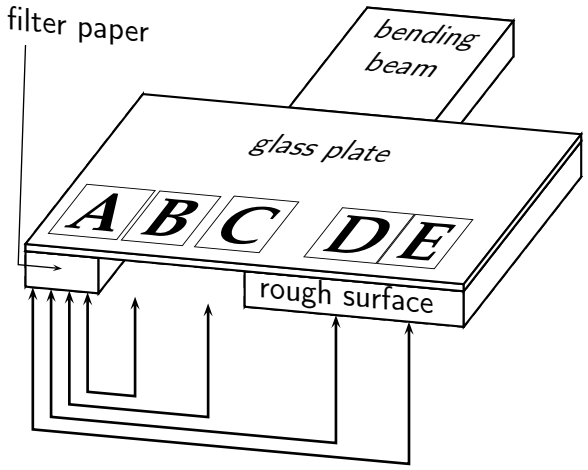

Figure 2.4: Simplified diagram of movement pattern for consecutive pull-offs testing forces between "smooth" (positions B and C) and "rough" surface (positions D and E). Position A represents contact with filter paper to deplete adhesive fluid. Double headed arrows indicate movement and location of attachment pad. Analysing "little" secretion would bring the pad in contact in the following order: A-B-A-D-A-C-A-E. For "accumulated" secretion the pad would not be brought in contact with position A but multiple times with position B (or C): B-B-B-B.

periment. Fig. 2.4 shows a simplified diagram of the movement pattern. To determine if the time the arolium spent in contact with the substratum influenced detachment forces, the experiment was performed with a short (0.5 s) and a long (20 s) contact time. Since the feedback mechanism had a loop time of approximately 100 ms it was necessary to adapt the movement pattern for short contact times (0.5 s) to ensure a constant normal force of 1 mN. This was achieved by preceding each pull-off with a contact using the feedback mechanism for 2 s. The subsequent pull-off was performed with a lateral offset of 500 µm to exclude effects of the pad secretion deposited during the feedback. Note that no contact area for both experiments was measured as the rough surface was not transparent and therefore no video images could be captured.

A Two-way within-subject ANOVA was used to analyse the data testing for effects of the factors "secretion", "contact time" and "surface" as well as for interactions between these factors.

2.6.2 *Mode of detachment*

2.6.2.1 *Normal force & velocity*

To test the influence of normal force F_N and velocity v on potentially adhesion related variables (i. e. pull-off force; see below for details) the following experiment was performed: The pad was brought into contact with the glass cover slip four times for 10 s with loads of 0.01 mN, 0.1 mN, 1 mN and 2 mN. The load force was kept constant via the feedback mechanism during this time. Afterwards the pad was pulled off with a velocity of $10\,\mu m\,s^{-1}$. The experiment was then repeated with increasing pull-off velocities ($10\,\mu m\,s^{-1}$, $50\,\mu m\,s^{-1}$, $100\,\mu m\,s^{-1}$, $500\,\mu m\,s^{-1}$ and $5000\,\mu m\,s^{-1}$). To ensure that the amount of secretion would not influence the results each experiment was preceded by five consecutive pull-offs performed on the same spot to accumulate secretion. Besides pull-off force, the following variables were measured: Contact area during maximal pull-off force ($A_{F_{max}}$) and during detachment (A_{F_0}), force per area ($F_P/A_{F_{max}}$) and work of adhesion (WOA1, $WOA2_{mean}$ and $WOA2_{max}$). All dependent variables were log-transformed for analyses.

CALCULATION OF WORK OF ADHESION Two different approaches were used to estimate work of adhesion (referred to as WOA1 and WOA2). Both have in common that they do not cater for elasticity effects as predicted from contact mechanics models such as the JKR theory. However, measuring the displacement of the motor will also include effects not related directly to the region of contact.

WOA1: This approach describes the work to separate the pad from the surface. The viscous dissipation energy which is lost during detachment was calculated from the integral of adhesive force F and motor displacement s in normal direction. This energy was then divided by the contact area when force equaled zero (A_{F_0}).

$$W = \frac{\int_{t=F_0}^{t=F_P} F_t \cdot ds}{A_{F_0}} \tag{2.1}$$

If pads peel due to elastic forces, WOA1 would be small.

WOA2: For the second approach a peeling tape model was implied (see Fig. 2.5). Under the assumption of a 90° peeling

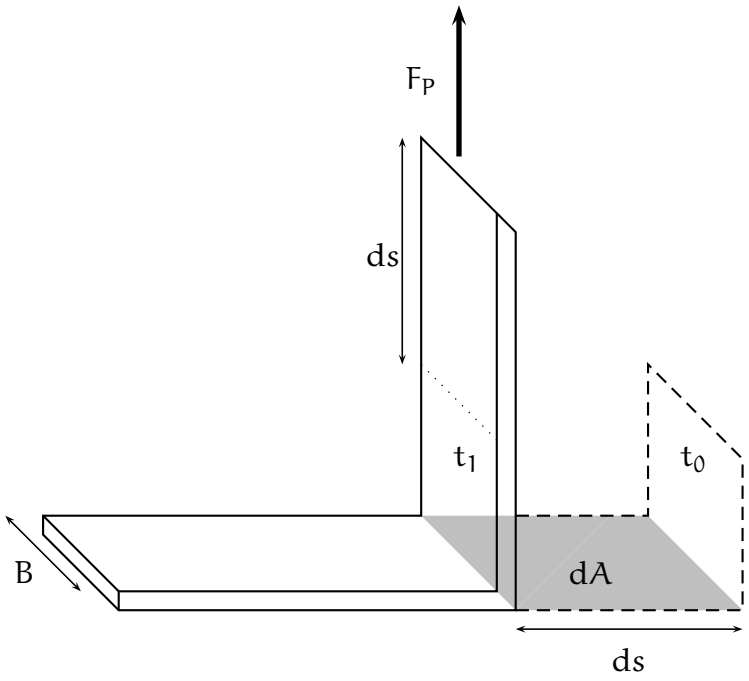

Figure 2.5: Calculation of work of adhesion using peeling model (perpendicular pull-off). Pulling force F_P is constant over time ($t_0 < t_1$). B is the length of the peeling edge, ds is the peeling distance, dA is the difference in contact area.

angle the vertical displacement equals the peeling length. The energy of the newly created surface $dA = B_t \cdot ds$ times the work of adhesion equals the product of force F_t and peeling distance ds:

$$F_t \cdot ds = \underbrace{B_t \cdot ds}_{dA} \cdot W_t \tag{2.2}$$

$$F_t \cdot ds = dA \cdot W_t \tag{2.3}$$

For a circular contact area the peeling distance ds can be described by (Fig. 2.6):

$$ds = \frac{dA}{2r_t\pi} \tag{2.4}$$

Substituting ds in equation Equ. 2.3 with equation Equ. 2.4

$$F_t \cdot \frac{dA}{2r_t\pi} = dA \cdot W_t \tag{2.5}$$

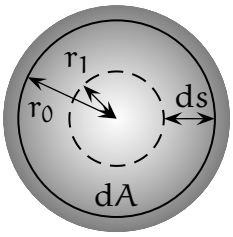

Figure 2.6: Calculation of work of adhesion using peeling model with circular contact area. Difference in decreasing contact areas are displayed by solid and dashed circles. The outer circle depicts the circumference of the contact area at time t_0 (radius r_0), inner circle at time t_1 (radius r_1). Length ds indicates the distance travelled (also see Fig. 2.5). The area in-between these two circles (dA) shows the difference in contact area.

and solving for W_t

$$W_t = \frac{F_t}{2r_t\pi}. \tag{2.6}$$

With $r_t = \sqrt{\frac{A_t}{\pi}}$ this results in:

$$W_t = \frac{F_t}{2\sqrt{A_t\pi}} \tag{2.7}$$

Since this approach includes a work of adhesion value for each point in time WOA2 was split into two different values, the first representing the maximum value during each trial ($WOA2_{max}$) whereas the second value ($WOA2_{mean}$) described the mean of this trial.

The data was analysed taking into account the following considerations: There were two explanatory variables (normal force F_N and velocity v) and seven continuous response variables: pull-off force F_P, contact area (A_{F_0} and $A_{F_{max}}$), force per area ($F_P/A_{F_{max}}$) and work of adhesion (WOA1, $WOA2_{mean/max}$). In theory the analysis can be done in three different ways:

- Explanatory variables can be considered categorial (Two-Way ANOVA).
- Explanatory variables can be considered as continuous (multiple linear regression).
- One explanatory variable can be considered continuous, the other categorial (ANCOVA).

Since only four normal forces and five velocities were tested multiple linear regressions as well as ANCOVA were dropped in favour of Two-way ANOVAs. To also examine if there was an interaction between the explanatory variables a Two-way within-subjects ANOVA was performed. When no interaction was found subsequent model reduction was applied. This consisted of dropping the interaction term (see Tbl. A.21 to Tbl. A.22 on page 114).

Tukey's Honest Significance Differences (Tukey's HSD) was performed to determine differences between factor levels when ANOVA results indicated significant differences in the respective factor. This test was only applied in the absence of interaction between factors (see Tbl. A.36 to Tbl. A.39 on pages 122–125).

2.6.2.2 *Scaling of single leg forces*

To analyse possible contribution of viscoelasticity in the adhesive pad of the stick insect I measured scaling effects of pull-off forces against velocity and normal force using the data set from the previous section ($N = 20$). Scaling analyses were performed on the relationship between pull-off force F_P and body mass m and contact areas at $F_P = 0$ (A_{F_0}) and at F_{max} ($A_{F_{max}}$). Scaling coefficients were calculated using ordinary least square (OLS) regression as well as standardized major axis (SMA) regression (see section 2.8 for details).

The measured scaling coefficients were compared to theoretical scaling coefficients derived from different theories: Contact mechanics models predict that forces will scale with contact area. The scaling coefficient is expected to be 2/3 when scaling adhesive force against body mass and 1 when scaling against measured contact area. Peeling theory predicts force scaling with a length. In this case the scaling coefficient of force against body mass and contact area is expected to be 1/3 and 1/2, respectively.

Body masses ranged from 84.45 mg to 1012.03 mg and were normally distributed after log-transformation (Shapiro-Wilks normality test: $W = 0.95$, $P > 0.3$).

2.7 CENTRIFUGE APPARATUS FOR MEASURING WHOLE BODY FORCES

To measure whole animal pull-off forces in stick insects a centrifuge technique similar to the one described in Federle et al. (2000) was applied. The same motor was used (gradual acceleration from 0 to 6000 rev min^{-1}).

The original apparatus was conceived for small animals such as ants and consisted of a cylindrical surface to which the insects attached. To prevent comparatively large stick insects from grasping around a cylindrical surface, and therefore additionally applying a friction force, the surface was redesigned using a plane surface (see Fig. 2.7). Using plane surfaces permitted an easy way of exchanging surfaces. Standard glass plates were used ($R_a = 4.6$ nm). Before each experiment, the plates was carefully cleaned with a lens cloth and 25 % ethanol. The detachment phase of the stick insect was recorded from above with a camera (Basler A602f, Basler AG, Ahrensburg, Germany). The latter was triggered using a light reflector whose signals where recorded for angular velocity calculation.

24 animals were tested. Measurement of contact areas was performed for each animal after the experiment using reflected light as described in section 2.2. Attachment forces F_P were calculated by measuring body mass m, radius of body center r and angular velocity ω at the time of detachment: $F_P = m\omega^2 r$. The insect's body was assumed to have a homogeneous density and therefore body mass m was set equal to volume V.

All data were log transformed. Although only force was normally distributed ($P > 0.05$, see Tbl. A.43) all data were analysed with parametric regression methods.

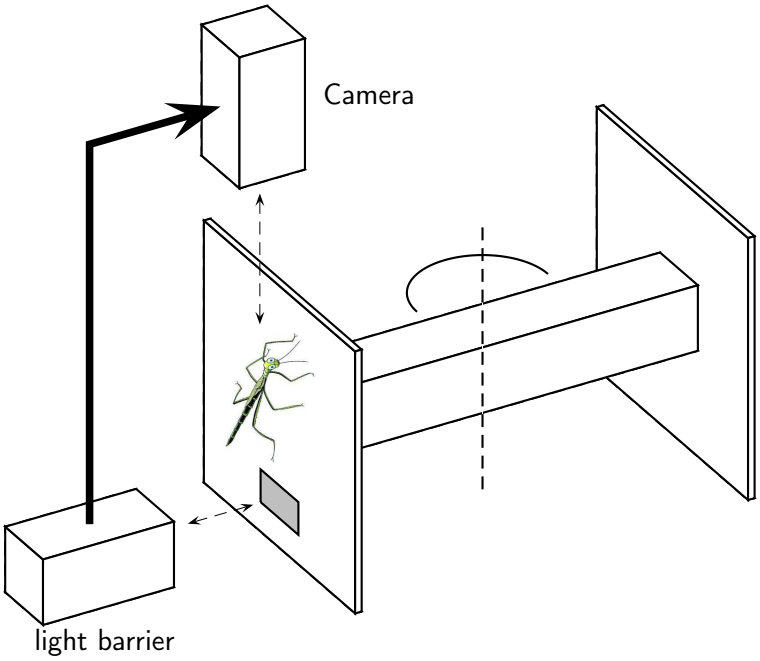

(a)

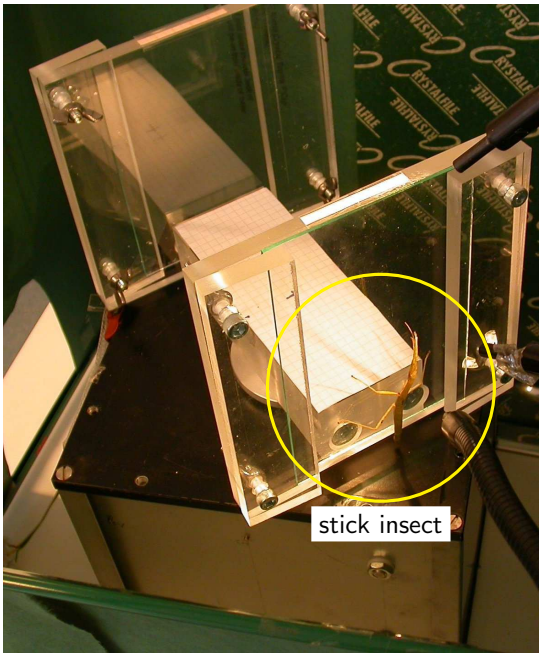

(b)

Figure 2.7: Diagram (a) and photography (b) of centrifuge apparatus. A beam connects two glass plates. A reflective tape (gray area below insect in (a)) is attached to one of the glass plates activating a photoelectric sensor which in turn triggers the camera. The stick insect sits on an exchangeable glass plate.

2.8 STATISTICS

All data were tested for the presence of normal distribution (Shapiro-Wilk test) and homogeneity of variances (Bartlett's test). If both conditions were met, parametric tests were performed, otherwise their non-parametric equivalents.

For comparisons between multiple groups analyses of variance (ANOVA = parametric) or Kruskal-Wallis tests (non-parametric) were used. Page's non-parametric L-test (Page, 1963) was used to test for monotonic changes between groups (see section 3.1.2, and section 3.1.5, consecutive pull-offs). The indices of the L-value ($L_{m,n}$) denote "conditions" (m) and "number of samples" (n).

Experiments with multiple independent variables were analyzed using multifactorial analysis of variance (i. e. Two-way ANOVA). Graphical representations of multifactorial analyses comply to Heiberger and Holland (2004) and Crawley (2005).

Line-fitting methods in regression analysis were chosen according to the general key given by Warton et al. (2006): When predicting the value of one variable from another, ordinary least square regression (OLS) was used. This regression is also referred to as linear regression or "model I" regression. If lines were fitted to estimate how one variable scales against another (allometric and isometric questions as in 3.2.2.2) standardized major axis regression (SMA) was performed. The latter is also referred to as "model II regression" or "reduced major axis regression" (RMA). Warton and Weber, 2002 have not only described a solution for calculating SMA regression slopes, but also tests if a slope equals a specific value or multiple slopes share a common value (Warton et al., 2006). It should be noted that the commonly used squared correlation coefficient R^2 does not express the *nature* of the relationship between variables but its *strength*. These are two independent properties of the relation.

Graphical representations in form of box plots comply to Chambers et al. (1983); outliers are not displayed. Data values given within the text are either medians in case of not normally distributed data or means with standard deviation in case of normally distributed data. To assure balanced designs were necessary, missing data points were imputed by inserting medians as proposed by Harrell, 2001, Chap. 3.

All statistic analysis were performed using the open source software R (R Development Core Team, 2007).

3

RESULTS

3.1 FRICTION FORCE MEASUREMENTS IN STICK INSECTS

3.1.1 *Anisotropy*

To assess anisotropic friction properties of adhesive pads (arolia) in stick insects (*Carausius morosus*), long distance sliding movements in proximal and distal directions at different velocities were performed. To account for material properties of the adhesive pad and those of the pretarsus, friction forces were measured with "immobilized" and "footloose" pretarsi (see Fig. 2.1). Fig. 3.1 shows an example measurement of friction force, contact area and shear stress (force per unit area) for the "immobilized" and "footloose" conditions.

The main result obtained from the "footloose" experiments was the fact that the pretarsus regularly detached during distal movement. Hence a statistical comparison of proximal and distal friction forces was not needed. Comparing proximal and distal movement directions of "immobilized" arolia showed a significantly larger contact area during proximal direction. No significant difference was present for friction force. Shear stress was therefore larger in the distal direction.

Different types of analysis were performed: First, all velocities were pooled to test for effects between proximal and distal directions of movement (Fig. 3.2). This analysis was repeated for unpooled data comparing direction dependence for each velocity (Fig. 3.3). Finally, the effect of velocity was analyzed.

"Immobilized" arolia showed no significant difference in friction force between proximal and distal direction (all velocities pooled; paired Wilcoxon test; $V = 144$, $P = 0.87$, $N = 6$). In contrast, contact areas were significantly larger in proximal than in distal directions (all velocities pooled; paired Wilcoxon test; $V = 0$, $P < 0.0001$, $N = 6$). Shear stress was therefore larger in the distal than in the proximal direction for "immobilized" arolia (all velocities pooled; paired Wilcoxon test; $V = 268$, $P < 0.0001$, $N = 6$).

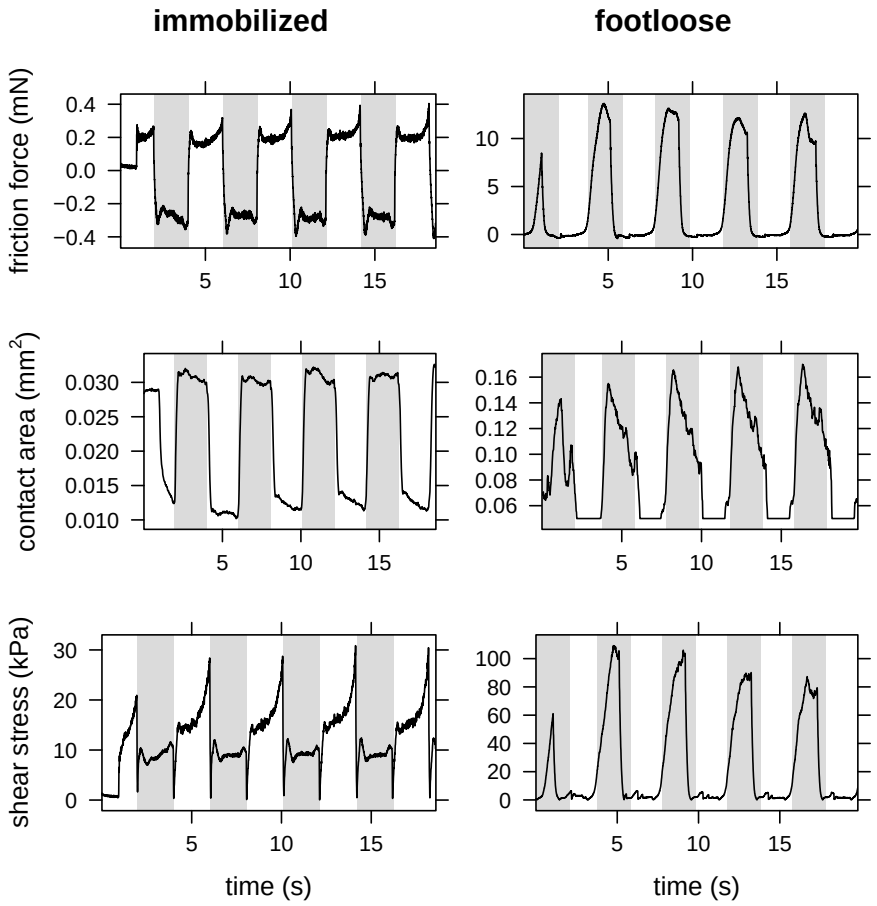

Figure 3.1: Example friction force, contact area and shear stress curves of five consecutive proximal and distal sliding movements for "immobilized" (plots on the left) and "footloose" (plots on the right) adhesive pads in stick insects. Gray areas depict proximal movement. Shear stress values were rectified. Amplitude was 1 mm and 2 mm for immobilized and footloose data, respectively and velocity was 500 µm s^{-1}.

A comparison between proximal and distal movement of "immobilized" arolia for each velocity showed no significant difference in friction force (paired Wilcoxon test; $V > 6$; $P > 0.1$). Contact area differed significantly at velocities 100 µm s^{-1}, 250 µm s^{-1} and 500 µm s^{-1} (paired Wilcoxon test; $V = 0$; $P < 0.05$). Shear stress was significantly different at 100 µm s^{-1} and 250 µm s^{-1} (paired Wilcoxon test; $V = 21$; $P < 0.05$).

Analysis of velocity dependence was performed with all data sets. Normality as well as homogeneity of variances was not present in any of the data sets. Therefore Page's L-test was per-

formed on "immobilized" (in proximal as well as distal direction) and "footloose" data to test the influences of velocity on friction. For "immobilized" data sets no significant effect of velocity was found for any of the studied physical parameters (friction force, contact area, shear stress), independent of the movement direction (one value imputed).

Due to the small sample size (N = 3) Page's L-test with "footloose" data sets did not reveal any significant influence of velocity on friction force, contact area or shear stress. Nevertheless, friction forces (Fig. 3.3b) and shear stress (Fig. 3.3f) show a tendency of increasing with increasing velocity.

Analysis of movement direction was performed without using the feedback mechanism for controlling normal force. Median normal forces were $-2.2\,\mathrm{mN}$ in the distal and $0.9\,\mathrm{mN}$ in the proximal direction.

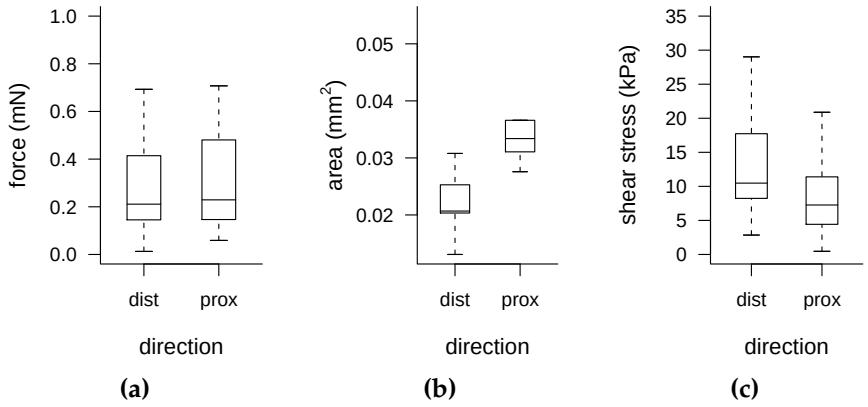

Figure 3.2: Anisotropy of (a) friction, (b) area and (c) shear stress for immobilized adhesive pads in proximal ("prox") and distal ("dist") directions (N = 6). All velocities are pooled.

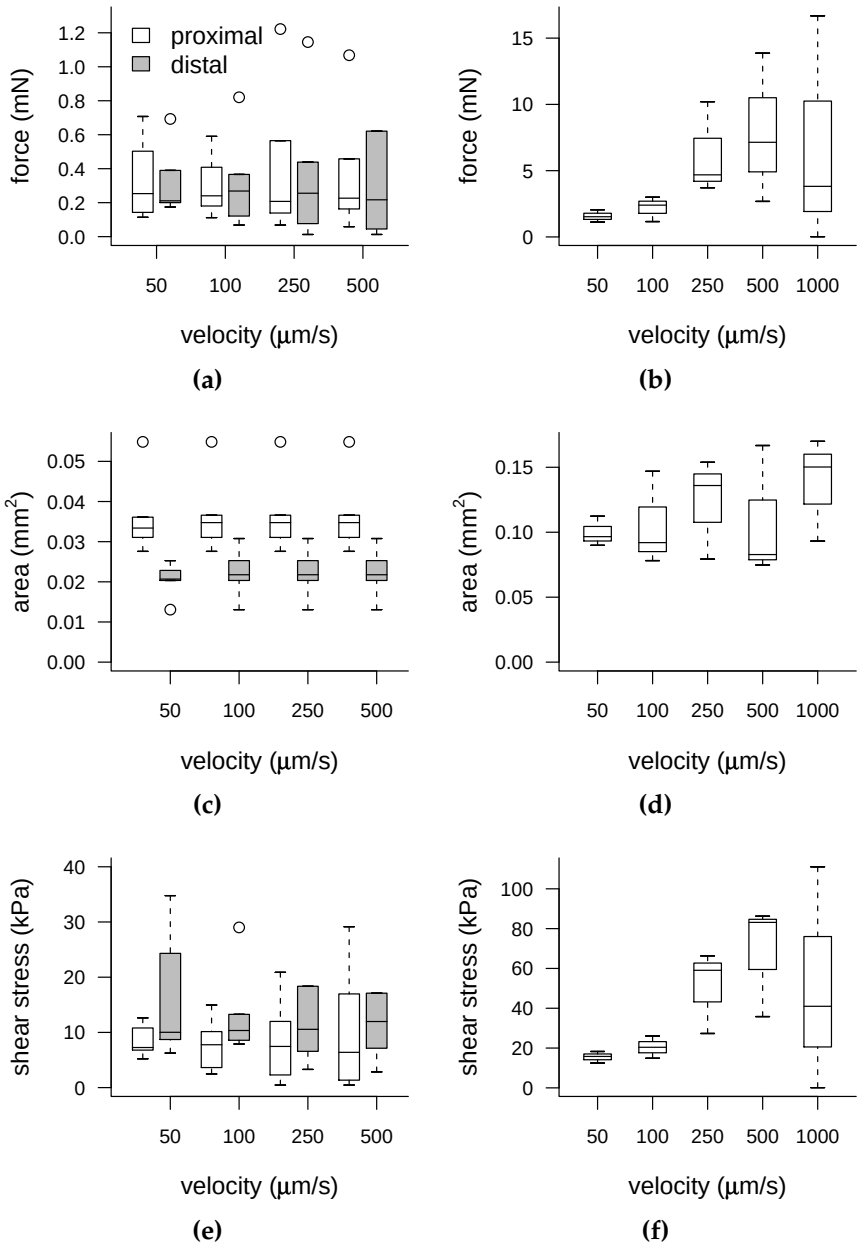

Figure 3.3: Velocity and direction dependence during anisotropic friction measurements. Left column of boxplots (a, c, e): "Immobilized" arolia. Six animals where tested using four velocities (50 µm s^{-1}, 100 µm s^{-1}, 250 µm s^{-1} and 500 µm s^{-1}); Amplitude: 1 mm; Right column of boxplots (b, d, f): "Footloose" pretarsal pads. Three animals where tested using five velocities (same as "immobilized" plus 1000 µm s^{-1}); Amplitude: 2 mm. White boxes denote proximal movement, grey boxes distal movement.

3.1.2 *Role of pad secretion*

To evaluate the friction characteristics of adhesive pads in stick insects, long distance sliding movements of front and hind leg pads on glass were performed. Friction and shear stress steadily increased in the course of each slide and only began to reach a plateau after approx. 15 s (corresponding to 7.5 mm distance covered, Fig. 3.4a). Friction force and shear stress were highly reproducible between consecutive slides when they were performed at new positions of the glass plate ("little secretion", Fig. 3.4a). However, when the consecutive sliding movements were repeated at the same position, forces decreased from trial to trial in a highly regular pattern ("accumulated" secretion, Fig. 3.4b). Shear stress in the last slide amounted to only 32 % of that of the first slide (medians: first slide 101 kPa, last slide 38 kPa). For "accumulated" secretion, the decrease of shear stress was highly significant (Fig. 3.4d; Page's L-test: $L_{9,10} = 1037$, $P < 0.001$), whereas no change was found for "little secretion" (Fig. 3.4c; ANOVA for effect of slide number and individual pad; effect of slide number: $F_{1,47} = 0.284$, $P > 0.1$). Normal force was 1 mN, sliding velocity was 500 µm s^{-1}, covering a distance of 8 mm.

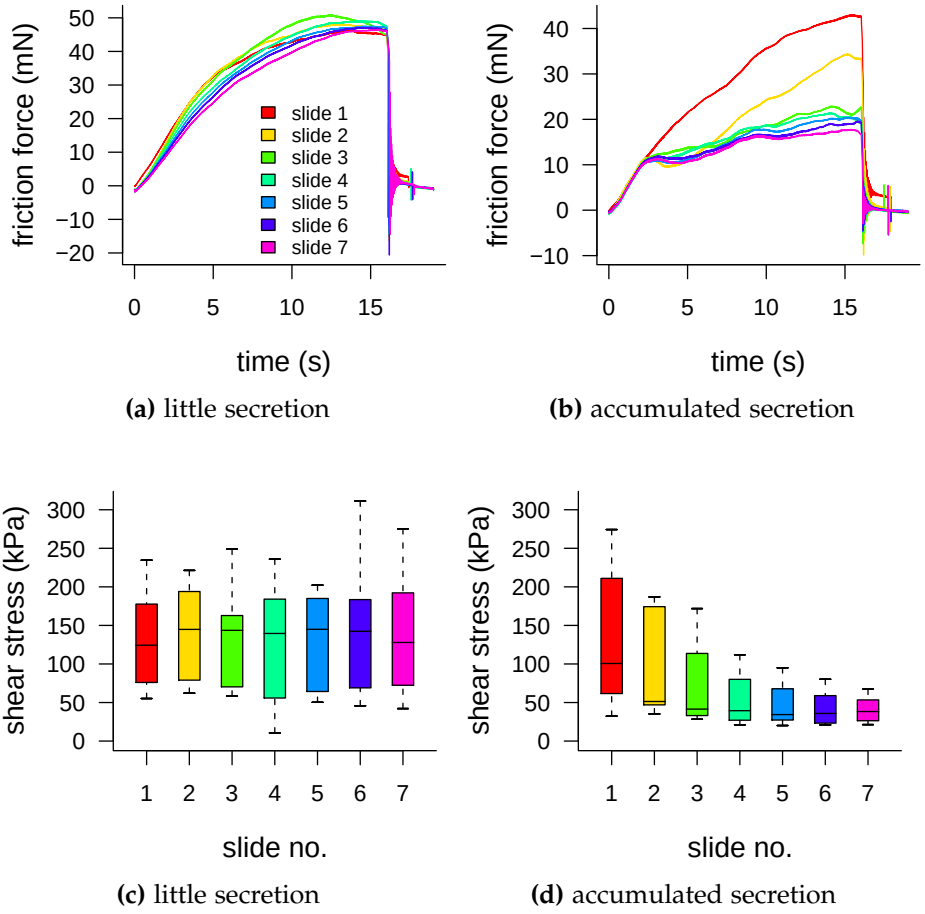

(a) little secretion

(b) accumulated secretion

(c) little secretion

(d) accumulated secretion

Figure 3.4: Shear stress measurement in single adhesive pads of *Carausius morosus*. (a): friction force in experiment consisting of seven consecutive long distance slides performed on a clean smooth glass plate ("little secretion"), (b): same as (a), but consecutive slides performed at the same position ("accumulated secretion"); (c) and (d): shear stress data, pooled results from ten pads. Grayscales indicate identical slide numbers in all plots. Normal force was 1 mN and sliding velocity was 500 µm s^{-1}, covering a distance of 8 mm.

3.1.3 *Normal force*

Both for "little" and "accumulated" secretion, normal forces had a significant influence on friction force and contact area (Fig. 3.5a and b, ANOVA; "little secretion": Force: $F_{1,19} = 8.05, P < 0.01$, Area: $F_{1,19} = 45.8, P < 0.001$; "accumulated secretion": Force $F_{1,19} = 74.86, P < 0.001$, Area: $F_{1,19} = 106.87, P < 0.001$). However, normal forces had no effect on shear stress for "little secretion" (Fig. 3.5c, ANOVA: $F_{1,19} = 0.09, P > 0.05$). Only for

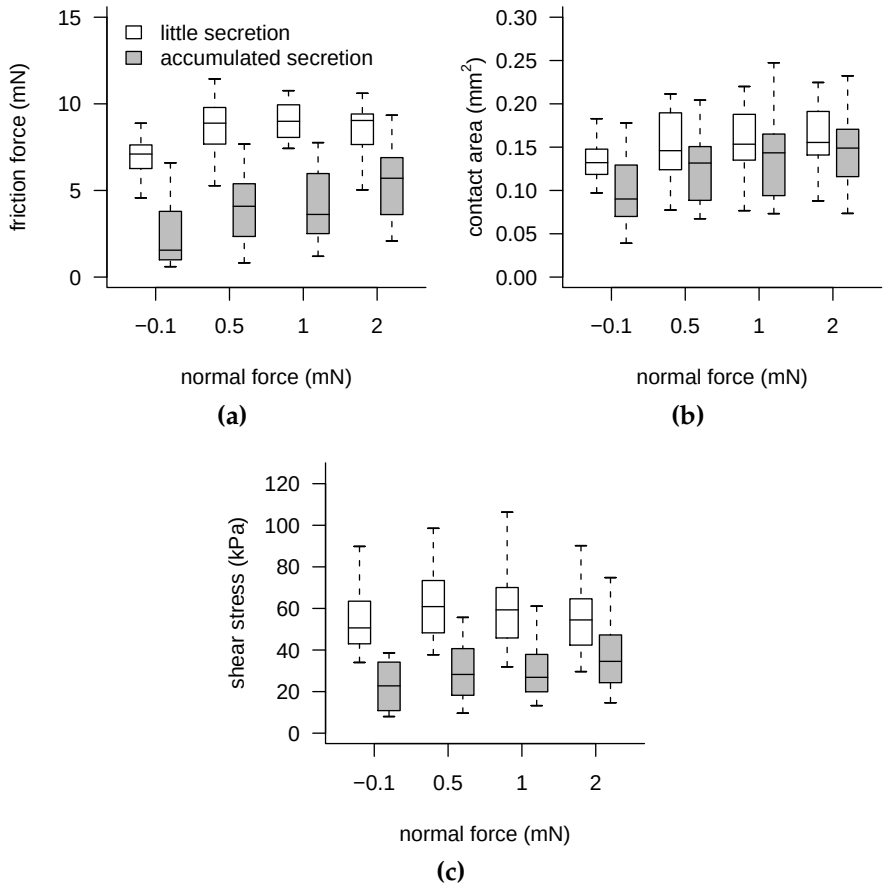

Figure 3.5: Influence of normal force on friction force (a), contact area (b) and shear stress (c) (sliding velocity: 100 µm s^{-1}; amplitude: 4 mm; N = 20). All pads were preloaded with 2 mN for 1 s before being set to the desired normal force by unloading.

"accumulated secretion" was shear stress dependent on normal force (Fig. 3.5c, ANOVA: $F_{1,19} = 15.37, P < 0.001$), but it explained less variation of friction than pad contact area. Thus, the increase of friction with normal force is mainly based on an increase of contact area (at least when no secretion has accumulated). Sliding velocity was 500 µm s^{-1}, covering a distance of 4 mm.

3.1.4 *Humidity*

I could not detect any effects of humidity and fluid evaporation on pad friction (Fig. 3.6). Friction forces and shear stress did

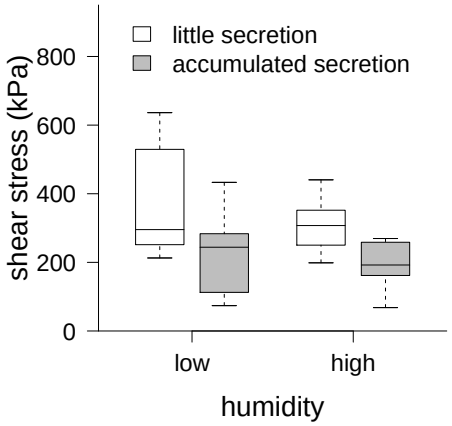

Figure 3.6: Influence of humidity on shear stress. There is no significant difference between low (< 30 %) and high (> 80 %) humidity for either "little" or "accumulated" secretion (sliding velocity: 500 µm s^{-1}; amplitude: 10 mm; $N = 11$).

not differ significantly between low (< 30 %) and high (> 80 %) humidity (Wilcoxon signed rank tests: $P > 0.4$ for both force and shear stress with "little" and "accumulated" secretion; $N = 11$).

3.1.5 *Velocity*

Friction forces and corresponding shear stress increased significantly with velocity in the presence of secretion ("accumulated secretion"). This increase was highly significant no matter whether force was measured after a constant time of 16 s (Fig. 3.7b) or after a constant amplitude of 4 mm (Page's L-tests: $L_{4,14} > 291$ and $P < 0.001$ for friction and shear stress). To estimate the relation between shear stress and velocity, linear regressions were performed for each individual pad (constant amplitude). Intercepts were positive in 100 % of all pads for "accumulated" ($N = 14$) secretion. Using the medians of the slopes and intercepts, the relationship between velocity v and shear stress τ can be written as: $\tau = 31.4 + 0.2 \cdot v$ (τ in kPa, v in µm s^{-1}; see Fig. 3.7c).

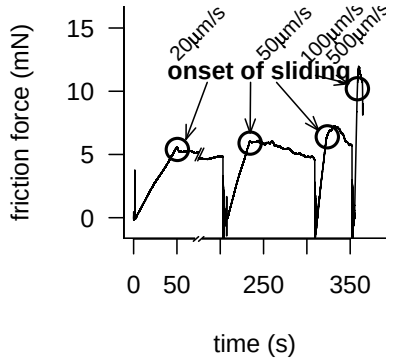

(a) Example force measurement.

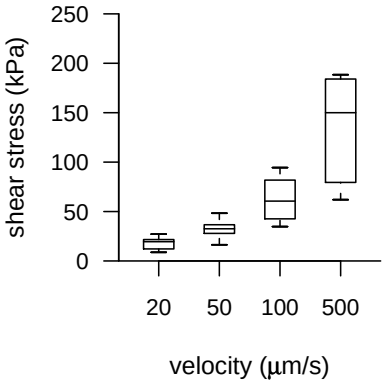

(b) Shear stress summary.

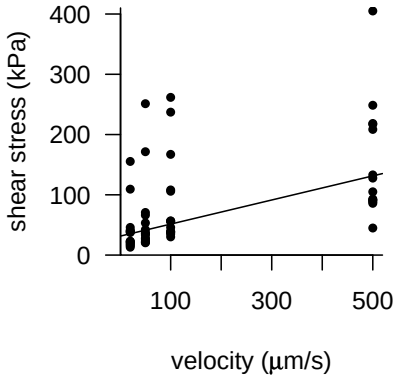

(c) Relationship between shear stress and velocity.

Figure 3.7: Single pad friction force (a) and shear stress (b) at four different velocities with "accumulated" secretion. Outliers are not displayed. (c): Scatterplot of (b) showing the linear regression between velocity and shear stress calculated from medians of individual slopes and intercepts. Shear stress τ can be described as $\tau = 31.4 + 0.2 \cdot v$ (τ in kPa, v in $\mu m\,s^{-1}$). All measurements were taken after a constant sliding time of 16 s (amplitude: 10 mm; normal force: 1 mN; N = 14).

3.1.6 *Static friction*

As the friction forces at the onset of sliding were velocity dependent and thus questionable as evidence in favour of static friction, I tested for the presence of static friction by measuring

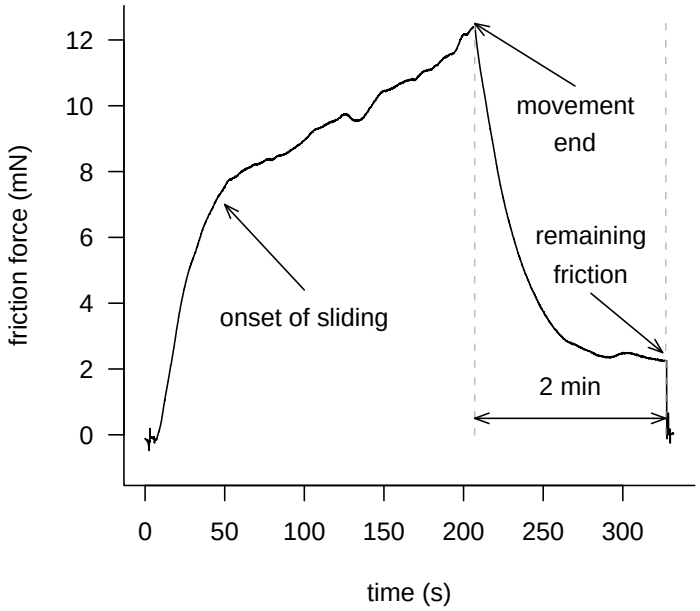

Figure 3.8: Friction force during and two minutes after a slow sliding movement ($20\,\mu m\,s^{-1}$). Onset of sliding was determined from the video recording.

the remaining friction force after the end of a sliding movement (Fig. 3.8). Even two minutes after the movement had ended, I still measured a considerable friction under both conditions (median "little" secr.: 3.36 mN, $N = 88$; median "accumulated" secr.: 3.8 mN, $N = 13$). However, shear stress was smaller for "accumulated" secretion (Wilcoxon rank sum test: $W = 280, P < 0.01$, median "little": 64 kPa, median "accumulated": 28 kPa; Fig. 3.9).

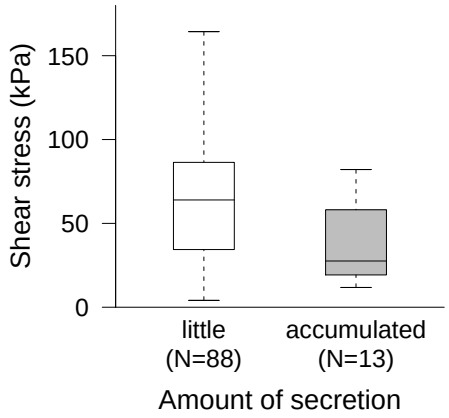

Figure 3.9: Comparison of remaining shear stress with little and accumulated secretion two minutes after movement had ended. Note that independent of the amount of fluid between pad and surface, shear stress was always present. Shear stress was significantly larger when less secretion was present ($P < 0.01$).

3.2 ADHESION FORCE MEASUREMENTS IN STICK INSECTS

Adhesion force were measured to answer questions concerning the role of pad secretion (amount of secretion, surface roughness) as well as the mode of detachment (fast versus slow detachment, influence of normal force, differences between single leg and whole body measurements).

3.2.1 *Role of pad secretion, surface roughness & contact time*

Two experiments were performed to analyse the influence of pad fluid on detachment forces in stick insects. In the first experiment, as described in section 2.6.1 on page 36 and illustrated in Fig. 3.10a, alternative pull-offs from smooth and rough substrates were preceded by contact with filter paper to accelerate the depletion of pad fluid. Forces significantly increased when consecutive pull-offs where performed at "new" positions on the smooth glass substrate (Page's L-test: $L_{9,10} = 2647$, $P < 0.05$; white boxes in Fig. 3.10). This effect was similar to the build-up of force seen during each long distance sliding experiment (Fig. 3.4). On the rough aluminium oxide substrate ($R_a = 16\,\mu m$), however, a different effect was found. Here, pull-off forces did not increase but, against expectations, actually

Table 3.1: Two-way within-subject ANOVA table testing the influence of surface (rough vs. smooth expoxy surface), secretion (little vs. accumulated) and contact time (short vs. long) as well as their interaction (denoted by "A:B" or "A:B:C"). There are significant effects for "surface" and "contact time", but not for interactions between any of the factors. ($N = 10$).

	Df	Sum Sq	Mean Sq	F	P
surface	1	0.280	0.280	37.17	0.000
Residuals	9	0.068	0.008		
secretion	1	0.007	0.007	2.72	0.134
Residuals	9	0.025	0.003		
contacttime	1	0.032	0.032	18.42	0.002
Residuals	9	0.016	0.002		
surface:secretion	1	0.000	0.000	0.36	0.563
Residuals	9	0.004	0.000		
surface:contacttime	1	0.001	0.001	1.99	0.192
Residuals	9	0.006	0.001		
secretion:contacttime	1	0.001	0.001	1.62	0.235
Residuals	9	0.004	0.000		
surface:secretion:contacttime	1	0.001	0.001	1.98	0.193
Residuals	9	0.003	0.000		

decreased (Page's L-test: $L_{9,10} = 2450$, $P < 0.01$; gray boxes in Fig. 3.10b).

For the second experiment, comparing smooth and rough epoxy surfaces, amount of secretion and contact time, a Two-Way within-subject ANOVA was performed to test for effects of these factors as well as for interactions between them (see section 2.6.1 on page 36 for a description of the experiment and Fig. 3.11 and Tbl. 3.1 for the results). There was no significant interaction between the factors "secretion", "contact time" and "surface" (all $P > 0.1$). Pull-off forces were significantly larger on smooth surfaces ($R_a \approx 0\,\mu m$) than on rough surfaces ($R_a \approx 16\,\mu m$): $F_{1,9} = 37.17$, $P < 0.001$. Similarly, long contact time (120 s) resulted in larger pull-off forces than short contact time (0.5 s): $F_{1,9} = 18.42$, $P < 0.01$. The amount of secretion ("little" vs. "accumulated") had no significant effect on pull-off forces: $F_{1,9} = 2.72$, $P > 0.1$.

Note that no contact area for both experiments was measured as the rough surface was not transparent and therefore no video images could be captured.

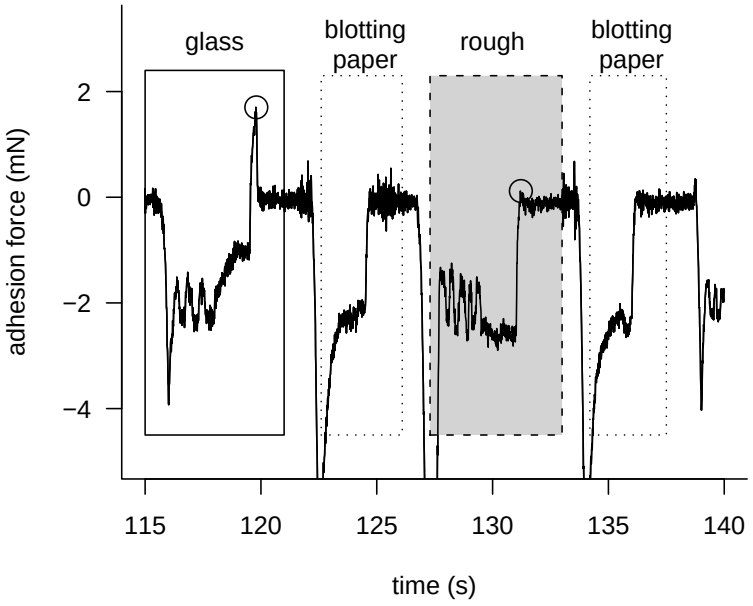

(a)

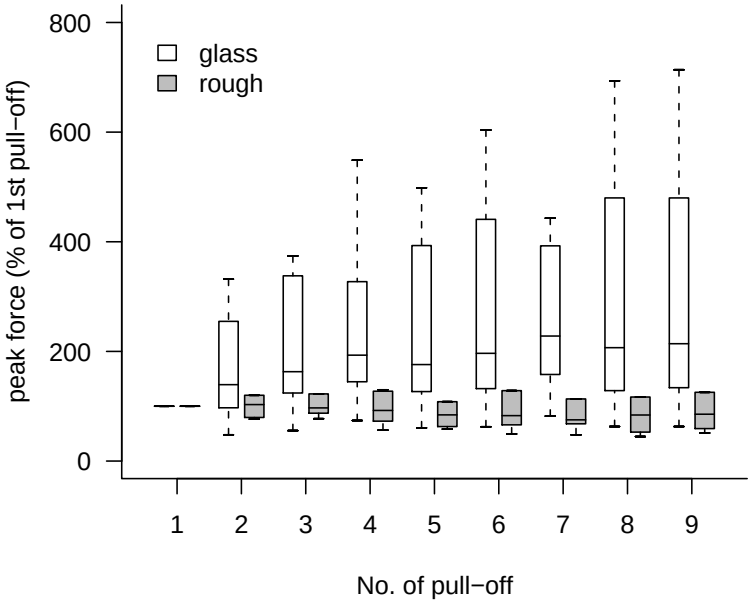

(b)

Figure 3.10: Consecutive, alternating pull-offs of *Carausius morosus* adhesive pads from glass and rough aluminium oxide ($R_a = 0.5\,\mu m$) substrates. (a): Example force curve. Each pull-off is preceded by contact with blotting paper to produce a reduction in fluid with successive pull-offs. Circles indicate pull-off force. (b): Pull-off forces increase with the number of pull-offs on glass surface, whereas they decrease slightly on the rough surface. Forces are shown as percentage of the first pull-off ($N = 10$).

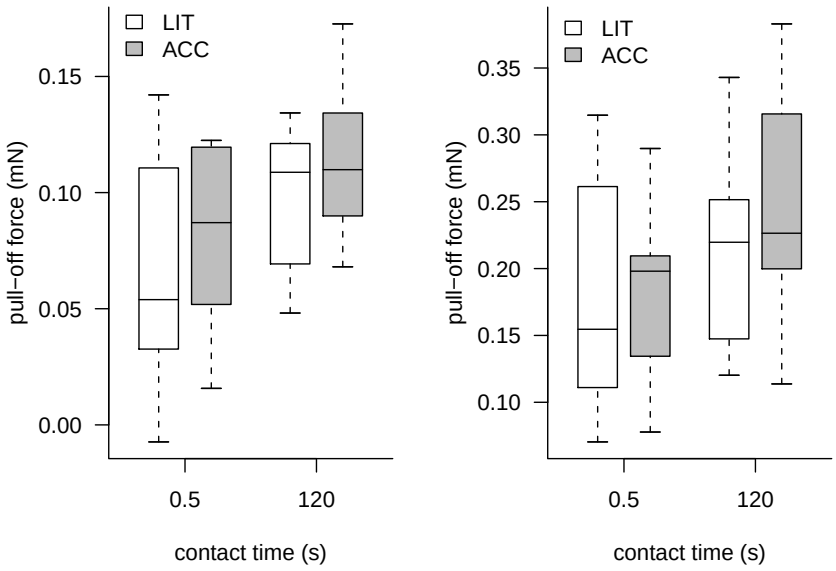

(a) rough surface **(b)** smooth surface

Figure 3.11: Effect of contact time and secretion on pull-off forces from a rough ($R_a \approx 16\,\mu m$; left plot) and a smooth ($R_a \approx 0\,\mu m$; right plot) epoxy surface ($N = 10$). Contact time was 0.5 s ("short") and 120 s ("long"). LIT/ACC: "little"/"accumulated" secretion.

3.2.2 *Mode of detachment*

3.2.2.1 *Normal force and velocity*

To test whether and how insect adhesive forces are influenced by pull-off velocity and preloads, single leg pull-off experiments in stick insects were performed with varying normal forces and velocities as described in section 2.6.2.1 (N = 20). An example measurement of force, area and displacement is given in Fig. 3.12.

The results are summarized in Tbl. 3.2 and Fig. 3.13. Normal force and velocity both had significant main effects on

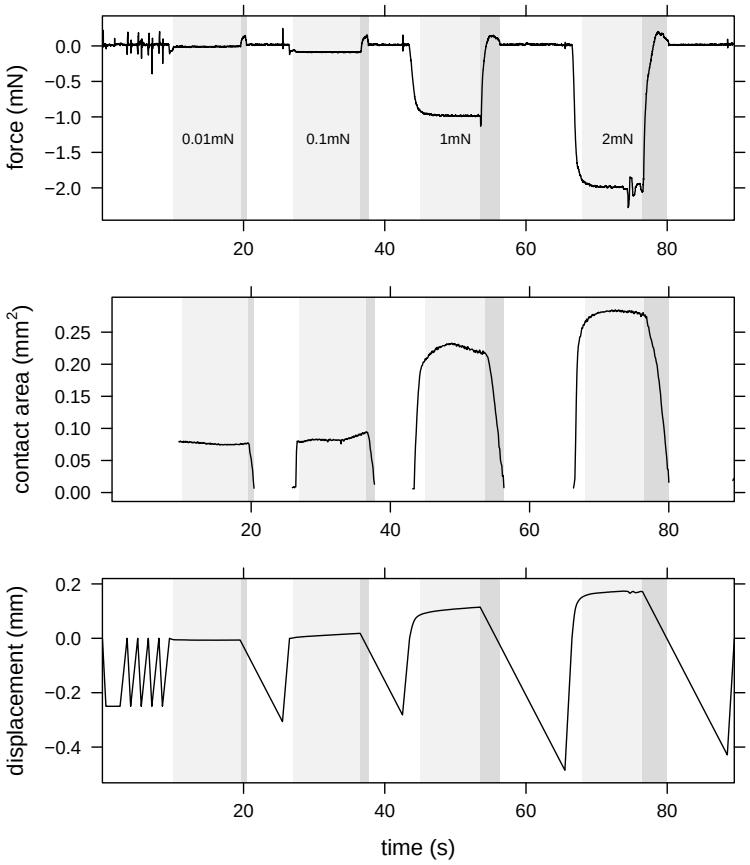

Figure 3.12: Example measurement of stick insect's single leg detachments at different normal forces. Light gray areas show different preload (from left to right: 0.01 mN, 0.1 mN, 1 mN and 2 mN). Dark gray areas show the corresponding detachment phases. Pull-off velocity: 50 µm s^{-1}.

pull-off force, contact area, force per area and work of adhesion WOA1. Furthermore, there was significant interaction between normal force and velocity for work of adhesion WOA2 (see section 2.6.2.1 for details on WOA calculation). Work of adhesion WOA2 increased more strongly with normal force at higher velocities.

Two-way mixed measures ANOVAs were carried out to examine the interaction between normal force F_N and and velocity v on all dependent variables. Missing data values (3 out of 400) were imputed by medians.

Although statistically not significant, there was a trend of pull-off forces (Fig. 3.13a, Fig. A.3) as well as contact areas (Fig. 3.13c, Fig. A.4) increasing more strongly with increasing normal force. This trend is supported by one-way ANOVAs on pull-off force (Tbl. A.25–Tbl. A.29) and contact area (Tbl. A.30–Tbl. A.34) testing for differences between normal forces for each measured velocity: Increasing velocities resulted in increasing differences in normal forces (corresponding to decreasing P-values). In contrast, force per area had a tendency to decrease with increasing normal force (Fig. 3.13d, Fig. A.6).

Table 3.2: Summary of Two-way ANOVAs analysing the influence of normal force F_N and velocity v on dependent variables in single leg detachment measurements of stick insects. Main effects were not analysed in the presence of interaction. Otherwise the model was simplified by removing the interaction term and testing for presence of main effects. If main effects were present, Tukey's Honest Significance Test (HSD) was performed. Detailed statistics are referred to in brackets. F_P: pull-off force, A_{F_0}: contact area during pull-off, $A_{F_{max}}$: contact area during max. pull-off, WOA: work of adhesion.

Variable	Interaction present?	Main effect F_N and v present?
F_P	no (Tbl. A.13, Fig. A.3)	yes (Tbl. A.20, Tbl. A.35)
A_{F_0}	no (Tbl. A.14, Fig. A.4)	yes (Tbl. A.21, Tbl. A.36)
$A_{F_{max}}$	no (Tbl. A.15, Fig. A.5)	yes (Tbl. A.22, Tbl. A.37)
F_P/A_{F_0}	no (Tbl. A.16, Fig. A.6)	yes (Tbl. A.23, Tbl. A.38)
WOA1	no (Tbl. A.17, Fig. A.7)	yes (Tbl. A.24, Tbl. A.39)
$WOA2_{mean}$	yes (Tbl. A.18, Fig. A.8)	no
$WOA2_{max}$	yes (Tbl. A.19, Fig. A.9)	no

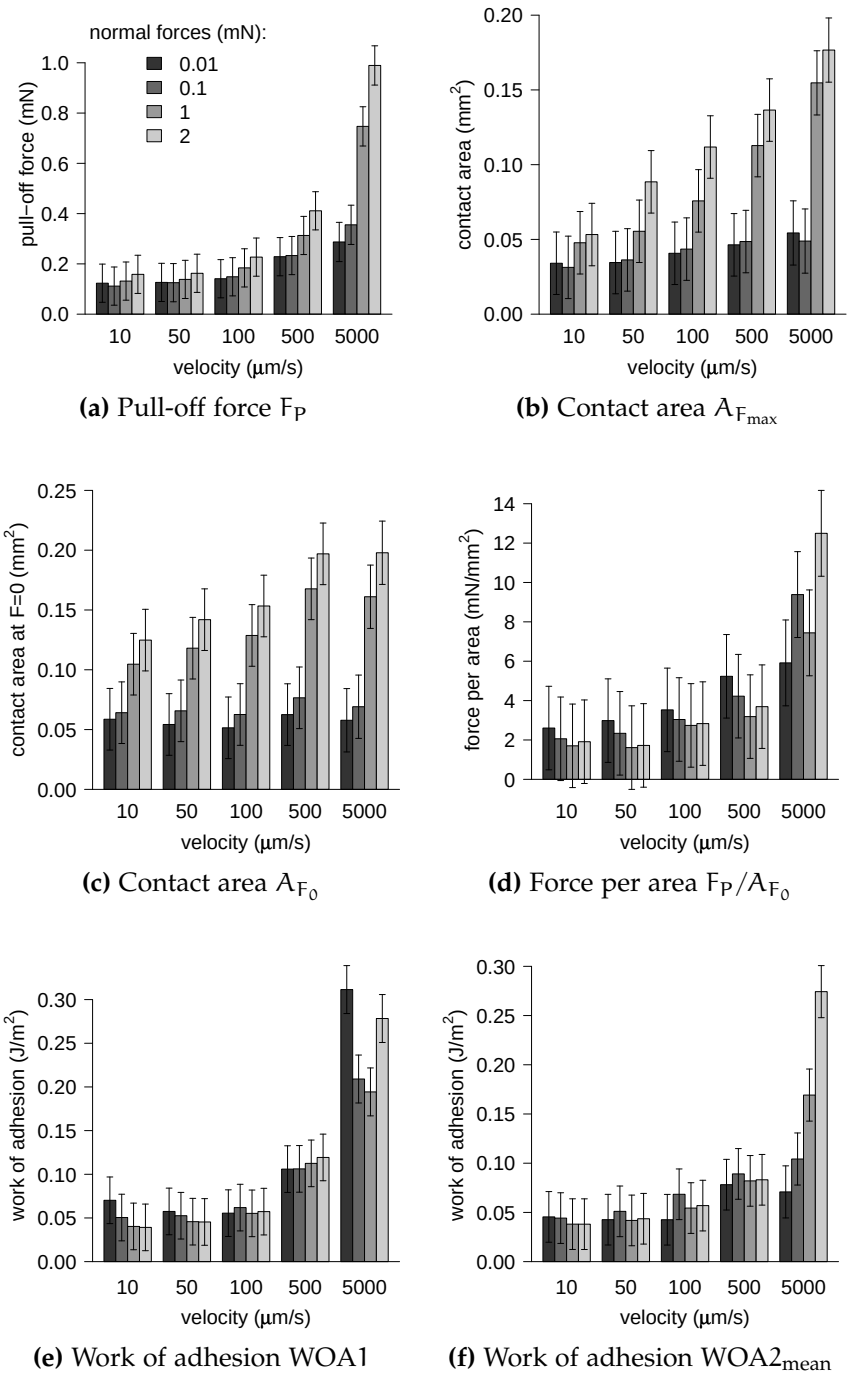

(a) Pull-off force F_P **(b)** Contact area $A_{F_{max}}$

(c) Contact area A_{F_0} **(d)** Force per area F_P/A_{F_0}

(e) Work of adhesion WOA1 **(f)** Work of adhesion $WOA2_{mean}$

Figure 3.13: Results of stick insect's single pad detachment experiments analysing the influence of normal force and velocity on all dependent variables (N = 20). Bars represent means, error bars are least significant differences (LSD).

3.2.2.2 *Scaling of single pad adhesive forces*

Using the data set from the previous section I examined if scaling coefficients were influenced by changes in preload and detachment velocity. Scaling analyses were performed on the relationship between pull-off force F_P and body mass m, contact area at $F_P = 0$ (A_{F_0}) and contact area at F_{max} ($A_{F_{max}}$). As described section 2.8, scaling coefficients were calculated using ordinary least square (OLS) regression as well as standardized major axis (SMA) regression. The measured scaling coefficients β_{OLS} and β_{SMA} were compared to predicted scaling coefficients β_{pred} derived from theoretical models such as contact mechanics models and peeling theory (see section 2.6.2.2 for details).

Ordinary least square regression analysis showed no significant correlation between pull-off force and body mass (Tbl. 3.3, Fig. 3.14). Correlations between pull-off force and contact areas A_{F_0} and $A_{F_{max}}$ were also very weak: Only 3 of 20 (A_{F_0}: Tbl. 3.4, Fig. 3.15) and 7 of 20 ($A_{F_{max}}$: Tbl. 3.5, Fig. 3.16) combinations of preload and velocity were significantly correlated. Almost all OLS regression slopes β_{OLS} were well below any of the slopes predicted from theoretical models.

In contrast, the scaling coefficients of standardized major axis regression analysis were in the predicted range of force scaling with a length or contact area (Tbl. 3.6–Tbl. 3.8, Fig. 3.14–Fig. 3.16). There was no statistical difference in scaling coefficients between velocities or normal forces due to large confidence intervals (all $P > 0.05$, see Tbl. 3.9–Tbl. 3.11). However, scaling of force versus body mass and force versus contact area $A_{F_{max}}$ had a trend of scaling with a length at low and contact area at high velocities (Fig. 3.17a, Fig. 3.17e).

Even though scaling coefficients had a tendency to increase with velocity, this effect was statistically not significant. Preload also had no significant influence on scaling (Fig. 3.17). Although these results do not confirm that rapid detachment increases scaling, they provide some indication that slow detachment scales with length (peeling) whereas rapid detachment scales with area (contact mechanics models).

The variance in data was caused by large differences between individual animals. Furthermore I had difficulties immobilizing very small insects. The weak forces produced by these small animals also resulted in poor signal to noise ratios complicating

Table 3.3: Scaling of stick insect's single adhesive pads pull-off force against body mass m using ordinary least square (OLS) regression (=model I regression). Regression slopes were tested against slopes of $1/3$ (length scaling), $2/3$ (area scaling) and 1 (volume scaling). The table only displays those comparisons with the least difference between predicted slope and measured slope (confidence level: 5 %). β_{OLS}: OLS regression slope, P_{H_0}: P value of regression slope differing from slope 0, R^2: squared correlation coefficient, P_{H_1}: P value of regression slope differing from predicted slope, β_{pred}: predicted regression slope, F_N: normal force, v: velocity (in $\mu m\,s^{-1}$).

m	β_{OLS}	P_{H_0}	R^2	P_{H_1}	β_{pred}
$F_N = 0.01\,mN$					
$v = 10$	0.053	0.693	0.009	0.048	0.33
$v = 50$	0.059	0.578	0.017	0.018	0.33
$v = 100$	0.032	0.800	0.004	0.027	0.33
$v = 500$	0.057	0.729	0.007	0.101	0.33
$v = 5000$	0.139	0.386	0.047	0.231	0.33
$F_N = 0.1\,mN$					
$v = 10$	0.095	0.508	0.025	0.108	0.33
$v = 50$	0.063	0.557	0.019	0.020	0.33
$v = 100$	0.022	0.859	0.002	0.020	0.33
$v = 500$	0.037	0.790	0.004	0.042	0.33
$v = 5000$	0.544	0.043	0.232	0.628	0.67
$F_N = 1\,mN$					
$v = 10$	−0.040	0.796	0.004	0.024	0.33
$v = 50$	−0.051	0.672	0.010	0.005	0.33
$v = 100$	−0.199	0.200	0.089	0.002	0.33
$v = 500$	−0.022	0.904	0.001	0.066	0.33
$v = 5000$	0.131	0.603	0.017	0.425	0.33
$F_N = 2\,mN$					
$v = 10$	−0.270	0.121	0.128	0.002	0.33
$v = 50$	−0.066	0.648	0.012	0.011	0.33
$v = 100$	−0.097	0.577	0.018	0.021	0.33
$v = 500$	0.032	0.873	0.001	0.145	0.33
$v = 5000$	0.191	0.278	0.073	0.413	0.33

analyses. Also the potential difference in pad elasticity between young and old insects might have influenced the results.

Table 3.4: Scaling of stick insect's single adhesive pads pull-off force against contact area A_{F_0} using ordinary least square (OLS) regression (=model I regression). Regression slopes were tested against slopes of 0.5 (length scaling), 1 (area scaling) and 1.5 (volume scaling). The table only displays those comparisons with the least difference between predicted slope and measured slope (confidence level: 5 %). β_{OLS}: OLS regression slope, P_{H_0}: P value of regression slope differing from slope 0, R^2: squared correlation coefficient, P_{H_1}: P value of regression slope differing from predicted slope, β_{pred}: predicted regression slope, F_N: normal force, v: velocity (in $\mu m\,s^{-1}$).

A_{F_0}	β_{OLS}	P_{H_0}	R^2	P_{H_1}	β_{pred}
$F_N = 0.01\,mN$					
$v = 10$	0.417	0.008	0.348	0.556	0.50
$v = 50$	0.243	0.079	0.162	0.065	0.50
$v = 100$	0.310	0.040	0.213	0.192	0.50
$v = 500$	0.152	0.460	0.031	0.101	0.50
$v = 5000$	0.370	0.057	0.208	0.482	0.50
$F_N = 0.1\,mN$					
$v = 10$	0.538	0.001	0.458	0.787	0.50
$v = 50$	0.286	0.051	0.195	0.134	0.50
$v = 100$	0.233	0.153	0.110	0.105	0.50
$v = 500$	0.176	0.318	0.055	0.075	0.50
$v = 5000$	0.444	0.033	0.254	0.774	0.50
$F_N = 1\,mN$					
$v = 10$	0.272	0.131	0.122	0.201	0.50
$v = 50$	0.165	0.242	0.075	0.024	0.50
$v = 100$	−0.084	0.611	0.015	0.002	0.50
$v = 500$	0.145	0.434	0.034	0.065	0.50
$v = 5000$	0.371	0.071	0.190	0.512	0.50
$F_N = 2\,mN$					
$v = 10$	0.140	0.504	0.025	0.097	0.50
$v = 50$	0.192	0.212	0.085	0.053	0.50
$v = 100$	0.085	0.608	0.015	0.020	0.50
$v = 500$	0.212	0.273	0.066	0.140	0.50
$v = 5000$	0.154	0.261	0.078	0.019	0.50

Table 3.5: Scaling of stick insect's single adhesive pads pull-off force against contact area $A_{F_{max}}$ using ordinary least square (OLS) regression (=model I regression). Regression slopes were tested against slopes of 0.5 (length scaling), 1 (area scaling) and 1.5 (volume scaling). The table only displays those comparisons with the least difference between predicted slope and measured slope (confidence level: 5 %). β_{OLS}: OLS regression slope, P_{H_0}: P value of regression slope differing from slope 0, R^2: squared correlation coefficient, P_{H_1}: P value of regression slope differing from predicted slope, β_{pred}: predicted regression slope, F_N: normal force, v: velocity (in $\mu m\,s^{-1}$).

$A_{F_{max}}$	β_{OLS}	P_{H_0}	R^2	P_{H_1}	β_{pred}
$F_N = 0.01\,mN$					
$v = 10$	0.215	0.057	0.197	0.015	0.50
$v = 50$	0.136	0.311	0.057	0.012	0.50
$v = 100$	0.427	0.007	0.336	0.611	0.50
$v = 500$	0.149	0.399	0.040	0.056	0.50
$v = 5000$	0.194	0.303	0.066	0.112	0.50
$F_N = 0.1\,mN$					
$v = 10$	0.281	0.029	0.239	0.080	0.50
$v = 50$	0.371	0.005	0.368	0.274	0.50
$v = 100$	0.347	0.037	0.219	0.336	0.50
$v = 500$	0.190	0.244	0.075	0.064	0.50
$v = 5000$	0.359	0.151	0.125	0.560	0.50
$F_N = 1\,mN$					
$v = 10$	0.258	0.033	0.228	0.044	0.50
$v = 50$	0.297	0.016	0.281	0.087	0.50
$v = 100$	0.200	0.197	0.091	0.059	0.50
$v = 500$	0.214	0.255	0.071	0.134	0.50
$v = 5000$	0.409	0.035	0.250	0.616	0.50
$F_N = 2\,mN$					
$v = 10$	0.248	0.054	0.190	0.052	0.50
$v = 50$	0.215	0.057	0.187	0.015	0.50
$v = 100$	0.196	0.187	0.095	0.047	0.50
$v = 500$	0.319	0.083	0.157	0.314	0.50
$v = 5000$	0.222	0.074	0.186	0.029	0.50

Table 3.6: Scaling of stick insect's single adhesive pads pull-off force against body mass m using standardized major axis (SMA) regression (=model II regression). Regression slopes were tested against slopes of $1/3$ (length scaling), $2/3$ (area scaling) and 1 (volume scaling). The table only displays those comparisons with the least difference between predicted slope and measured slope. Opposite signs in β_{SMA} and β_{pred} result in undefined P values. β_{SMA}: SMA regression slope, $CI_{lower/upper}$: lower and upper confidence intervals (confidence level: 5 %), P: P value of regression slope differing from predicted slope, β_{pred}: predicted regression slope, F_N: normal force, v: velocity (in $\mu m\,s^{-1}$).

m	β_{SMA}	CI_{lower}	CI_{upper}	P	β_{pred}
$F_N = 0.01\,mN$					
$v = 10$	0.546	0.335	0.890	0.416	0.67
$v = 50$	0.450	0.280	0.722	0.210	0.33
$v = 100$	0.533	0.331	0.858	0.349	0.67
$v = 500$	0.683	0.424	1.098	0.920	0.67
$v = 5000$	0.639	0.389	1.050	0.865	0.67
$F_N = 0.1\,mN$					
$v = 10$	0.605	0.377	0.969	0.680	0.67
$v = 50$	0.455	0.284	0.730	0.193	0.33
$v = 100$	0.520	0.323	0.837	0.300	0.67
$v = 500$	0.578	0.359	0.930	0.548	0.67
$v = 5000$	1.131	0.721	1.772	0.582	1.00
$F_N = 1\,mN$					
$v = 10$	−0.643	−0.399	−1.035		0.67
$v = 50$	−0.509	−0.317	−0.819		0.67
$v = 100$	−0.666	−0.422	−1.051		0.67
$v = 500$	−0.772	−0.479	−1.244		0.67
$v = 5000$	0.997	0.602	1.650	0.991	1.00
$F_N = 2\,mN$					
$v = 10$	−0.753	−0.481	−1.177		0.67
$v = 50$	−0.604	−0.376	−0.970		0.67
$v = 100$	−0.728	−0.454	−1.169		0.67
$v = 500$	0.839	0.521	1.351	0.464	1.00
$v = 5000$	0.705	0.432	1.152	0.818	0.67

Table 3.7: Scaling of stick insect's single adhesive pads pull-off force against contact area A_{F_0} using standardized major axis (SMA) regression (=model II regression). Regression slopes were tested against slopes of 0.5 (length scaling), 1 (area scaling) and 1.5 (volume scaling). The table only displays those comparisons with the least difference between predicted slope and measured slope. Opposite signs in β_{SMA} and β_{pred} result in undefined P values. β_{SMA}: SMA regression slope, $CI_{lower/upper}$: lower and upper confidence intervals (confidence level: 5 %), P: P value of regression slope differing from predicted slope, β_{pred}: predicted regression slope, F_N: normal force, v: velocity (in $\mu m\,s^{-1}$).

A_{F_0}	β_{SMA}	CI_{lower}	CI_{upper}	P	β_{pred}
$F_N = 0.01\,mN$					
$v = 10$	0.707	0.473	1.057	0.089	0.50
$v = 50$	0.606	0.390	0.939	0.384	0.50
$v = 100$	0.671	0.438	1.027	0.171	0.50
$v = 500$	0.868	0.542	1.389	0.548	1.00
$v = 5000$	0.811	0.514	1.279	0.357	1.00
$F_N = 0.1\,mN$					
$v = 10$	0.795	0.556	1.136	0.199	1.00
$v = 50$	0.646	0.420	0.995	0.235	0.50
$v = 100$	0.703	0.447	1.104	0.136	0.50
$v = 500$	0.748	0.470	1.189	0.214	1.00
$v = 5000$	0.882	0.567	1.375	0.570	1.00
$F_N = 1\,mN$					
$v = 10$	0.779	0.497	1.220	0.267	1.00
$v = 50$	0.601	0.380	0.952	0.424	0.50
$v = 100$	−0.696	−0.433	−1.118		0.50
$v = 500$	0.781	0.488	1.248	0.295	1.00
$v = 5000$	0.852	0.538	1.350	0.485	1.00
$F_N = 2\,mN$					
$v = 10$	0.884	0.552	1.416	0.602	1.00
$v = 50$	0.658	0.417	1.040	0.232	0.50
$v = 100$	0.696	0.433	1.117	0.168	0.50
$v = 500$	0.821	0.517	1.302	0.394	1.00
$v = 5000$	0.550	0.337	0.897	0.695	0.50

Table 3.8: Scaling of stick insect's single adhesive pads pull-off force against contact area $A_{F_{max}}$ using standardized major axis (SMA) regression (=model II regression). Regression slopes were tested against slopes of 0.5 (length scaling), 1 (area scaling) and 1.5 (volume scaling). The table only displays those comparisons with the least difference between predicted slope and measured slope. Opposite signs in β_{SMA} and β_{pred} result in undefined P values. β_{SMA}: SMA regression slope, $CI_{lower/upper}$: lower and upper confidence intervals (confidence level: 5 %), P: P value of regression slope differing from predicted slope, β_{pred}: predicted regression slope, F_N: normal force, v: velocity (in $\mu m\,s^{-1}$).

$A_{F_{max}}$	β_{SMA}	CI_{lower}	CI_{upper}	P	β_{pred}
$F_N = 0.01\,mN$					
$v = 10$	0.485	0.311	0.756	0.889	0.50
$v = 50$	0.568	0.357	0.904	0.582	0.50
$v = 100$	0.736	0.497	1.091	0.123	1.00
$v = 500$	0.745	0.467	1.190	0.213	1.00
$v = 5000$	0.753	0.460	1.232	0.252	1.00
$F_N = 0.1\,mN$					
$v = 10$	0.574	0.378	0.874	0.507	0.50
$v = 50$	0.611	0.416	0.897	0.295	0.50
$v = 100$	0.742	0.485	1.134	0.163	1.00
$v = 500$	0.694	0.438	1.100	0.158	0.50
$v = 5000$	1.016	0.630	1.637	0.948	1.00
$F_N = 1\,mN$					
$v = 10$	0.539	0.353	0.823	0.719	0.50
$v = 50$	0.561	0.373	0.844	0.572	0.50
$v = 100$	0.663	0.420	1.046	0.219	0.50
$v = 500$	0.801	0.506	1.270	0.339	1.00
$v = 5000$	0.819	0.525	1.277	0.366	1.00
$F_N = 2\,mN$					
$v = 10$	0.569	0.370	0.877	0.547	0.50
$v = 50$	0.498	0.323	0.767	0.983	0.50
$v = 100$	0.636	0.403	1.002	0.294	0.50
$v = 500$	0.805	0.518	1.250	0.326	1.00
$v = 5000$	0.515	0.325	0.817	0.898	0.50

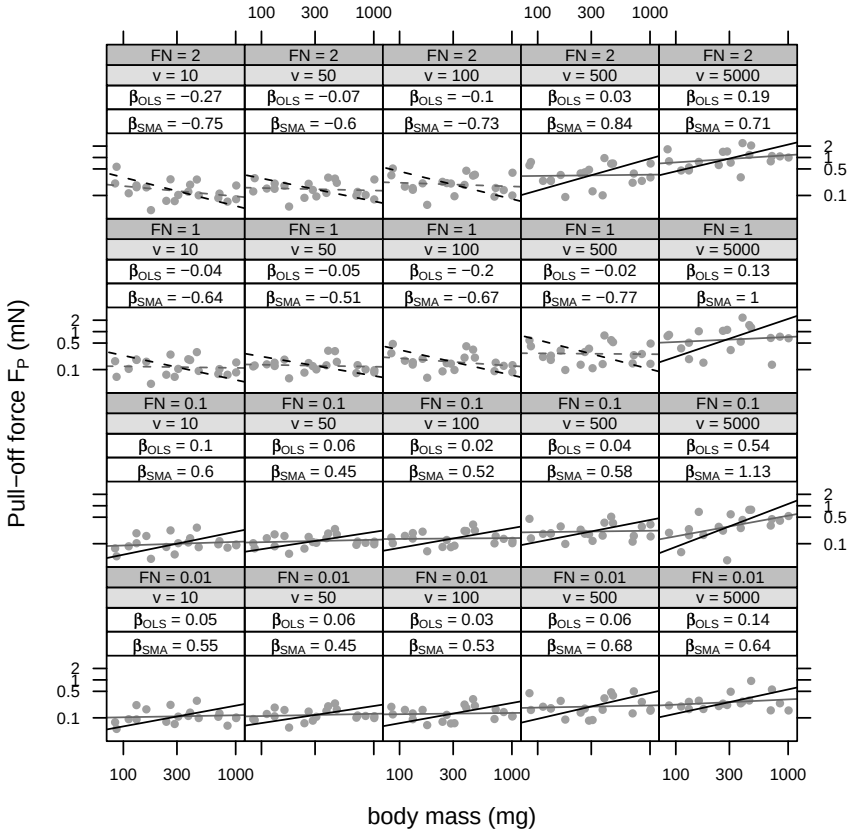

Figure 3.14: Scaling of stick insect's single leg pull-off forces F_P plotted against body mass. Each subplot shows one combination of velocity v (in $\mu m\,s^{-1}$) and normal force F_N (in mN). Gray and black lines depict OLS regressions β_{OLS} (=model I) and SMA regressions β_{SMA} (=model II), respectively. Dashed lines indicate negative slopes ($N = 20$; see Tbl. 3.3 and Tbl. 3.6 for detailed statistics).

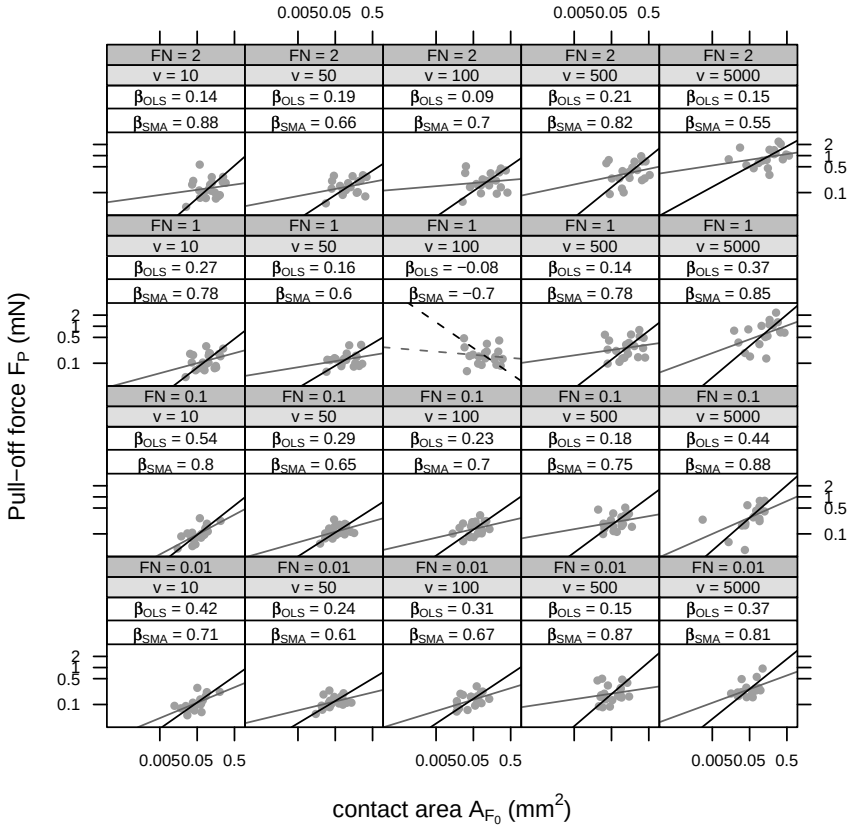

Figure 3.15: Scaling of stick insect's single leg pull-off forces F_P plotted against contact area A_{F_0}. Each subplot shows one combination of velocity v (in $\mu m\,s^{-1}$) and normal force F_N (in mN). Gray and black lines depict OLS regressions β_{OLS} (=model I) and SMA regressions β_{SMA} (=model II), respectively. Dashed lines indicate negative slopes ($N = 20$; see Tbl. 3.4 and Tbl. 3.7 for detailed statistics).

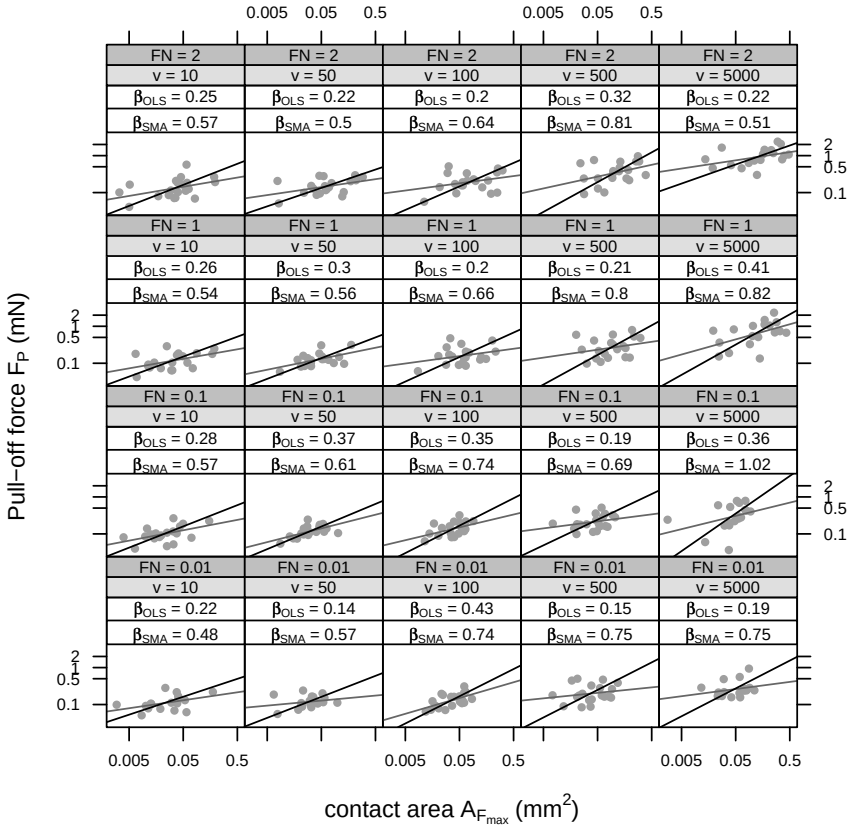

Figure 3.16: Scaling of stick insect's single leg pull-off forces F_P plotted against contact area $A_{F_{max}}$. Each subplot shows one combination of velocity v (in $\mu m\,s^{-1}$) and normal force F_N (in mN). Gray and black lines depict OLS regressions β_{OLS} (=model I) and SMA regressions β_{SMA} (=model II), respectively. Dashed lines indicate negative slopes ($N = 20$; see Tbl. 3.5 and Tbl. 3.8 for detailed statistics).

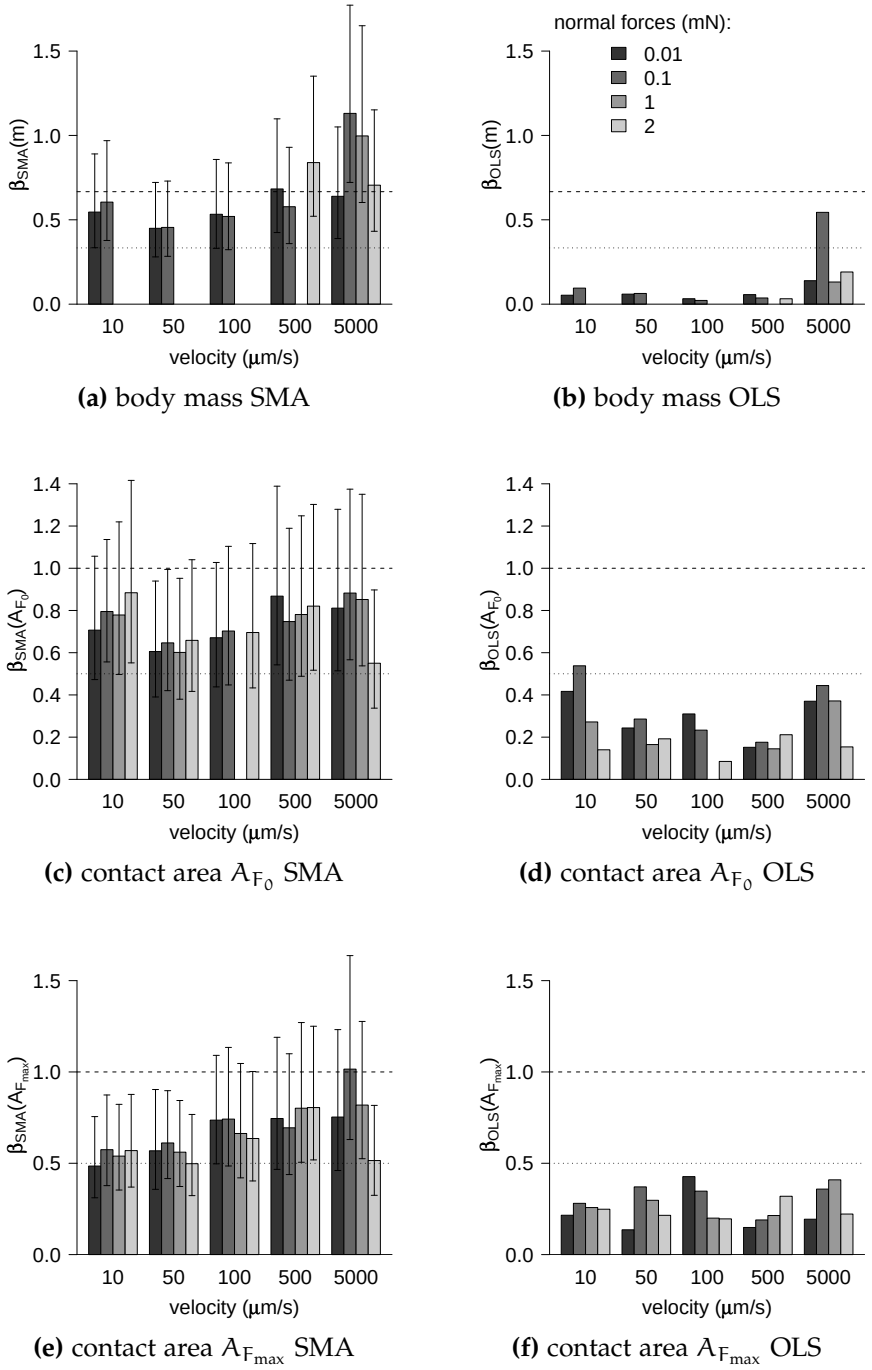

(a) body mass SMA

(b) body mass OLS

(c) contact area A_{F_0} SMA

(d) contact area A_{F_0} OLS

(e) contact area $A_{F_{max}}$ SMA

(f) contact area $A_{F_{max}}$ OLS

Figure 3.17: Summary of stick insect's single leg scaling coefficients using OLS (=model I) and SMA (=model II) regressions (N = 20). Scaling coefficients β_{SMA} are shown on the left side and β_{OLS} are shown on the right side. Negative slopes are excluded. Error bars in SMA regressions indicate lower and upper confidence intervals. Dotted and dashed lines indicate theoretical scaling coefficients of length and area scaling, respectively.

Table 3.9: Warton's test for common slope $\hat{\beta}_{SMA}$ between different velocities v during stick insect single leg measurements using standard major axis (SMA) regression. Scaling coefficients (β_{SMA}) represent SMA slopes derived from pull-off force F_P vs. body mass m after log transformation. F_N: normal force, $CI_{lower/upper}$: lower and upper confidence intervals, P: P-value of Warton's common slope test. Note that no common slope $\hat{\beta}_{SMA}$ is calculated with Warton's SMA method if there is a difference in signs.

F_P vs. m	velocity v ($\mu m\,s^{-1}$)						
	10	50	100	500	5000	$\hat{\beta}_{SMA}$	P
$F_N = 0.01\,mN$							
β_{SMA}	0.55	0.45	0.53	0.68	0.64	0.56	0.76
CI_{lower}	0.33	0.28	0.33	0.42	0.39	0.45	
CI_{upper}	0.89	0.72	0.86	1.10	1.05	0.70	
$F_N = 0.1\,mN$							
β_{SMA}	0.60	0.45	0.52	0.58	1.13	0.62	0.06
CI_{lower}	0.38	0.28	0.32	0.36	0.72	0.50	
CI_{upper}	0.97	0.73	0.84	0.93	1.77	0.77	
$F_N = 1\,mN$							
β_{SMA}	−0.64	−0.51	−0.67	−0.77	1.00		
CI_{lower}	−0.40	−0.32	−0.42	−0.48	0.60		
CI_{upper}	−1.04	−0.82	−1.05	−1.24	1.65		
$F_N = 2\,mN$							
β_{SMA}	−0.75	−0.60	−0.73	0.84	0.71		
CI_{lower}	−0.48	−0.38	−0.45	0.52	0.43		
CI_{upper}	−1.18	−0.97	−1.17	1.35	1.15		

Table 3.10: Warton's test for common slope $\hat{\beta}_{SMA}$ between different velocities v during stick insect single leg measurements using standard major axis (SMA) regression. Scaling coefficients (β_{SMA}) represent SMA slopes derived from pull-off force F_P vs. contact area A_{F_0} after log transformation. F_N: normal force, $CI_{lower/upper}$: lower and upper confidence intervals, P: P-value of Warton's common slope test. Note that no common slope $\hat{\beta}_{SMA}$ is calculated with Warton's SMA method if there is a difference in signs.

F_P vs. A_{F_0}	velocity v ($\mu m\,s^{-1}$)						
	10	50	100	500	5000	$\hat{\beta}_{SMA}$	P
$F_N = 0.01\,mN$							
β_{SMA}	0.71	0.61	0.67	0.87	0.81	0.72	0.80
CI_{lower}	0.47	0.39	0.44	0.54	0.51	0.59	
CI_{upper}	1.06	0.94	1.03	1.39	1.28	0.87	
$F_N = 0.1\,mN$							
β_{SMA}	0.80	0.65	0.70	0.75	0.88	0.75	0.88
CI_{lower}	0.56	0.42	0.45	0.47	0.57	0.63	
CI_{upper}	1.14	0.99	1.10	1.19	1.37	0.91	
$F_N = 1\,mN$							
β_{SMA}	0.78	0.60	−0.70	0.78	0.85		
CI_{lower}	0.50	0.38	−0.43	0.49	0.54		
CI_{upper}	1.22	0.95	−1.12	1.25	1.35		
$F_N = 2\,mN$							
β_{SMA}	0.88	0.66	0.70	0.82	0.55	0.71	0.66
CI_{lower}	0.55	0.42	0.43	0.52	0.34	0.58	
CI_{upper}	1.42	1.04	1.12	1.30	0.90	0.88	

Table 3.11: Warton's test for common slope $\hat{\beta}_{SMA}$ between different velocities v during stick insect single leg measurements using standard major axis (SMA) regression. Scaling coefficients (β_{SMA}) represent SMA slopes derived from pull-off force F_P vs. contact area $A_{F_{max}}$ after log transformation. F_N: normal force, $CI_{lower/upper}$: lower and upper confidence intervals, P: P-value of Warton's common slope test.

F_P vs. $A_{F_{max}}$	velocity v ($\mu m\,s^{-1}$)						
	10	50	100	500	5000	$\hat{\beta}_{SMA}$	P
$F_N = 0.01\,mN$							
β_{SMA}	0.48	0.57	0.74	0.75	0.75	0.65	0.53
CI_{lower}	0.31	0.36	0.50	0.47	0.46	0.53	
CI_{upper}	0.76	0.90	1.09	1.19	1.23	0.79	
$F_N = 0.1\,mN$							
β_{SMA}	0.57	0.61	0.74	0.69	1.02	0.70	0.43
CI_{lower}	0.38	0.42	0.49	0.44	0.63	0.57	
CI_{upper}	0.87	0.90	1.13	1.10	1.64	0.84	
$F_N = 1\,mN$							
β_{SMA}	0.54	0.56	0.66	0.80	0.82	0.66	0.52
CI_{lower}	0.35	0.37	0.42	0.51	0.53	0.54	
CI_{upper}	0.82	0.84	1.05	1.27	1.28	0.80	
$F_N = 2\,mN$							
β_{SMA}	0.57	0.50	0.64	0.81	0.51	0.59	0.55
CI_{lower}	0.37	0.32	0.40	0.52	0.32	0.49	
CI_{upper}	0.88	0.77	1.00	1.25	0.82	0.73	

3.2.2.3 *Scaling of whole body adhesive forces (centrifuge measurements)*

To analyse the detachment of unrestrained stick insect, whole body scaling coefficients were acquired by measuring forces of stick insects detaching from an accelerating centrifuge as described in section 2.7. Scaling coefficients were derived from pull-off force against body mass, contact area and body length, respectively. Whole body forces scaled with contact area.

Tbl. 3.12 summarizes the results by comparing predicted slopes β_{pred} with the measured slopes β_{SMA}. Fig. 3.18a–Fig. 3.18c show results of ordinary least square (OLS = model I) and standardized major axis regression (SMA = model II) for force versus body length, contact area and body mass, respectively. Stick insects' whole body adhesive forces clearly scale with their pad's contact area ($P > 0.1$). Similar results have been acquired by

Table 3.12: Comparison of SMA regression slopes (β_{SMA}) with predicted slopes (β_{pred}) for centrifuge data set. All P-values are Bonferroni corrected. P_{sig} show P-values at common α-levels. n.s.: No significant difference between measured slope and predicted slope. There is no difference in P-values at the α-level of 5 %, no matter if Bonferroni's correction is applied or not. Therefore the displayed table values can be considered as statistically conservative. Forces scale with contact area. Furthermore contact area A scales isometrically with body length L.

	β_{pred}	β_{SMA}	P	P_{sig}
F_P vs. L ($N = 26$)				
$\propto L$	1	1.789	$7.35e-05$	< 0.0001
$\propto A$	2	1.789	1	> 0.05 (n.s.)
$\propto V$	3	1.789	0.0003384	< 0.001
F_P vs. A ($N = 24$)				
$\propto L$	0.5	0.933	0.0002721	< 0.001
$\propto A$	1	0.933	1	> 0.05 (n.s.)
$\propto V$	1.5	0.933	0.0052103	< 0.01
F_P vs. m ($N = 26$)				
$\propto L$	0.33	0.702	$4e-07$	< 0.0001
$\propto A$	0.67	0.702	1	> 0.05 (n.s.)
$\propto V$	1	0.702	0.0064212	< 0.01
A vs. L ($N = 24$)				
	3	1.917	$1.5e-06$	< 0.0001
	2	1.917	1	> 0.05 (n.s.)
	1	1.917	0	< 0.0001
m vs. L ($N = 26$)				
	3	2.547	0.0334584	< 0.05
	2	2.547	0.0014565	< 0.01
	1	2.547	0	< 0.0001

Barnes (2007) for tree frogs (scaling coefficient of adhesive force against contact area: 1.14).

The scaling coefficient of stick insect contact area versus body length was 1.97 (Fig. 3.18d). This value did not differ significantly from the predicted allometric growth scaling factor of $\beta_{pred} = 2$ ($P > 0.05$; see A vs. L in Tbl. 3.12). In contrast, the measured scaling coefficient of body mass versus body length ($\beta_{SMA} = 2.5$) was less then the predicted allometric growth coefficient $\beta_{pred} = 3$ and differed significantly from it ($P < 0.01$; see m vs. L in Tbl. 3.12 and Fig. 3.18e). This means that adult stick insects were significantly lighter for their length then would be expected from allometric growth. Similar results have been

obtained for mature frogs in a study by Smith et al. (2006b): Scaling coefficients ranged from 2.5 to approximately 2.8.

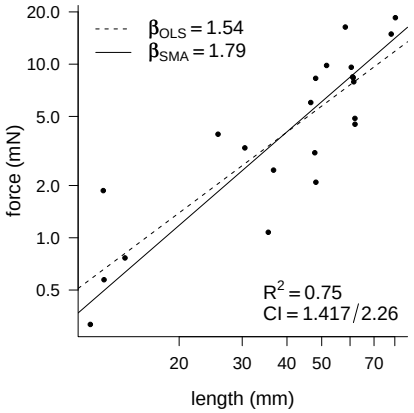

(a) Force versus body length

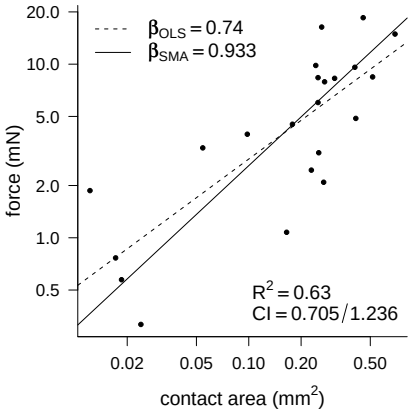

(b) Force versus contact area

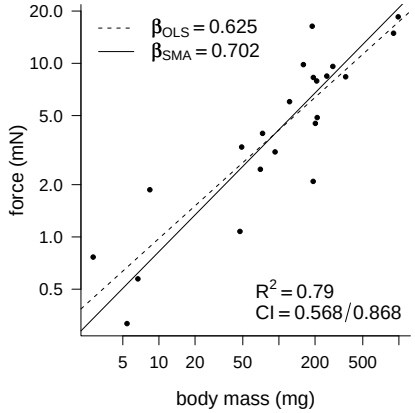

(c) Force versus body mass

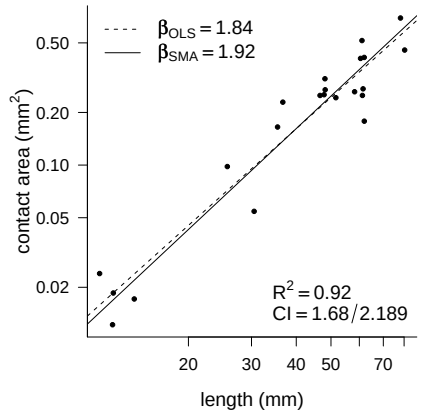

(d) Contact area versus body length

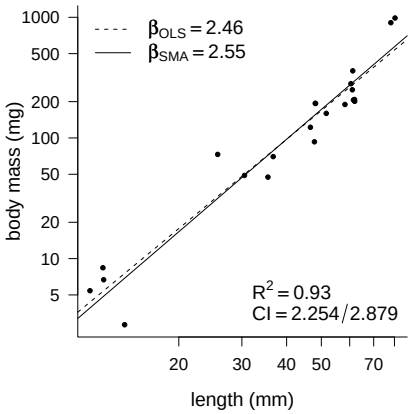

(e) Body mass versus body length

Figure 3.18: Scaling results of stick insect whole body measurements (centrifuge technique). (a)–(c): Regression slopes of force versus body length (a), contact area (b) and body mass (c). (d) and (e): Contact area and body mass versus body length. Dashed and solid lines depict ordinary least square regression slopes β_{OLS} (= model I) and standardized major axis regression slopes β_{SMA} (= model II), respectively. All P values of $\beta_{OLS} < 0.0001$, R: correlation coefficient, CI: lower and upper confidence intervals of SMA regression.

3.2.2.4 *Comparison of single pad forces and whole body forces*

To test whether the detachment mode of stick insects differs between single leg and whole body measurements, the scaling coefficients of the previous two sections were compared with each other. Contrary to expectations, Warton's test for common slopes amongst several allometric regressions (Warton and Weber, 2002) revealed no significant difference between single leg and whole body measurements.

Comparing the scaling coefficients of single leg and whole body measurements was analysed using the single leg data at normal force 0.1 mN derived from pull-off force over body mass and contact area $A_{F_{max}}$ showed no statistical difference between the two (F_P vs. m: common scaling coefficient $\hat{\beta}_{SMA} = 0.76$, $P > 0.05$; F_P vs. $A_{F_{max}}$: common scaling coefficient $\hat{\beta}_{SMA} = 0.9$, $P > 0.05$; see Tbl. 3.13 for details).

Table 3.13: Warton's test for common slopes between stick insect single leg at normal force $F_N = 0.1\,mN$ and whole body measurements using SMA regression of pull-off force against body mass and contact area. Since there was no significant difference between velocities (see Tbl. 3.9–Tbl. 3.11) they were pooled for comparison with whole body measurements. There was no significant difference between single leg and whole body scaling coefficients (F_P vs. m: $P = 0.24$, F_P vs. $A_{F_{max}}$: $P = 0.74$). β_{SMA}: SMA regression slope after pooling, $CI_{lower/upper}$: lower and upper confidence intervals. Note that the single leg scaling coefficients differ from the previous calculations in Tbl. 3.9 and Tbl. 3.11 as data was pooled, therefore ignoring differences in the elevation of slopes.

$F_N = 0.1\,mN$	single leg	whole body	common slope	P
F_P vs. m				
β_{SMA}	0.833	0.702	0.764	0.241
CI_{lower}	0.683	0.568	0.665	
CI_{upper}	1.016	0.868	0.892	
F_P vs. $A_{F_{max}}$				
β_{SMA}	0.884	0.933	0.900	0.743
CI_{lower}	0.739	0.705	0.773	
CI_{upper}	1.057	1.236	1.043	

3.3 FRICTION FORCE MEASUREMENTS IN TREE FROGS

To analyse friction forces in tree frogs, sliding movements were performed on a smooth surface (see section 2.5.7 for details) to

estimate the fluid film height as well as static friction. Similar to the results obtained for stick insects, shear stress measurements on single *L. caerulea* toe pads demonstrated that pads generate static friction. Static friction was not only evident from the build-up of force at the onset of sliding (Fig. 3.19, median shear stress 1.08 kPa) but also from the presence of a remaining shear force 2 min after the sliding motion had stopped (Fig. 3.19, median shear stress 1.12 kPa; see Tbl. 3.14).

As extremely slow sliding could be misinterpreted as 'static' contact, I measured the amount of pad sliding during the 2 min after the motor had stopped and performed regression analyses of pad position. The amount of pad sliding was measured at 12 points at 10 s intervals.

To estimate the fluid film height d, the velocity v at the end of the experiment was calculated assuming hydrodynamic lubrication: $d = \eta v/\sigma$ (η: dynamic viscosity, σ: pressure). Pad velocity of the distance L travelled after the motor had stopped was derived after fitting the data. The fitting was done exponentially because

- the force implied on the toe pad was proportional to its displacement ($F \propto L$) and
- the sliding velocity was nearly proportional to force ($v = dL/dt \propto F$).

The data was analysed using a non-linear exponential model ($L(t) = a - b \cdot e^{-c \cdot t}$), with b corresponding to the respective intercept. By replacing force F with $-bL(t)$ this resulted in

$$v = \frac{dL}{dt} = -b \cdot L(t) \tag{3.1}$$

$L(t)$ can be expressed as follows for linear and non-linear exponential regression analyses:

$$L(t) = a - b \cdot e^{-c \cdot t} \tag{3.2}$$

Deriving this equation by time t results in

$$v = \frac{dL}{dt} = b \cdot c \cdot e^{-c \cdot t}. \tag{3.3}$$

Using the dynamic viscosity of water ($\eta = 10^{-3}\,\mathrm{Pa\,s}$) and a pressure of $\sigma = 1.12\,\mathrm{kPa}$ this results in

$$d = \frac{v \cdot \eta}{\sigma} \tag{3.4}$$

$$= \frac{v \cdot 10^{-3}\,\mathrm{Pa\,s}}{1.12\,\mathrm{kPa}} \tag{3.5}$$

These analyses indicated that, if the pads had indeed still been sliding after 2 min, the mean remaining sliding velocity was less than $12\,\mathrm{nm\,s^{-1}}$.

Assuming a continuous mucus film of thickness d to be present in the entire pad contact zone, the film thickness predicted from simple hydrodynamic lubrication ($d = \eta v/\sigma \approx 1.5 \cdot 10^{-4}\,\mathrm{nm}$; η: dynamic viscosity, v: velocity, σ: pressure) is much less than a single molecular layer of water. An analogous calculation for pads sliding at $500\,\mu\mathrm{m\,s^{-1}}$ velocity yields film thicknesses in the order of 1–2 water layers ($d = \eta v/\sigma \approx 0.4\,\mathrm{nm}$).

These results indicate that tree frogs are able to bring their pads into very close contact with the surface. The friction in tree frogs is therefore not primarily caused by the viscosity and surface tension of the mucus film, but from boundary friction of the toe pad epidermis on the substrate (Persson, 1998).

Table 3.14: Descriptive statistics of friction experiments in tree frogs *Litoria caerulea* during 'onset' of movement, 'sliding', and two minutes after movement had ended ('remaining'). F_F: friction force, A: contact area, F/A: shear stress.

	N_{total}	onset N = 30	sliding N = 30	remaining N = 30
F_F (mN)	87	1.5 **2.9** 6.0	7.5 **10.0** 12.5	2.3 **4.6** 8.1
A (mm^2)	87	1.4 **2.8** 4.8	3.7 **5.0** 5.9	4.3 **5.1** 6.7
F_F/A (kPa)	87	0.81 **1.08** 1.62	1.42 **2.12** 3.10	0.54 **1.12** 1.36

a **b** c represent the lower quartile a, the median b, and the upper quartile c for continuous variables.
N is the number of non–missing values.

3.3.1 *Possible contribution of surface tension forces to shear stress in tree frogs*

It is possible that surface tension forces of the mucus film contribute to static and dynamic shear forces. When the toe pad

slides across the surface, the fluid meniscus will be deformed so that the contact angle with the substrate may become larger at the leading and smaller at the trailing edge. The retentive force acting on a thread of fluid moving through a tube is (West, 1911):

$$F = 2\pi r \gamma_L (\cos \alpha_2 - \cos \alpha_1) \tag{3.6}$$

where $2\pi r$ is the inner perimeter of the tube, γ_L the fluid's surface tension and α_1, α_2 are the advancing and receding contact angles, respectively. For simplicity, I modeled the contact area as a square (side length B) and assumed the contact angle deformation to be constant over the leading and trailing edges of the pad contact zone. The static shear force for one pad due to surface tension was:

$$F = 2B\gamma_L (\cos \alpha_1 - \cos \alpha_2) \ll 4B\gamma_L \tag{3.7}$$

Estimating B as $2 \cdot (\text{contact area}/\pi)^{0.5} \approx 2.6\,\text{mm}$ and the surface tension of mucus ($70\,\text{mN}\,\text{m}^{-1}$), I obtained:

$$F \ll 4B\gamma_L \approx 0.73\,\text{mN} \tag{3.8}$$

With a pad contact area of $5.3 \pm 1.8\,\text{mm}^2$ (mean $\pm$ s.d.) this maximal estimate corresponded to a static shear stress of 0.14 kPa, which is considerably less than the measured static shear stress (Fig. 3.19b). Thus, the presence of static shear stress in frog toe pads cannot be explained by surface tension forces alone.

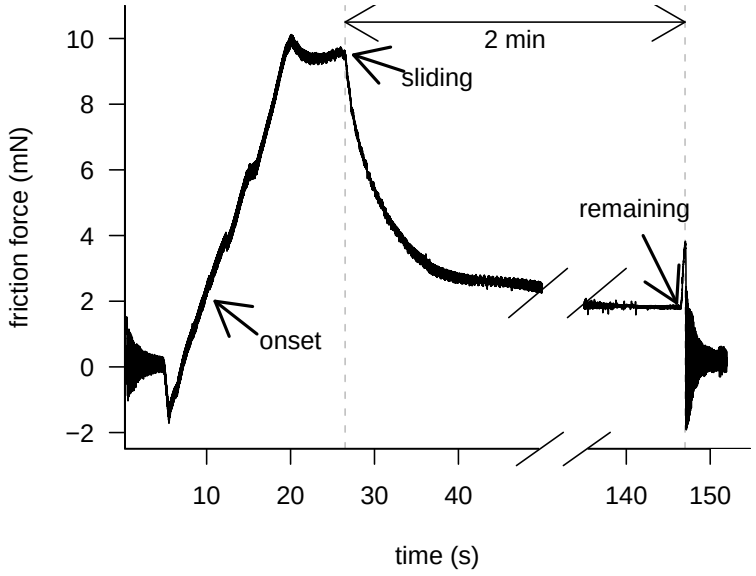

(a) Example of friction force measurement.

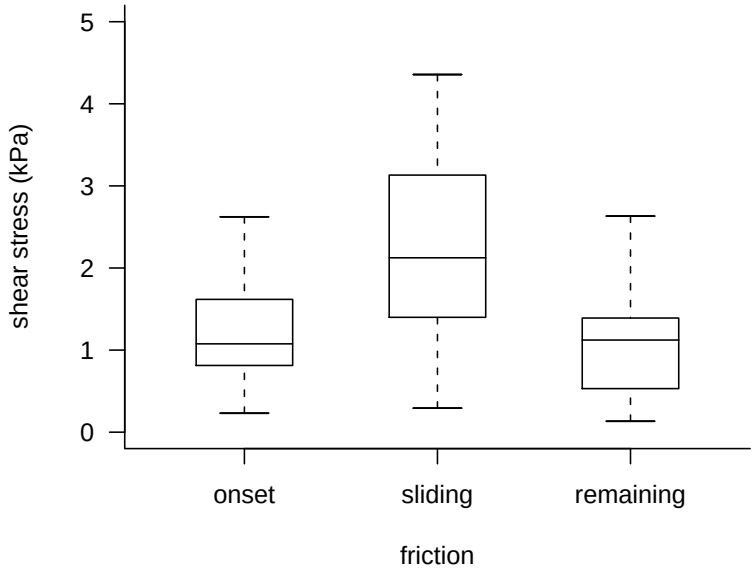

(b) Summary of shear stress measurements.

Figure 3.19: Shear stress measurement in single toe pads of *Litoria caerulea*. (a): Friction force during a sliding experiment consisting of 20 s sliding toward the body (500 µm s^{-1}) followed by 2 min standstill. (b): Toe pad shear stress at the transition from rest to sliding ('onset'), during steady sliding ('sliding') and 2 min after the end of the motor movement ('remaining'). Data from 10 toe pads of three frogs (N = 27, 3 missing values). See Tbl. 3.14 for descriptive statistic details.

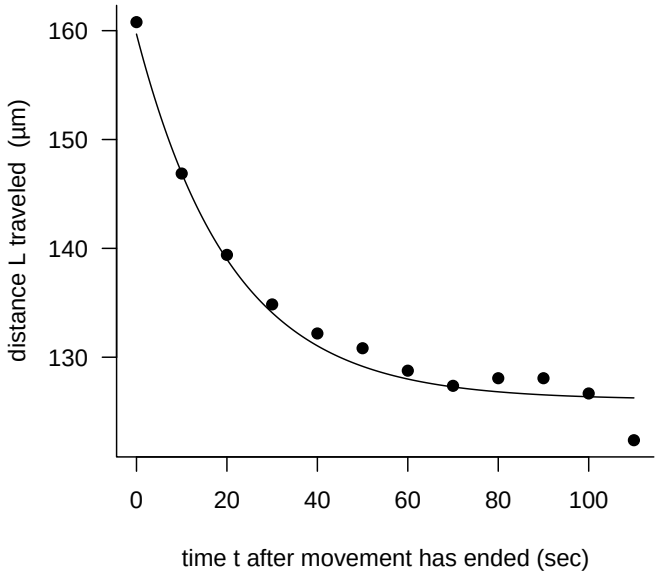

Figure 3.20: Example data set to estimate fluid height between frog toe pad and substratum using non-linear regressions. Data points depict the distance the frog toe pad travelled during 2 min after the motor had stopped. Non-linear least-square regression calculated using $L = a - be^{-ct}$ (solid line): $a = 126.09$, $b = 33.597$, $c = 0.048$. Calculated velocity $v = 0.008\,\mu m\,s^{-1}$ and fluid film height $d = 7.332 \cdot 10^{-6}$ nm.

4

DISCUSSION

4.1 FRICTIONAL ANISOTROPY

Many insects combine fast running performance with strong resistance to detachment forces. This capacity requires an effective control of attachment and detachment forces of the adhesive system. As described earlier, this control can be achieved at different hierarchical levels (see section 1.2.1 on page 12). An attachment device which is dependent on movement direction could facilitate this behaviour. It has been shown in unrestrained ants and flies that they can detach more easily when twisting or rolling their adhesive pads (Federle et al., 2002; Niederegger and Gorb, 2003; Federle and Endlein, 2004). Similar to a study in bush crickets by Gorb and Scherge (2000), this study confirmed a strong direction dependence of friction when comparing proximal to distal movements. Sliding the unrestrained stick insect's pretarsus ("footloose" condition) in distal direction regularly resulted in detachment of the pad. In other words: Attachment force was only present when sliding the pad towards the body.

There are two possible explanations for this behaviour. Either (i) shear stress is increased in proximal direction or (ii) the area of contact is increased in proximal direction. To examine which of these hypotheses is true, the sliding of "immobilized" arolia was analysed. This resulted in higher shear stress values in *distal* direction (Fig. 3.2c), clearly disproving the first hypothesis.

In contrast to findings by Gorb and Scherge (2000), I could not confirm any anisotropy in friction forces in "immobilized" arolia (Fig. 3.2a). The frictional anisotropy of "immobilized" arolia in form of shear stress resulted mainly from changes in contact area, which was larger in the proximal direction (Fig. 3.2b).

As the pretarsus of the stick insect is composed of multiple joints it will buckle under compression and the ground angle will be smaller in proximal than in distal direction (even with the direction of the force vector reversing its direction). If the

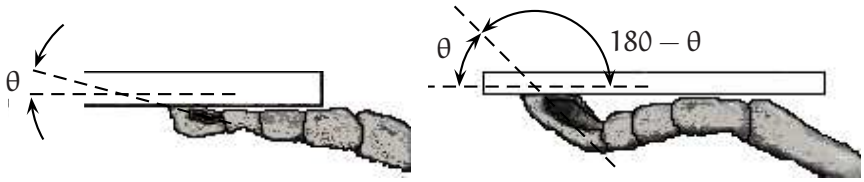

(a) proximal **(b)** distal

Figure 4.1: "Footloose" arolium moving (a) in proximal and (b) distal directions on a glass surface. The angle θ between the pretarsus and the surface is larger in the distal than in the proximal direction, which, according to peeling theory, reduces attachment forces in the distal direction. This still holds true when the pad detaches distally by means of buckling (see angle $180 - \theta$).

pad detaches by way of peeling, a large contact angle will ease detachment (Kendall, 1971). This was confirmed by the "footloose" experiments (see Fig. 3.3d and Fig. 4.1), supporting previous research that insects can detach their adhesive organs by rolling (Niederegger and Gorb, 2003) or peeling (Federle et al., 2002; Federle and Endlein, 2004).

Preliminary observations of "footloose" insect friction forces indicated the ability to produce friction even in distal direction by using attachment organs located on the pretarsal segments (i. e. euplantulae). Further research on the usage of arolium and euplantula for frictional anisotropy are needed.

Even though no anisotropy in friction force was present in the immobilized condition a large contact area in proximal direction is still beneficial for many adhesion processes, as will be discussed in the following two sections.

4.2 ROLE OF PAD SECRETION

4.2.1 *Role of pad secretion for attachment to smooth and rough substrates*

This study on the biomechanics of smooth adhesive organs in stick insects demonstrates the role of the tarsal fluid secretion for adhesion and friction. Previous studies on insects suggested that the pad fluid generally enhances adhesion (Edwards and Tarkanian, 1970; Dixon et al., 1990). However, the presented data show that both friction and adhesion of insect pads on

smooth glass are greater when *less* secretion is present (see Fig. 3.4). This behavior is consistent with physical models of fluid-based adhesion and lubrication (Israelachvili, 1992b; Francis and Horn, 2001; Bhushan, 2003; Piau et al., 2005). A thinner fluid film between the pad and the surface not only results in more strongly curved menisci and thus more negative Laplace pressures but it will also increase forces due to viscosity. If adhesion and friction are enhanced for smaller amounts of pad secretion, however, the question arises as to why insects don't conserve energy resources and simply secrete less or even no fluid.

The present findings indicate that perhaps the most important function of adhesive secretion is to provide sufficient attachment to rough substrates. When the pads were depleted from secretion in the course of multiple consecutive pull-offs on a rough substrate, adhesive forces decreased. A similar effect was found in toe pads of tree frogs, where attachment to very rough surfaces was improved by wetting the surface with a stream of water (Barnes et al., 2002). The influence of fluid films on the adhesion between two solids has been studied in a classical paper by McFarlane and Tabor (1950). They found that increasing the surface roughness of glass by abrasion resulted in strongly reduced adhesion due to a loss of contact area, which was partly restored by applying water films or high humidity. Whether the substrate cavities can be filled out by the fluid depends on the relation between the height of the surface peaks and the thickness of the fluid layer (Fig. 4.2). Maximum adhesion will be reached when there is just enough fluid to fill out the substrate cavities, in which case the fluid layer thickness is in the same magnitude as the surface roughness amplitude (Bhushan, 2003; Persson et al., 2005).

The effect of surface roughness can not only be compensated by a fluid film but also if one of the adherends is very soft, so that it can adapt to the surface profile (Fuller and Tabor, 1975). Smooth adhesive pads of insects are indeed extremely soft and deformable (Gorb et al., 2000). In other animals, e. g. flies, beetles, spiders and lizards, compliance is achieved by a "hairy" design of adhesive pads (Stork, 1983). However, if adhesive contacts are not extremely fine as in the "dry" adhesive systems of spiders and lizards, the surface roughness to which even a very soft smooth pad or a larger adhesive seta can make

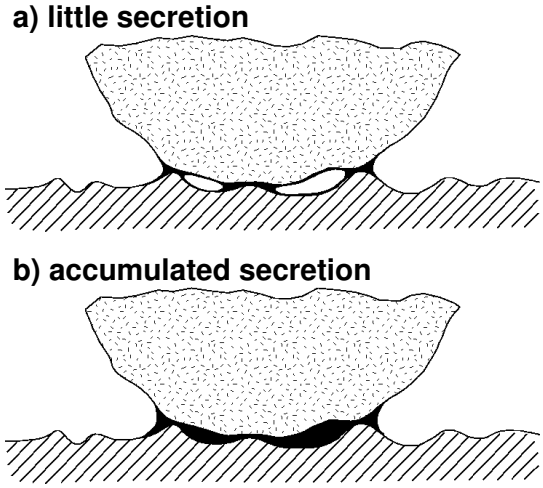

Figure 4.2: Schematic diagram illustrating the adhesion-enhancing role of insect pad secretion on a rough substrate. Due to the high surface roughness, the pad cannot completely fill out the substrate cavities. When there is only little secretion (**a**), only small menisci form at the tips of surface asperities and the real area of contact is small. If there is more fluid present in the contact zone (**b**, "accumulated secretion"), the small menisci merge and create a larger contact area, which gives rise to greater effective adhesion.

complete contact, is limited (Fuller and Tabor, 1975; Persson, 2002). Thus, insect pad secretion can enhance adhesion on very rough surfaces where a dry pad would make only partial contact (Fig. 4.2a). Most of the substrates that insects encounter in nature are in fact not perfectly smooth but characterized by some degree of surface roughness. In the course of evolution, adhesive pads may have been optimized for better attachment to these "real" substrates rather than for superior contact to smooth surfaces.

4.2.2 *Role of pad secretion for friction forces*

The second important result emerging from this study concerns the presence of static friction and the role of the fluid secretion for static and dynamic forces. Even though shear forces of insect pads have often been measured (Stork, 1980; Gorb and Scherge, 2000; Gorb et al., 2001; Betz, 2002; Federle et al., 2004; Gorb and Gorb, 2004), the presence of a static component of friction has never been directly demonstrated. These results confirm previous conclusion by Federle et al. (2004), that, despite

the presence of a liquid in the contact zone, smooth adhesive pads generate static friction. In contrast to the classical concept of static friction between two solids, the forces at the onset of sliding did not always show a peak and were velocity dependent (Fig. 3.7a). This indicates that the transition from rest to sliding is associated with a dynamic, rate-dependent process, which may involve the release of the contact zone by peeling. To demonstrate that pads can indeed sustain a "static" shear stress, the friction force was measured for 2 minutes after a sliding movement had stopped. The remaining shear stress was considerable both for "little" and "accumulated" secretion.

The friction of smooth adhesive pads has been reported to increase with normal load (Gorb and Scherge, 2000; Gorb et al., 2002). Even though the current friction measurements are much larger than the values reported by Gorb and Scherge (2000), (taken with only 10 µm amplitude and probably with "accumulated" secretion) the findings in this study confirm this effect and demonstrate that it is mainly based on changes in adhesive contact area. In contrast, shear stress itself was relatively insensitive to variations of normal force at least when no secretion had accumulated. This behavior is consistent with the view that friction depends on the "real" area of contact (Bowden and Tabor, 1950). Scaling of friction with contact area has been found mainly in situations of close contact where friction is dominated by adhesion (Homola et al., 1990) such as the sliding friction of rubber on glass (Barquins and Roberts, 1986). Thus, in order to be able to sustain larger friction forces, insects need to maximize their pad contact area. Under natural conditions, this is only rarely achieved by increasing the load on foot pads. On the contrary, the pad contact area of ants was found to increase with a stronger pull away from the surface (Federle and Endlein, 2004). Insects take advantage of direction-dependent pad designs and active and passive unfolding mechanisms, and can increase contact area by pulling their legs toward the body (Federle et al., 2001; Niederegger et al., 2002).

Several possible mechanisms might explain the ability to sustain static shear forces in insects and frogs. First, the meniscus of the fluid film between pad and substrate may be deformed when the pad is displaced horizontally. Due to the tendency of the contact angle to return to equilibrium, there will be a reten-

tive force. However, a quantitative estimate analogous to previous analysis by Federle et al. (2004) shows that the maximum possible shear stress in insects due to surface tension amounts to only $\tau \approxeq 0.5\,\mathrm{kPa}$ and is therefore two orders of magnitude smaller than the measured static shear stress. Furthermore, the static shear stress measured in tree frogs is also too large to be explained by deformation and the resulting retentive force of the fluid film's meniscus (see section 3.3.1). This confirms that the contribution of surface tension forces cannot explain the observed static friction.

Second, the adhesive pad could make direct contacts to the substrate. This could be related to the direct contact of surface asperities with the cuticle across the adhesive liquid film, if surface roughness is greater than the fluid film thickness (Roberts, 1971a). Using interference reflection microscopy, Federle et al. (2002) estimated the thickness of the adhesive liquid film in *Carausius morosus* and *Oecophylla smaragdina* ants to range between 90 nm and 160 nm near the edge of the pad contact zone. Secretion films of up to 50 nm thickness get deposited at the trailing edge of sliding pads (Federle et al., 2002, and unpublished results). Even though the deposited fluid volume during the "accumulated secretion" experiments was not quantified in this study, the visible trails of deposited secretion indicated that pads slid on secretion films of considerable thickness. Moreover, the fact that shear stress was sensitive to normal force only in the "accumulated" but not in the "little secretion" condition confirms that the fluid films were very thick (Fig. 3.5). As the surface roughness of glass is probably much smaller than the thickness of the fluid film, at least in the "accumulated" condition, it is unlikely that the penetration of asperities can explain static friction.

Alternatively, "dry" contacts could form by dewetting of a metastable, triboactive liquid film (Brochard-Wyart and de Gennes, 1994; Martin and Brochard-Wyart, 1998; Martin et al., 2002). Federle et al. (2002) did not observed any evidence for such a process using interference reflection microscopy. Moreover, the wetting properties of the fluid suggest that dewetting is unlikely to occur. The stability of the thin fluid film between the pad cuticle and the surface depends on the sign of the spreading coefficient $S = \gamma_{GC} - (\gamma_{GF} + \gamma_{FC})$, where γ_{GC}, γ_{GF} and γ_{FC} are the glass/cuticle, glass/fluid, and fluid/cuticle interfacial

tensions, respectively (Martin et al., 2001). The fluid film is stable if S is positive (Martin and Brochard-Wyart, 1998). As insect adhesive secretion completely wets the pad cuticle and forms only small contact angles with glass (Federle et al., 2002; Vötsch et al., 2002), both γ_{GF} and γ_{FC} are probably small and the film may be stable.

Third, it is possible that the pad secretion has non-Newtonian, shear-thinning properties, which could involve a solid-like behavior for small shear stresses (Granick, 1991; Zhang et al., 2002). In fact, such a "yield stress" is a characteristic feature of emulsions, especially if the volume fraction of the disperse phase is large (Barnes, 1994; Tadros, 1994). The rate-dependence of shear stress in insect adhesive pads as observed in this work and in a previous study on ants by Federle et al. (2004) could be fully explained by the rheological behavior of an emulsion. In many emulsions, shear stress is an approximately linear function of shear rate, with a positive intercept corresponding to the yield stress. The relationship between velocity and shear stress in insect pads also shows a positive intercept (Federle et al., 2004 and Fig. 3.7c).

The current findings provide evidence in favour of the "emulsion" mechanism. Static friction was still clearly present even when secretion had accumulated. Based on the above considerations, neither meniscus deformation nor direct contacts between the cuticle and the surface are plausible explanations in insects. By virtue of its yield stress, even a relatively thick and continuous film of adhesive emulsion could sustain static friction forces. Further work is required to clarify in detail how the composition of this emulsion is related to its rheological properties and to its adhesive and frictional performance.

I assume that using a thixotropic (= shear thinning) emulsion as an adhesive fluid is an advantageous strategy, because it conveys the benefits of wet adhesion and particularly the superior performance on rough substrates without sacrificing the ability to withstand shear forces. The combination of both factors, sufficient contact to rough substrates and resistance against sliding, might be an essential prerequisite for the insects' capability to manoeuvre on plant surfaces.

In contrast, the small fluid film height measured in tree frogs suggest that static friction is governed by boundary lubrication (see section 3.3). This effect is facilitated by the microstructured

surface of the toe pad (Fig. 1.11), which allows fluid drainage from the contact zone (Persson, 2007a,b), similar to the way car tires grip firmly to wet road surfaces (Roberts, 1971b). Analogous to stick insects, non-Newtonian properties of the mucus (Granick, 1991; Zhang et al., 2002) might play an important role in providing tree frogs with sufficient static friction.

4.3 MODE OF DETACHMENT

How are insects able to maintain their maneuverability while hanging upside down from smooth surfaces? Maneuverability obviously relies on being able to control the adhesive forces between the pad and the substratum. Many mechanisms have been put forward describing animal adhesion to smooth surfaces (see section 1.3.3). The underlying models have in common that they either rely on elastic spheres *or* rigid plates. This study has shown that the factors velocity, preload and contact time prior to detachment all have an effect on pull-off forces:

(a) Larger preload increased contact area and pull-off forces (section 3.2.2.1, Fig. 3.13a–Fig. 3.13c). This effect was more pronounced at higher velocities (Tbl. A.25–Tbl. A.34).

(b) Pull-off force per area had a tendency to decrease with increasing preload (Fig. 3.13d, Fig. A.6).

(c) Longer contact times prior to detachment increased adhesive forces (section 3.2.1, Fig. 3.11). Whether this effect was be due to an increase in contact area *or* an increased force per area could not be determined, as no contact area was measured during these experiments.

(d) Scaling coefficients of adhesive forces as well as contact areas had a tendency to increase with velocity (Fig. 3.17a, Fig. 3.17e).

These results indicate that the detachment process relies on viscoelasticity. How can these findings be brought in unison with theories derived from purely elastic or purely rigid bodies? Viscoelastic materials, often modeled as a combination of dashpots and springs (i. e. Kelvin-Voigt model; see section 1.1.4 on page 10 and Fig. 1.6), will behave more like a Hookean elastic spring, if the system is moved slowly. This is consistent with

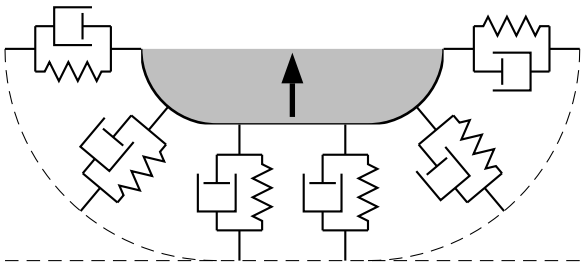

Figure 4.3: Proposed viscoelastic detachment model. The adhesive pad is composed of viscous and elastic filaments, depicted as Kelvin-Voigt models (see Fig. 1.6b for model details and Fig. 1.9 and Fig. 1.11 for a morphological comparison). During equilibrium the part of the pad in contact with the substratum is compressed fully. A rapid detachment will at first show no effect. Only gradually the dashpots will lengthen. During this time the adhesive force is spread over the complete contact area (load sharing). Once the dashpot elements have reached their maximum elongation, the stiffness of the springs will determine the behaviour of the system by detaching ("peeling") from the edge of the contact zone.

attachment models peeling from the edge of the contact zone, for instance contact mechanics models such as the JKR theory (Johnson et al., 1971) or the theory as proposed by Schargott et al. (2006). In contrast, the material will behave stiffer if the viscous elements (Newtonian dashpots) are moved quickly, as the daspots need more time to lengthen. This corresponds to a sudden detachment of two rigid plates or load sharing (Bhushan, 2003). The proposed rate-dependent detachment model of a viscoelastic attachment pad is shown in Fig. 4.3.

The viscoelasticity model is supported by (a) and (b): Large preloads increased contact area (Fig. 3.13c). During rapid detachment the material did not have enough time to retract elastically. In model terms, the dashpot components "prohibited" elastic retraction The material will be stiffer, resulting in load sharing. In contrast, the contact area was able to retract elastically during slow detachment. This resulted in the pull-off force being concentrated at the circumference of the contact area (JKR). The fact that force per area had a tendency to decrease with increasing preload (Fig. 3.13d, Fig. A.6) seems to confirm these results. These results confirm findings by Jiao et al. (2000), who have shown that normal force influences detachment force of smooth adhesive pads in insects. But in addition to the results of Jiao et al. (2000), these results also show

that the relationship between pull-off force and preload is dependent upon detachment velocity.

The increased detachment forces measured during prolonged attachment prior to detachment (section 3.2.1, Fig. 3.11) can be interpreted as a further indication of viscoelastic behaviour: A short compression of the pad material would not give the viscous dashpot components of the attachment system enough time to compress fully. In contrast, a longer contact time prior to detachment would give the dashpots enough time to move, hereby increasing the area of contact. Further investigations on the effect of contact time are necessary, as the contact area was not measured during these experiments. Therefore the increased pull-off force could also result from an increase in force per area at longer contact times prior to detachment. A possible explanation for the latter could be a decreasing distance between pad and substrate due to fluid drainage from the contact zone (Persson, 2007b). This in turn might increase the force per area.

Allometric analyses of the influence of velocity showed weak trends of increasing scaling coefficients with increasing velocity, supporting the hypothesis that the pad material is viscoelastic. Scaling coefficients derived from pull-off force versus body mass (Fig. 3.17a) as well as pull-off force versus contact area (Fig. 3.17e) increased from approximately 0.5 at low velocities ($\leqslant 100\,\mu m\,s^{-1}$) to about 1 at high velocities ($> 100\,\mu m\,s^{-1}$). The large variance of the data was mainly caused by differences between individual animals. I also had difficulties immobilizing very small insects. The weak forces produced by these small animals also resulted in poor signal to noise ratios complicating analyses. Furthermore the potential difference in pad elasticity between young and old insects might have influenced the results. As the amount of pad secretion can not be controlled in detail, differences in secretion present during detachment will have had an uncontrollable effect on pull-off forces (see previous section).

Scaling analysis of insect whole body detachment showed that forces clearly scaled with contact area (Fig. 3.18), supporting the wet adhesion model. This effect might be facilitated by the pad having had enough time to attach firmly prior to detachment by virtue of viscoelastic material properties (see earlier discussion). As the insect was able to move freely on the

centrifuge, it can not be ruled out that attachment forces were additionally altered by changes to body posture or leg position (i. e. angle between leg and surface). Allometric studies in tree frogs also confirm detachment forces scaling with contact area (Barnes et al., 2006; Smith et al., 2006a,b).

Additional support for the viscoelastic properties of soft attachments pads is provided by morphological results of this study and recent findings analysing the material properties of the ultrastructure of soft attachment pads in insects: The pad material is softer towards the surface (see Fig. 1.9 and Gorb and Scherge, 2000; Beutel and Gorb, 2001; Scholz et al., 2007).

Because quick viscoelastic detachment will increase adhesion and therefore contradicts fast locomotion, animals need further control over the detachment process. Indeed, mechanisms such as changes in gait pattern or posture as well as rolling or peeling of the attachment pad have been shown to be present in studies in ants and flies (see section 1.3.3 on page 23 and Federle et al., 2001; Gorb, 2001; Federle et al., 2002; Niederegger and Gorb, 2003; Federle and Endlein, 2004). To test whether stick insects actually use a different mode of detachment, whole body measurements of unrestrained stick insects where compared to single leg measurements (section 3.2.2.4). As previously mentioned, the scaling data was very variable. The comparison of single leg measurements and centrifuge measurements did not reveal a significant difference (Tbl. 3.13).

Aside from the presence of an adhesive fluid as described in the previous section, all smooth adhesive systems in animals studied so far are characterized by the presence of micro- or nanostructured surfaces (see Fig. 1.10, Fig. 1.11 and Mizuhira, 2004; Goodwyn et al., 2006; Smith et al., 2006a; Barnes, 2007). Microstructured surfaces have been described to increase adhesion by inhibiting crack propagation (Hui et al., 2004, 2005; Glassmaker et al., 2007). A further advantage of this surface geometry, which has recently been proposed, is that fluid drainage is facilitated due to the presence of channels between the microstructured surface. This effect can facilitate adhesion especially to wetted surfaces or when the pad is submerged (Persson, 2007b). When a microstructured surface is in contact with a dry surface, these properties will serve the opposite function and ease detachment. Independent of the state of wetting, friction forces will be increased by these microstructures.

I therefore propose the following model for animals adhering by virtue of a smooth attachment organ: Smooth attachment pads in insects and tree frogs are viscoelastic in nature. This material property guarantees good contact to a wide range of surfaces by virtue of the elastic and viscous components of the material. Furthermore, the area of real contact on rough surfaces can be enhanced by the presence of an adhesive fluid (see previous section). The viscous material component is able to compensate involuntary (rapid) detachments by increasing the elasticity of the pad. Surface roughness can be compensated by virtue of the pad material being softer (=decreased modulus of elasticity) towards its surface. Finally, adhesion can be enhanced by fluid drainage through the presence of channels in the structured surface of the adhesive pad.

5

SUMMARY

Animals are able to control the attachment process on many different levels (ranging from body locomotion and posture to actively or passively controlling material properties of their attachment pad). The aim of this study was to characterize the biomechanical principles underlying the attachment mechanism of smooth adhesive pads as present in many insects and tree frogs under controlled conditions.

The first result of this study showed that friction in insect attachment pads is anisotropic: Attachment pads regularly detached when slid away from the body. Further analyses of "immobilized" arolia revealed that this anisotropy is *not* caused by an increased shear stress in proximal direction.

The second part of this study analysed the role of the pad secretion present in insects and frogs. To understand the function of these fluid-based adhesive systems, I simultaneously measured force and contact area in single pads of both species. In stick insects, shear stress was largely independent of normal force and increased with velocity, seemingly consistent with the viscosity effect of a continuous fluid film. However, measurements of the remaining force two minutes after a sliding movement showed that adhesive pads could sustain considerable static friction in insects and tree frogs. Repeated sliding movements and multiple consecutive pull-offs of stick insect single legs to deplete adhesive secretion showed that on a smooth surface, friction and adhesion strongly increased with decreasing amount of fluid in insects. In contrast, stick insect pull-off forces significantly decreased on a rough substrate. Thus, the secretion does not generally increase attachment but does so only on rough substrates, where it helps to maximize contact area. When slides with stick insect arolia were repeated at one position so that secretion could accumulate, sliding shear stress decreased but static friction remained clearly present. This suggests that static friction in stick insects, which is biologically important to prevent sliding, is based on non-Newtonian properties of the adhesive emulsion rather than on a direct contact

between the cuticle and the substrate. In contrast, the very thin mucus film layer present in tree frogs suggests that they are also able to create static friction by boundary lubrication.

Finally, this study demonstrated that the mode of detachment is influenced by viscoelastic material properties as well as normal force and velocity. Previous attachment models have relied on either rigid *or* elastic material properties. The presence of viscoelasticity can bring these conflicting prerequisites in unison: Fast detachment will facilitate viscous behaviour, leading to adhesive forces being spread over the complete area of contact. This corresponds to forces scaling with an area, such as described by load sharing theories or the wet adhesion model. In contrast, the material will be elastic during slow detachments. The adhesive force will concentrate on the circumference of the contact area, therefore scaling with a length, supporting models such as the peeling theory. Although the many morphological similarities present between attachment organs of tree frogs and stick insects suggest that homologous processes might be involved in tree frog attachment, further research on tree frogs is needed to support this.

6

ZUSAMMENFASSUNG

Tiere sind in der Lage den Ablösevorgang auf verschiedenen hierarchischen Ebenen zu kontrollieren (angefangen von der Körperhaltung bis zur aktiven oder passiven Veränderung des Haftmaterials). Ziel dieser Arbeit war es, die Funktionsweise weicher Haftorgane von Insekten und Fröschen unter kontrollierten Bedingungen zu ermitteln.

Das erste Ergebnis dieser Arbeit war, dass Reibung von Insektenhaftorganen von der Bewegungsrichtung abhängt. Ein Haftorgan, das vom Körper weg bewegt wird (distale Richtung), löst sich sofort von der Oberfläche ab ("footloose"). Weitere Untersuchungen an "immobilisierten" Haftorganen zeigten, dass *keine* erhöhte Scherspannung in proximaler Richtung vorhanden ist.

Um die Funktionsweise der flüssigkeitsbasierten Haftsysteme von Insekten und Fröschen zu untersuchen, wurden Kräfte und Kontaktflächen beider Spezies gemessen. Bei Stabheuschrecken war die Scherspannung unabhängig von der Normalkraft und nahm mit der Bewegungsgeschwindigkeit zu, scheinbar in Einklang mit der viskosen Reibung eines kontinuierlichen Flüssigkeitsfilms. Jedoch ergaben Scherspannungsmessungen bei Stabheuschrecken und Fröschen selbst zwei Minuten nach einer Gleitbewegung ein beträchtliches Maß an statischer "Rest"-Reibung. Um den Einfluss geringer werdender Haftflüssigkeit zu untersuchen, wurden wiederholte Gleitversuche sowie aufeinanderfolgende Ablöseversuche auf glatten Oberflächen durchgeführt. Diese Experimente zeigten, dass sowohl die Reibungs- als auch die Adhäsionskraft mit abnehmender Flüssigkeitsmenge anstieg. Im Gegensatz hierzu nahm die Adhäsionskraft auf rauen Oberflächen mit abnehmender Haftflüssigkeitsmenge ab. Demzufolge führte die Haftflüssigkeit nur auf rauen Oberflächen zu einer Vergrößerung der Kontaktfläche und zu einer Erhöhung der Adhäsionskraft. Scherspannungen von Gleitreibungsversuchen auf glatten Oberflächen wurden bei Stabheuschrecken umso geringer, je häufiger der Versuch an ein und der selben Stelle durchgeführt wurde

(um die Menge an Haftflüssigkeit zu akkumulieren). Nichts desto trotz blieb immer eine statische Reibung vorhanden. Das Vorhandensein von statischer Reibung ist biologisch wichtig um das unfreiwillige Ausrutschen zu verhindern und deutet an, dass der Mechanismus der Haftflüssigkeit von Stabheuschrecken eher auf eine Emulsion mit nicht-Newtonschen Eigenschaften (scherverdünnend) zurückzuführen ist und nicht auf das Vorhandensein direkter Kontakte zwischen Kutikula und Untergrund. Im Gegensatz hierzu deutete die geringe Höhe des Flüssigkeitsfilms bei Baumfröschen an, dass diese zusätzlich "Grenzflächenschmierung" ("boundary lubrication") als Methode zur Erzeugung statischer Reibung verwenden.

Im letzten Teil dieser Arbeit wurde gezeigt, dass der Ablösevorgang von der Ablösegeschwindigkeit, der Normalkraft und den viskoelastischen Materialeigenschaften des Insektenhaftorgans abhängig ist. Bisherige Modelle zum Trennen zweier Körper gehen davon aus, dass beide Körper entweder starr *oder* elastisch sind. Das Vorhandensein von Viskoelastizität vereinigt diese bisher als widersprüchlich angesehenen Modelle: Bei einem schnellen Ablösen wird das Material sich viskos verhalten. Dies führt dazu, dass die Adhäsionskraft über die gesamte Kontaktfläche verteilt wird – die Kraft skaliert mit einer Fläche, wie von dem "wet adhesion" oder "load sharing" Modell vorhergesagt wird. Im Gegensatz dazu verhält sich das Material bei einem langsamen Ablöseprozess elastisch. In diesem Fall verteilt sich die Adhäsionskraft nicht auf die gesamte Kontaktfläche, sondern konzentriert sich auf den Umfang der Kontaktfläche. Das Haftorgan löst sich schälend und die Kraft skaliert mit einer Länge, wie z. B. von der "peeling" Theorie vorhergesagt. Obwohl die vielen morphologischen Ähnlichkeiten zwischen Baumfröschen und Stabheuschrecken es nahe legen, dass Baumfrösche einen homologen Mechanismus einsetzen können, sind hierfür weitere Untersuchungen an Baumfröschen nötig.

A

APPENDIX

A.1 MATERIAL AND METHODS

A.1.1 LABVIEW

The LABVIEW program consists of a front panel (the graphical user interface, GUI) and a block diagram containing the code. The latter is displayed in Fig. A.1 as a flowchart.

The front panel (see screenshots in Fig. A.2) offered a simple way of toggling between measurement mode and motor initialization, selecting a default directory and choosing the default movement direction of motors (depending upon the camera being above or below the glass plate).

Forces, movement pattern and raw voltage data where graphically displayed (see graphs marked as A–C in the bottom screenshot of Fig. A.2). Furthermore forces, voltage and time where displayed live during the measurement (marked E in Fig. A.2). The tables marked as D and F indicate the numeric values of the bending beam properties and the movement pattern, respectively. The physical parameters of each bending beam (such as spring constant and conversion from voltage to force) were stored in individual files and could be replaced on the fly. Similarly, movement patterns were also stored as text files and where loadable through the graphical user interface.

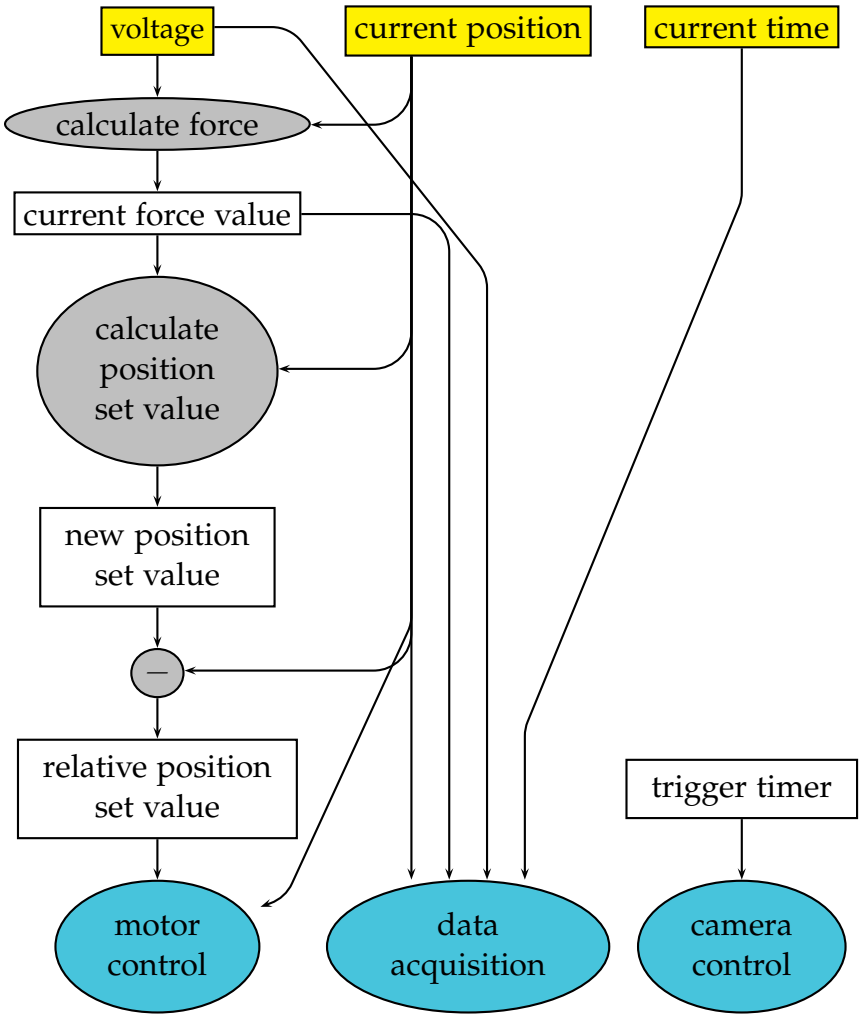

Figure A.1: Flowchart diagram of LABVIEW program displaying motor (incl. feedback) and camera control. Yellow boxes denote measurement values, white boxes are calculated values, gray oval boxes denote algorithms and blue boxes denote output values.

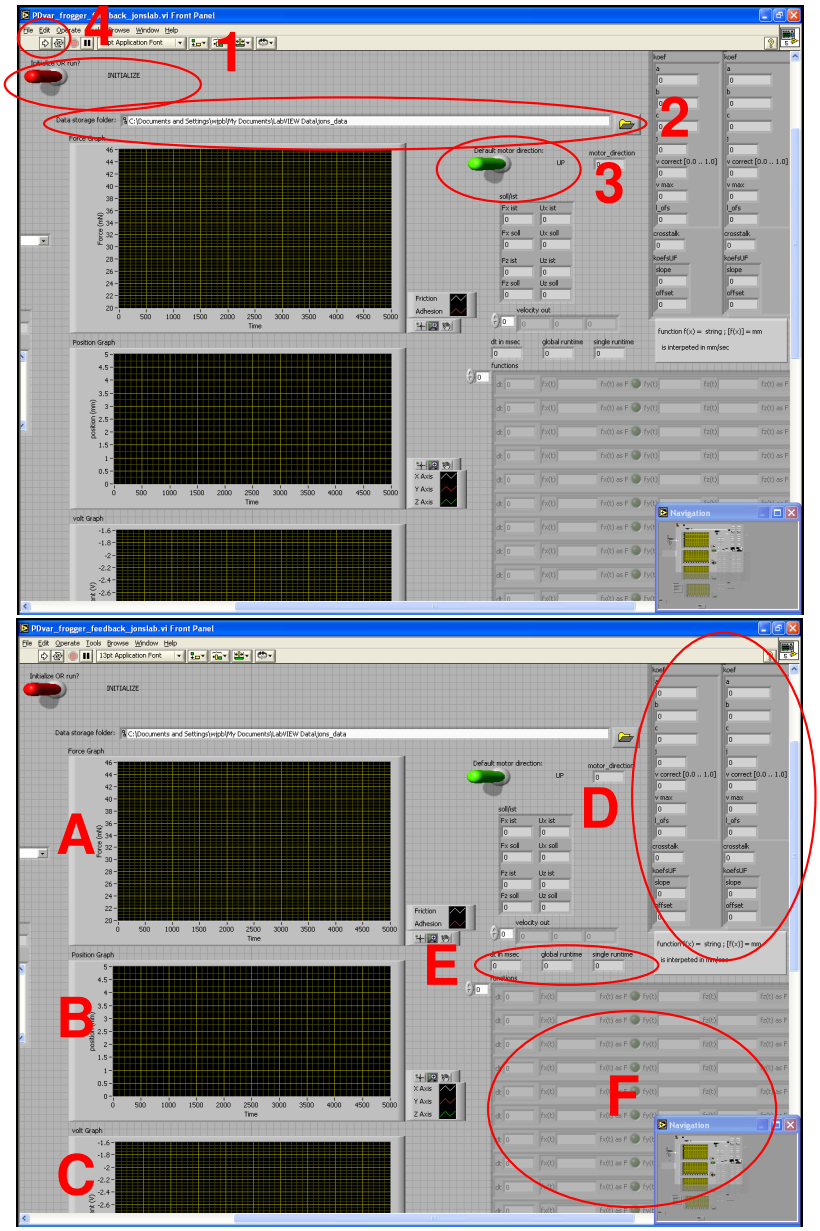

Figure A.2: Front panel of LABVIEW control program. **TOP:** The numbers 1–4 in the top screenshot indicate normal usage. 1.: Toggle between motor initialization and running a measurement. 2.: Selecting default directory. 3.: default movement direction of motors (up/down). 4.: Starting the LABVIEW program. **BOTTOM:** The letters in the bottom screenshot describe the output of the GUI. A–C: force, movement pattern and raw voltage data graphs. D: Bending beam coefficients. E: Live time counters. F: Movement pattern script.

A.1.2 MATLAB

Listing A.1: Main MATLAB algorithm used to calculate animal contact areas.

```
%% Loop over all video frames:
for j = workframes % Format: double array
    output(j).cdata = mov(j).cdata;
    output(j).colormap = mov(j).colormap;
    I1 = output(j).cdata;
    I2 = I1;
    %% "imhmax" suppresses all maxima in the
    %% intensity image "I" whose height
    %% is below threshold "value_imhmax".
    mov_imhmax = imhmax(I2, value_imhmax);
    %% Suppresses all minima in "I" whose depth is
    %% below threshold "value_imhmin":
    mov_imhmin = imhmin(mov_imhmax, value_imhmin);
    %% Low pass filter:
    mov_low_pass = mov_imhmin < value_low_pass;
    %% "bwlabeln": Label connected components in
    %% N-D binary image
    [mov_bin,num] = bwlabeln(mov_low_pass);
    %% Minimal area size: cutoff
    stats = regionprops(mov_bin,'Area');
    idx = find([stats.Area] >= mycutoff);
    bw2 = ismember(mov_bin,idx);
    %% Area and centroid (summed over all partial
    %% contact  areas):
    mov_bin2 = double(bw2);
    stats2 = regionprops(mov_bin2,'all');
    myCentroid_sum = [stats2.Centroid];

    %% Calculate area and centroid of totalframes area:
    [mov_bin3,num] = bwlabel(bw2);
    stats3 = regionprops(mov_bin3,'all');
    pad_area = [stats3.Area];
    pad_area = sort(pad_area);
    idx2 = find([stats3.Area] == max(pad_area));
    bw3 = ismember(mov_bin3,idx2);
    mov_bin4 = double(bw3);
    stats4 = regionprops(mov_bin4,'all');
    %% X and Y coordinates:
    myCentroid_max = [stats4.Centroid];
    ConvexHull = [stats4.ConvexHull];
    convexhull{j} = [ConvexHull];
    BoundingBox = [stats2.BoundingBox];
    bb{j} = [BoundingBox];

    if isempty(stats2)% <- no contact area
```

```
      pad_area = NaN;
      area_max(j) = pad_area;
      area_sum(j) = pad_area;
      D(j) = 0;    % <- movement within the frame
    else% <- contact area present
      %% Area calculation:
      %% Only include totalframes value:
      area_max(j) = max(pad_area);
      %% Include all values:
      area_sum(j) = sum(pad_area);
      if area_max(j) < mycutoff
        area_max(j) = 0;
      end
      if area_sum(j) < mycutoff
        area_sum(j) = 0;
      end

      %% Movement within frame:
      C = [];                          %
      for k = 1:num
        %% "r": row; "c": column
        [r,c] = find(bwlabel(mov_bin2)==k);
        C = [C;r];
      end
      D(j) = mean(C);
    end;
end;

area_max = (myfactor*sqrt(area_max)).^2;
area_sum = (myfactor*sqrt(area_sum)).^2;
```

A.2 RESULTS

A.2.1 *Adhesion single leg*

The data set was unbalanced due to missing values. After log-transforming pull-off force, contact area, force per area and work of adhesion were normally distributed and had homogeneous variances.

A.2.1.1 *Shapiro Wilks tests:*

Table A.1: log-transformed pull-off forces F_P. ($N = 20$): P-values of Shapiro-Wilks normality test for normal forces and velocities.

F_P	velocity v ($\mu m\, s^{-1}$)				
	10	50	100	500	5000
F_N (mN)					
0.01	0.8018	0.9846	0.8965	0.2017	0.0040
0.1	0.6567	0.9833	0.9321	0.5266	0.1288
1	0.5029	0.2078	0.7069	0.5759	0.0034
2	0.8309	0.6273	0.8039	0.3627	0.0000

Table A.2: log-transformed contact area $A_{F_{max}}$. ($N = 20$): P-values of Shapiro-Wilks normality test for normal forces and velocities.

$A_{F_{max}}$	velocity v ($\mu m\, s^{-1}$)				
	10	50	100	500	5000
F_N (mN)					
0.01	0.4960	0.1851	0.1855	0.7906	0.2387
0.1	0.9982	0.9738	0.1374	0.1629	0.0003
1	0.7225	0.9884	0.7803	0.8447	0.1847
2	0.0314	0.3291	0.6282	0.4716	0.2647

Table A.3: log-transformed force per area $F_P/A_{F_{max}}$. ($N = 20$): P-values of Shapiro-Wilks normality test for normal forces and velocities.

$F_P/A_{F_{max}}$	velocity v ($\mu m\, s^{-1}$)				
	10	50	100	500	5000
F_N (mN)					
0.01	0.2412	0.8579	0.7655	0.2568	0.2007
0.1	0.0351	0.6716	0.1535	0.3865	0.0043
1	0.5902	0.6028	0.5718	0.5778	0.2736
2	0.1746	0.7339	0.2040	0.0997	0.0445

Table A.4: log-transformed work of adhesion WOA1. (N = 20): P-values of Shapiro-Wilks normality test for normal forces and velocities.

WOA1	velocity v ($\mu m\,s^{-1}$)				
	10	50	100	500	5000
F_N (mN)					
0.01	0.4842	0.4916	0.4816	0.7653	0.0244
0.1	0.0216	0.0421	0.8097	0.7218	0.0006
1	0.0260	0.0016	0.0310	0.9799	0.0796
2	0.1871	0.2539	0.1870	0.6306	0.0201

Table A.5: log-transformed work of adhesion $WOA2_{mean}$. (N = 20): P-values of Shapiro-Wilks normality test for normal forces and velocities.

$WOA2_{mean}$	velocity v ($\mu m\,s^{-1}$)				
	10	50	100	500	5000
F_N (mN)					
0.01	0.0992	0.0791	0.1197	0.0393	0.0005
0.1	0.8731	0.9256	0.2837	0.1097	0.4586
1	0.8436	0.6303	0.9723	0.2051	0.4361
2	0.3626	0.7002	0.4894	0.9001	0.4373

Table A.6: log-transformed work of adhesion $WOA2_{max}$. (N = 20): P-values of Shapiro-Wilks normality test for normal forces and velocities.

$WOA2_{max}$	velocity v ($\mu m\,s^{-1}$)				
	10	50	100	500	5000
F_N (mN)					
0.01	0.9351	0.0657	0.1247	0.4053	0.3281
0.1	0.2744	0.9688	0.2333	0.3098	0.2062
1	0.3559	0.8997	0.0148	0.0259	0.6610
2	0.3091	0.0252	0.5628	0.3322	0.2700

A.2.1.2 *Bartlett tests:*

Table A.7: Bartlett Test of homogeneity of variances at the five velocities on log-transformed pull-off force (N = 20):

F_P	velocity v ($\mu m\,s^{-1}$)				
	10	50	100	500	5000
K	1.9704	2.1861	3.0788	2.8201	16.5373
df	3.0000	3.0000	3.0000	3.0000	3.0000
P	0.5786	0.5347	0.3796	0.4202	0.0009

Table A.8: Bartlett Test of homogeneity of variances at the five velocities on log-transformed contact area $A_{F_{max}}$ (N = 20):

$A_{F_{max}}$	velocity v ($\mu m\,s^{-1}$)				
	10	50	100	500	5000
K	1.0326	5.6610	6.5320	0.9822	5.8420
df	3.0000	3.0000	3.0000	3.0000	3.0000
P	0.7934	0.1293	0.0884	0.8056	0.1196

Table A.9: Bartlett Test of homogeneity of variances at the five velocities on log-transformed force per area $F_P/A_{F_{max}}$ (N = 20):

$F_P/A_{F_{max}}$	velocity v ($\mu m\,s^{-1}$)				
	10	50	100	500	5000
K	8.8015	3.3803	8.9828	2.2904	9.3652
df	3.0000	3.0000	3.0000	3.0000	3.0000
P	0.0320	0.3366	0.0295	0.5144	0.0248

Table A.10: Bartlett Test of homogeneity of variances at the five velocities on log-transformed work of adhesion WOA1 (N = 20):

WOA1	velocity v ($\mu m\,s^{-1}$)				
	10	50	100	500	5000
K	9.3761	9.1376	2.3651	2.2794	6.2963
df	3.0000	3.0000	3.0000	3.0000	3.0000
P	0.0247	0.0275	0.5002	0.5165	0.0981

Table A.11: Bartlett Test of homogeneity of variances at the five velocities on log-transformed work of adhesion $WOA2_{mean}$ ($N = 20$):

$WOA2_{mean}$	velocity v ($\mu m\, s^{-1}$)				
	10	50	100	500	5000
K	2.0421	19.8003	12.9517	13.2153	0.9951
df	3.0000	3.0000	3.0000	3.0000	3.0000
P	0.5637	0.0002	0.0047	0.0042	0.8024

Table A.12: Bartlett Test of homogeneity of variances at the five velocities on log-transformed work of adhesion $WOA2_{max}$ ($N = 20$):

$WOA2_{max}$	velocity v ($\mu m\, s^{-1}$)				
	10	50	100	500	5000
K	2.6956	4.5126	3.0418	1.3957	3.8369
df	3.0000	3.0000	3.0000	3.0000	3.0000
P	0.4410	0.2112	0.3852	0.7066	0.2796

A.2.1.3 *ANOVA tables and figures:*

Table A.13: Two-way ANOVA table showing effects of normal force F_N and velocity v (as well as their interaction) on log-tranformed pull-off force F_P ($N = 20$). Both explanatory parameters (F_N and v) have a highly significant effect on the response parameter F_P ($P < 0.0001$). There is no interaction present ($P > 0.05$).

F_P	Df	Sum Sq	Mean Sq	F value	Pr(>F)
F_N	3	14.5	4.82	12.6	$7.6e-08$
v	4	83.3	20.84	54.4	$3.9e-36$
F_N:v	12	6.4	0.53	1.4	$1.7e-01$
Residuals	376	144.1	0.38		

Table A.14: Two-way ANOVA table showing effects of normal force F_N and velocity v (as well as their interaction) on log-tranformed contact area $A_{F_{max}}$ ($N = 20$). Both explanatory parameters (F_N and v) have a highly significant effect on the response parameter F_P ($P < 0.0001$). There is no interaction present ($P > 0.05$).

$A_{F_{max}}$	Df	Sum Sq	Mean Sq	F value	Pr(>F)
F_N	3	45.7	15.25	23.04	$1.0e-13$
v	4	43.9	10.98	16.60	$1.5e-12$
F_N:v	12	5.7	0.48	0.72	$7.3e-01$
Residuals	376	248.8	0.66		

Table A.15: Two-way ANOVA table showing effects of normal force F_N and velocity v (as well as their interaction) on log-tranformed contact area at $A_{F=0}$ ($N = 20$). Both explanatory parameters (F_N and v) have a highly significant effect on the response parameter F_P ($P < 0.0001$). There is no interaction present ($P > 0.05$).

$A_{F=0}$	Df	Sum Sq	Mean Sq	F value	Pr(>F)
F_N	3	57.0	18.99	31.0	$6.5e-18$
v	4	3.1	0.78	1.3	$2.8e-01$
F_N:v	12	1.5	0.12	0.2	$1.0e-00$
Residuals	376	230.5	0.61		

Table A.16: Two-way ANOVA table showing effects of normal force F_N and velocity v (as well as their interaction) on log-tranformed force per area F_P/A_{F_0} ($N = 20$). Both explanatory parameters (F_N and v) have a highly significant effect on the response parameter F_P ($P < 0.0001$). There is no interaction present ($P > 0.05$).

F_P/A_{F_0}	Df	Sum Sq	Mean Sq	F value	Pr(>F)
F_N	3	17	5.79	9.50	$4.6e-06$
v	4	68	16.99	27.88	$2.7e-20$
F_N:v	12	7	0.58	0.96	$4.9e-01$
Residuals	376	229	0.61		

Table A.17: Two-way ANOVA table showing effects of normal force F_N and velocity v (as well as their interaction) on log-tranformed work of adhesion WOA1 ($N = 20$). Both explanatory parameters (F_N and v) have a highly significant effect on the response parameter F_P ($P < 0.0001$). There is no interaction present ($P > 0.05$).

WOA1	Df	Sum Sq	Mean Sq	F value	Pr(>F)
F_N	3	4.2	1.40	3.1	$2.6e-02$
v	4	131.1	32.77	73.0	$9.6e-46$
F_N:v	12	9.0	0.75	1.7	$7.0e-02$
Residuals	376	168.7	0.45		

Table A.18: Two-way ANOVA table showing effects of normal force F_N and velocity v (as well as their interaction) on log-tranformed work of adhesion $WOA2_{mean}$ ($N = 20$). Both explanatory parameters (F_N and v) have a highly significant effect on the response parameter F_P ($P < 0.0001$). The latter also show significant interaction between eachother ($P < 0.001$).

$WOA2_{mean}$	Df	Sum Sq	Mean Sq	F value	Pr(>F)
F_N	3	10	3.44	7.7	$5.2e-05$
v	4	54	13.61	30.5	$5.3e-22$
F_N:v	12	18	1.49	3.3	$1.2e-04$
Residuals	376	168	0.45		

Table A.19: Two-way ANOVA table showing effects of normal force F_N and velocity v (as well as their interaction) on log-tranformed work of adhesion $WOA2_{max}$ ($N = 20$). Both explanatory parameters (F_N and v) have a highly significant effect on the response parameter F_P ($P < 0.0001$). The latter also show significant interaction between eachother ($P < 0.01$).

$WOA2_{max}$	Df	Sum Sq	Mean Sq	F value	Pr(>F)
F_N	3	0.89	0.30	1.0	$3.8e-01$
v	4	26.57	6.64	23.3	$3.3e-17$
F_N:v	12	8.23	0.69	2.4	$5.3e-03$
Residuals	376	107.35	0.29		

Table A.20: Two-way ANOVA table showing effects of normal force F_N and velocity v (after dropping the interaction term) on log-transformed pull-off force F_P. Both explanatory parameters (F_N and v) have a highly significant effect on the response parameter F_P ($P < 0.0001$).

F_P	Df	Sum Sq	Mean Sq	F value	Pr(>F)
F_N	3	14	4.82	12	$9.0e-08$
v	4	83	20.84	54	$5.3e-36$
Residuals	388	151	0.39		

Table A.21: Two-way ANOVA table showing effects of normal force F_N and velocity v (after dropping the interaction term) on log-transformed contact areas $A_{F_{max}}$. Both explanatory parameters (F_N and v) have a highly significant effect on the response parameter $A_{F_{max}}$ ($P < 0.0001$).

$A_{F_{max}}$	Df	Sum Sq	Mean Sq	F value	Pr(>F)
F_N	3	46	15.25	23	$7.4e-14$
v	4	44	10.98	17	$1.1e-12$
Residuals	388	255	0.66		

Table A.22: Two-way ANOVA table showing effects of normal force F_N and velocity v (after dropping the interaction term) on log-transformed contact area A_{F_0}. Only normal force has a significant effect on A_{F_0} ($P < 0.0001$).

A_{F_0}	Df	Sum Sq	Mean Sq	F value	Pr(>F)
F_N	3	57.0	18.99	31.8	$2.2e-18$
v	4	3.1	0.78	1.3	$2.7e-01$
Residuals	388	232.0	0.60		

Table A.23: Two-way ANOVA table showing effects of normal force F_N and velocity v (after dropping the interaction term) on log-transformed pull-off force per area F_P/A_{F_0}. Both explanatory parameters (F_N and v) have a highly significant effect on the response parameter F_P/A_{F_0} ($P < 0.001$).

F_P/A_{F_0}	Df	Sum Sq	Mean Sq	F value	Pr(>F)
F_N	3	17	5.79	9.5	$4.5e-06$
v	4	68	16.99	27.9	$2.2e-20$
Residuals	388	236	0.61		

Table A.24: Two-way ANOVA table showing effects of normal force F_N and velocity v (after dropping the interaction term) on log-transformed work of adhesion WOA1. Both explanatory parameters (F_N and v) have a highly significant effect on the response parameter WOA1 ($P < 0.01$).

WOA1	Df	Sum Sq	Mean Sq	F value	Pr(>F)
F_N	3	4.2	1.40	3.1	$2.8e-02$
v	4	131.1	32.77	71.5	$2.4e-45$
Residuals	388	177.7	0.46		

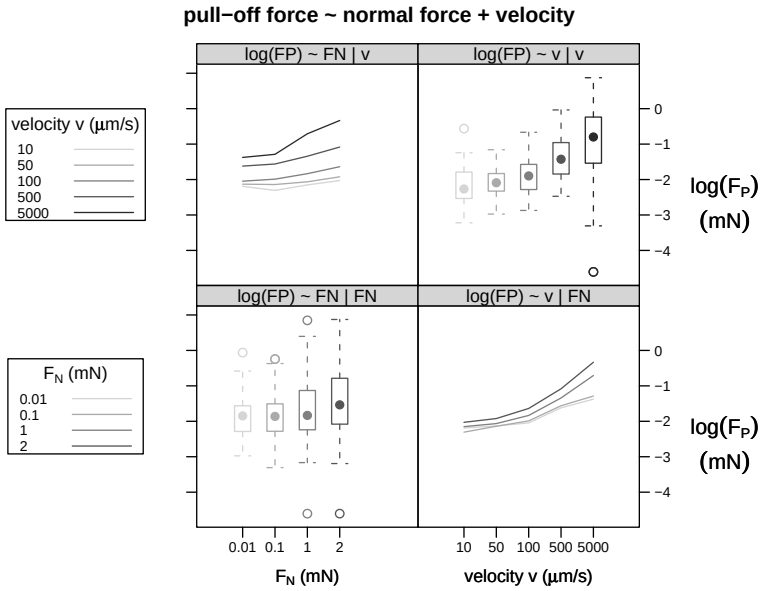

Figure A.3: Interaction plot showing the main effects and two-way interactions of log transformed pull-off force versus normal force and detachment velocity.

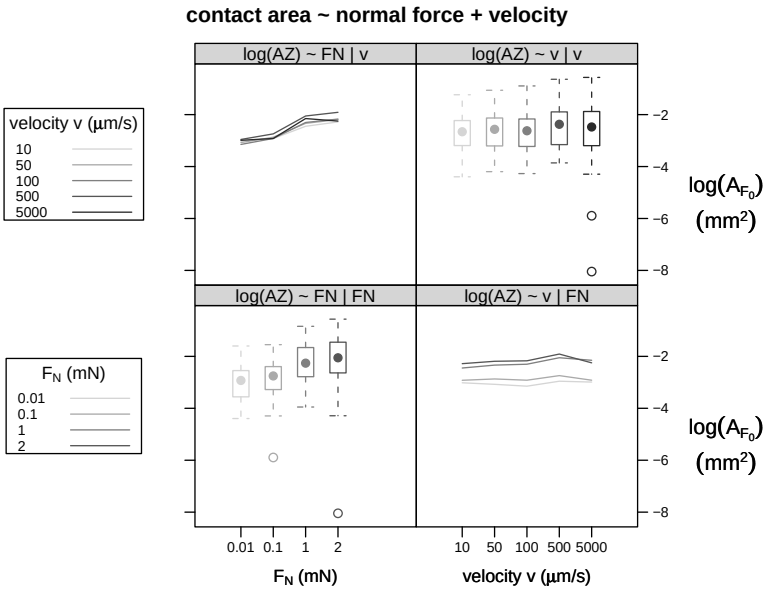

Figure A.4: Interaction plot showing the main effects and two-way interactions of log transformed contact area A_{F_0} versus normal force and detachment velocity.

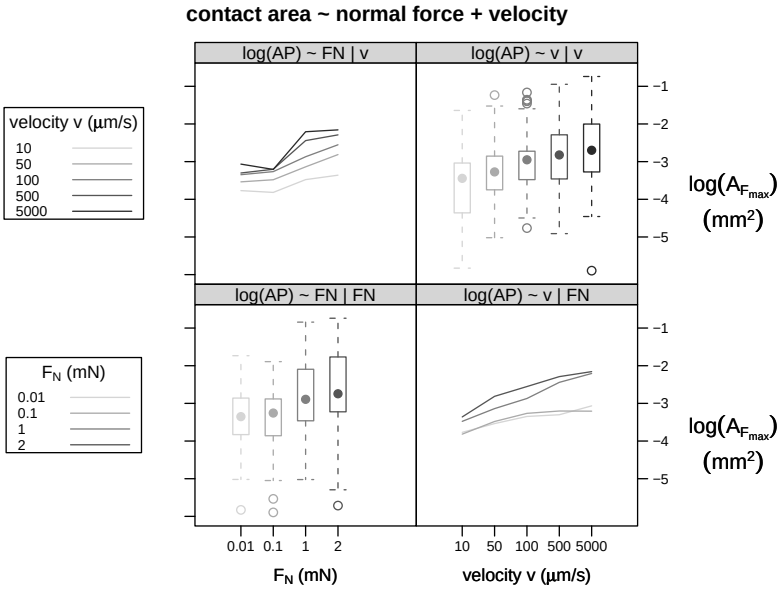

Figure A.5: Interaction plot showing the main effects and two-way interactions of log transformed contact area $A_{F_{max}}$ versus normal force and detachment velocity.

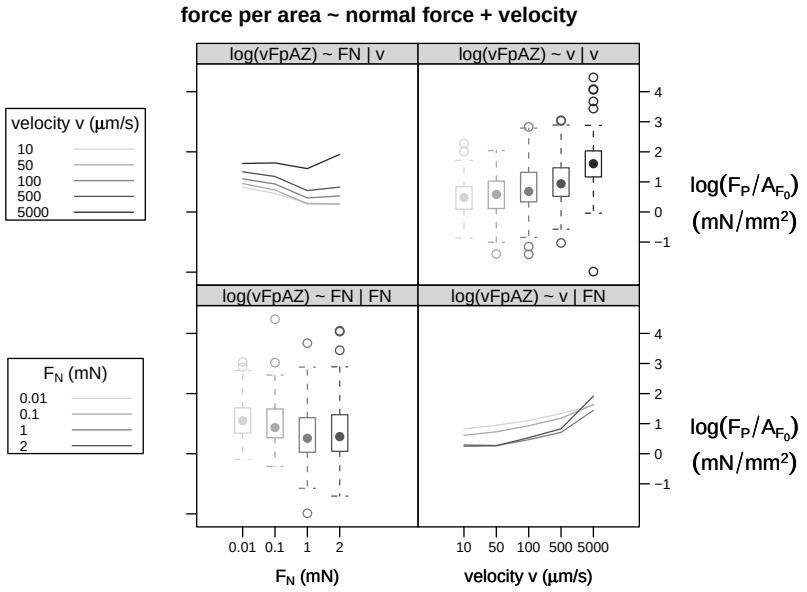

Figure A.6: Interaction plot showing the main effects and two-way interactions of log transformed force per contact area F_P/A_{F_0} versus normal force and detachment velocity.

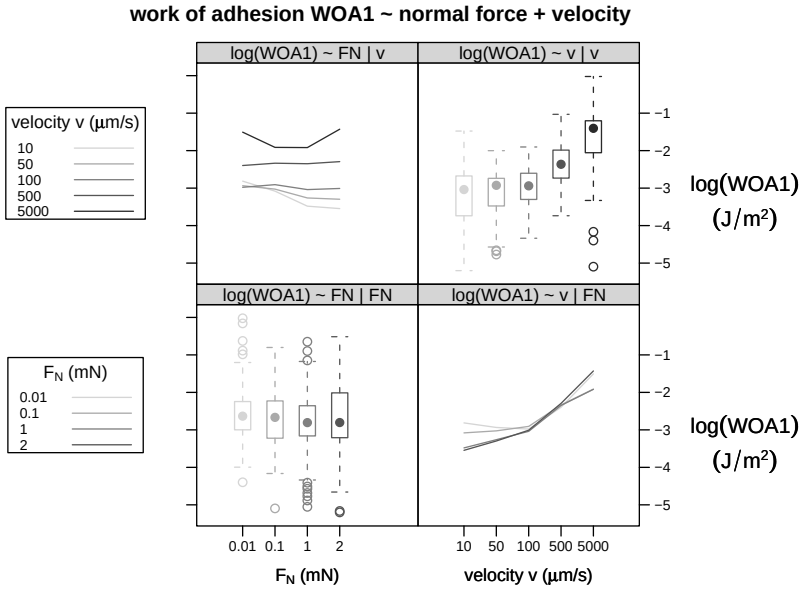

Figure A.7: Interaction plot showing the main effects and two-way interactions of log transformed work of adhesion WOA1 versus normal force and detachment velocity.

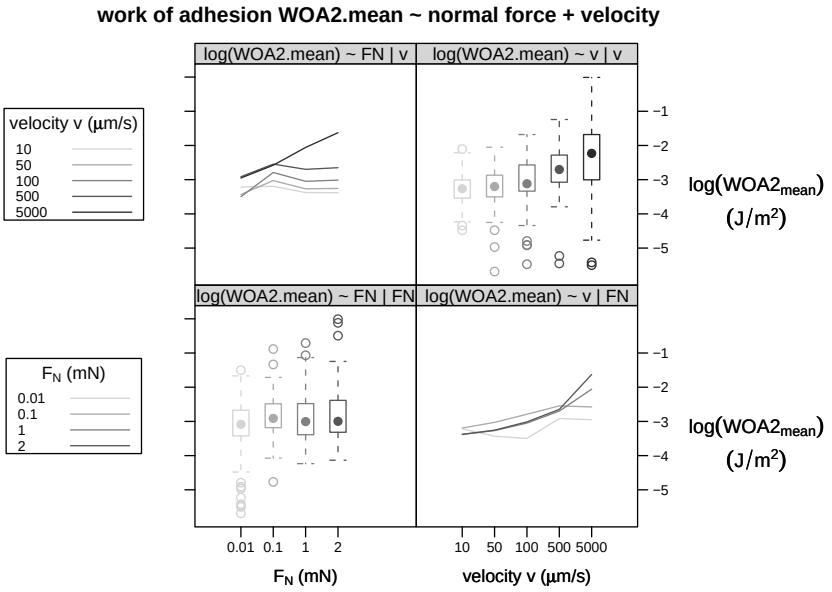

Figure A.8: Interaction plot showing the main effects and two-way interactions of log transformed work of adhesion $WOA2_{mean}$ versus normal force and detachment velocity.

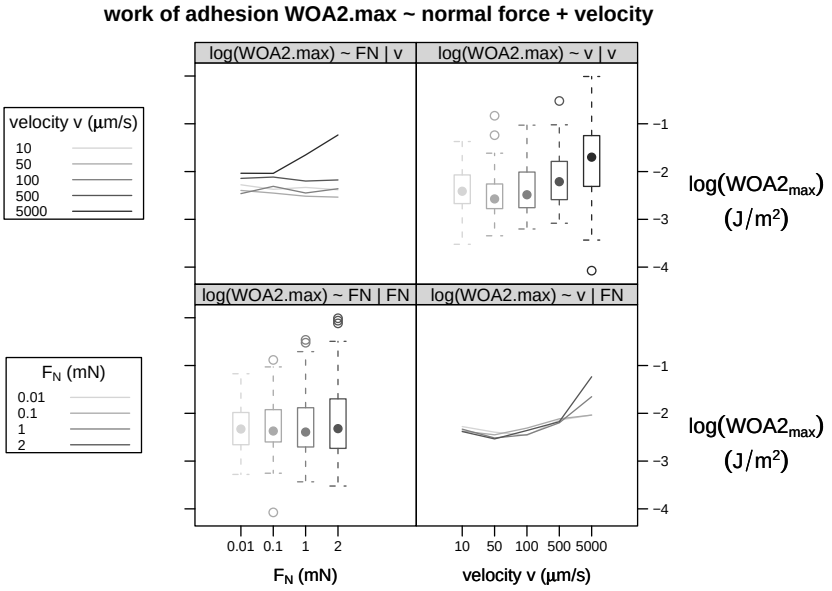

Figure A.9: Interaction plot showing the main effects and two-way interactions of log transformed work of adhesion $WOA2_{max}$ versus normal force and detachment velocity.

Table A.25: One-way ANOVA table showing effect of normal force F_N on F_P at velocity $v = 10\,\mu m\,s^{-1}$.

$F_P(10)$	Df	Sum Sq	Mean Sq	F value	Pr(>F)
F_N	3	0.79	0.26	0.99	0.4
Residuals	76	20.16	0.27		

Table A.26: One-way ANOVA table showing effect of normal force F_N on F_P at velocity $v = 50\,\mu m\,s^{-1}$.

$F_P(50)$	Df	Sum Sq	Mean Sq	F value	Pr(>F)
F_N	3	0.6	0.20	1.2	0.31
Residuals	76	12.6	0.17		

Table A.27: One-way ANOVA table showing effect of normal force F_N on F_P at velocity $v = 100\,\mu m\,s^{-1}$.

$F_P(100)$	Df	Sum Sq	Mean Sq	F value	Pr(>F)
F_N	3	2	0.67	2.7	0.05
Residuals	76	19	0.25		

Table A.28: One-way ANOVA table showing effect of normal force F_N on F_P at velocity $v = 500\,\mu m\,s^{-1}$.

$F_P(500)$	Df	Sum Sq	Mean Sq	F value	Pr(>F)
F_N	3	3.6	1.19	3.5	0.019
Residuals	76	25.7	0.34		

Table A.29: One-way ANOVA table showing effect of normal force F_N on F_P at velocity $v = 5000\,\mu m\,s^{-1}$.

$F_P(5000)$	Df	Sum Sq	Mean Sq	F value	Pr(>F)
F_N	3	14	4.63	5	0.0034
Residuals	72	67	0.93		

Table A.30: One-way ANOVA table showing effect of normal force F_N on $A_{F_{max}}$ at velocity $v = 10\,\mu m\,s^{-1}$.

$A_{F_{max}}(10)$	Df	Sum Sq	Mean Sq	F value	Pr(>F)
F_N	3	3.0	0.99	1.1	0.35
Residuals	76	68.0	0.89		

Table A.31: One-way ANOVA table showing effect of normal force F_N on $A_{F_{max}}$ at velocity $v = 50\,\mu m\,s^{-1}$.

$A_{F_{max}}(50)$	Df	Sum Sq	Mean Sq	F value	Pr(>F)
F_N	3	6.8	2.26	4	0.010
Residuals	76	42.5	0.56		

Table A.32: One-way ANOVA table showing effect of normal force F_N on $A_{F_{max}}$ at velocity $v = 100\,\mu m\,s^{-1}$.

$A_{F_{max}}(100)$	Df	Sum Sq	Mean Sq	F value	Pr(>F)
F_N	3	8.1	2.71	5.1	0.003
Residuals	76	40.8	0.54		

Table A.33: One-way ANOVA table showing effect of normal force F_N on $A_{F_{max}}$ at velocity $v = 500\,\mu m\,s^{-1}$.

$A_{F_{max}}(500)$	Df	Sum Sq	Mean Sq	F value	Pr(>F)
F_N	3	16	5.35	9.4	$2.4e-05$
Residuals	76	43	0.57		

Table A.34: One-way ANOVA table showing effect of normal force F_N on $A_{F_{max}}$ at velocity $v = 5000\,\mu m\,s^{-1}$.

$A_{F_{max}}(5000)$	Df	Sum Sq	Mean Sq	F value	Pr(>F)
F_N	3	18	5.85	7.8	0.00015
Residuals	72	54	0.75		

A.2.1.4 *Tukey HSD tables*

Table A.35: Tukey's HSD test showing effects of normal force F_N and velocity v (after dropping the interaction term) on log-tranformed pull-off force F_P. diff: difference in observed means, lwr/upr: lower and upper end points of interval, P_{adj}: P value after adjustment for the multiple comparisons. Highlighted P values are smaller than 5 %.

F_P	diff	lwr	upr	P_{adj}
F_N (mN)				
$0.1 - 0.01$	0.015	−0.212	0.242	0.998204
$1 - 0.01$	0.248	0.021	0.475	0.025716
$2 - 0.01$	0.466	0.239	0.693	0.000001
$1 - 0.1$	0.233	0.006	0.460	0.041448
$2 - 0.1$	0.451	0.224	0.678	0.000003
$2 - 1$	0.218	−0.010	0.445	0.066021
v ($\mu m\,s^{-1}$)				
$50 - 10$	0.105	−0.163	0.373	0.820692
$100 - 10$	0.293	0.024	0.561	0.024757
$500 - 10$	0.768	0.500	1.036	0.000000
$5000 - 10$	1.243	0.971	1.515	0.000000
$100 - 50$	0.188	−0.081	0.456	0.310412
$500 - 50$	0.663	0.395	0.931	0.000000
$5000 - 50$	1.138	0.866	1.410	0.000000
$500 - 100$	0.475	0.207	0.744	0.000017
$5000 - 100$	0.950	0.678	1.222	0.000000
$5000 - 500$	0.475	0.203	0.747	0.000024

Table A.36: Tukey's HSD test showing effects of normal force F_N and velocity v (after dropping the interaction term) on log-tranformed contact area $A_{F_{max}}$. diff: difference in observed means, lwr/upr: lower and upper end points of interval, P_{adj}: P value after adjustment for the multiple comparisons. Highlighted P values are smaller than 5 %.

$A_{F_{max}}$	diff	lwr	upr	P_{adj}
F_N (mN)				
$0.1 - 0.01$	0.011	−0.287	0.310	0.999674
$1 - 0.01$	0.574	0.276	0.873	0.000006
$2 - 0.01$	0.768	0.470	1.067	0.000000
$1 - 0.1$	0.563	0.265	0.862	0.000010
$2 - 0.1$	0.757	0.459	1.056	0.000000
$2 - 1$	0.194	−0.104	0.492	0.337269
v ($\mu m\,s^{-1}$)				
$50 - 10$	0.364	0.011	0.716	0.039224
$100 - 10$	0.597	0.245	0.950	0.000046
$500 - 10$	0.797	0.444	1.150	0.000000
$5000 - 10$	0.947	0.590	1.304	0.000000
$100 - 50$	0.233	−0.119	0.586	0.366234
$500 - 50$	0.433	0.081	0.786	0.007432
$5000 - 50$	0.583	0.226	0.940	0.000099
$500 - 100$	0.200	−0.153	0.552	0.529146
$5000 - 100$	0.349	−0.008	0.707	0.058524
$5000 - 500$	0.150	−0.207	0.507	0.779723

Table A.37: Tukey's HSD test showing effects of normal force F_N and velocity v (after dropping the interaction term) on log-tranformed contact area A_{F_0}. diff: difference in observed means, lwr/upr: lower and upper end points of interval, P_{adj}: P value after adjustment for the multiple comparisons. Highlighted P values are smaller than 5 %.

A_{F_0}	diff	lwr	upr	P_{adj}
F_N (mN)				
$0.1 - 0.01$	0.165	−0.123	0.452	0.451230
$1 - 0.01$	0.779	0.491	1.066	0.000000
$2 - 0.01$	0.879	0.591	1.166	0.000000
$1 - 0.1$	0.614	0.327	0.901	0.000000
$2 - 0.1$	0.714	0.427	1.001	0.000000
$2 - 1$	0.100	−0.187	0.387	0.805225
v ($\mu m\,s^{-1}$)				
$50 - 10$	0.049	−0.290	0.388	0.994843
$100 - 10$	0.032	−0.307	0.371	0.999017
$500 - 10$	0.251	−0.088	0.591	0.253214
$5000 - 10$	0.090	−0.254	0.434	0.952777
$100 - 50$	−0.017	−0.356	0.322	0.999921
$500 - 50$	0.203	−0.137	0.542	0.475375
$5000 - 50$	0.041	−0.303	0.385	0.997553
$500 - 100$	0.219	−0.120	0.559	0.391137
$5000 - 100$	0.058	−0.286	0.402	0.990685
$5000 - 500$	−0.162	−0.505	0.182	0.698327

Table A.38: Tukey's HSD test showing effects of normal force F_N and velocity v (after dropping the interaction term) on log-tranformed force per contact area F_P/A_{F_0}. diff: difference in observed means, lwr/upr: lower and upper end points of interval, P_{adj}: P value after adjustment for the multiple comparisons. Highlighted P values are smaller than 5 %.

F_P/A_{F_0}	diff	lwr	upr	P_{adj}
F_N (mN)				
$0.1 - 0.01$	−0.150	−0.436	0.137	0.533295
$1 - 0.01$	−0.530	−0.816	−0.244	0.000015
$2 - 0.01$	−0.413	−0.699	−0.126	0.001312
$1 - 0.1$	−0.381	−0.667	−0.094	0.003729
$2 - 0.1$	−0.263	−0.550	0.023	0.084344
$2 - 1$	0.117	−0.169	0.404	0.715023
v ($\mu m\,s^{-1}$)				
$50 - 10$	0.056	−0.282	0.394	0.991204
$100 - 10$	0.261	−0.078	0.599	0.217471
$500 - 10$	0.516	0.178	0.855	0.000343
$5000 - 10$	1.153	0.810	1.496	0.000000
$100 - 50$	0.205	−0.134	0.543	0.462074
$500 - 50$	0.460	0.122	0.799	0.002052
$5000 - 50$	1.097	0.754	1.440	0.000000
$500 - 100$	0.256	−0.082	0.594	0.233995
$5000 - 100$	0.892	0.550	1.235	0.000000
$5000 - 500$	0.637	0.294	0.979	0.000006

Table A.39: Tukey's HSD test showing effects of normal force F_N and velocity v (after dropping the interaction term) on log-tranformed work of adhesion (WOA1). diff: difference in observed means, lwr/upr: lower and upper end points of interval, P_{adj}: P value after adjustment for the multiple comparisons. Highlighted P values are smaller than 5 %.

WOA1	diff	lwr	upr	P_{adj}
F_N (mN)				
0.1 − 0.01	−0.124	−0.369	0.122	0.563340
1 − 0.01	−0.283	−0.528	−0.037	0.016685
2 − 0.01	−0.191	−0.437	0.054	0.186137
1 − 0.1	−0.159	−0.405	0.087	0.341472
2 − 0.1	−0.068	−0.313	0.178	0.893266
2 − 1	0.091	−0.154	0.337	0.772432
v ($\mu m\, s^{-1}$)				
50 − 10	0.100	−0.190	0.391	0.878580
100 − 10	0.247	−0.043	0.537	0.136852
500 − 10	0.887	0.596	1.177	0.000000
5000 − 10	1.539	1.245	1.833	0.000000
100 − 50	0.147	−0.143	0.437	0.636638
500 − 50	0.787	0.496	1.077	0.000000
5000 − 50	1.439	1.144	1.733	0.000000
500 − 100	0.640	0.349	0.930	0.000000
5000 − 100	1.292	0.998	1.586	0.000000
5000 − 500	0.652	0.358	0.946	0.000000

A.2.2 *Contact time and surface roughness*

Tbl. A.40 summarizes the data. All groups were normally distributed (Tbl. A.41) and had homogeneous variances (Tbl. A.42).

Table A.40: Mean ($\overline{F_P}$) and standard deviation (SD) of all groups.

surface, contact time, secretion	$\overline{F_P}$ (mN)	SD (mN)
smooth, short, little	0.188	0.063
smooth, long, little	0.247	0.079
smooth, short, accumulated	0.177	0.082
smooth, long, accumulated	0.214	0.071
rough, short, little	0.080	0.037
rough, long, little	0.112	0.033
rough, short, accumulated	0.064	0.046
rough, long, accumulated	0.096	0.031

Table A.41: Shapiro-Wilks normality test. All groups were normally distributed.

surface, contact time, secretion	P	W
smooth, short, little	0.89	0.97
smooth, long, little	0.78	0.96
smooth, short, accumulated	0.48	0.93
smooth, long, accumulated	0.69	0.95
rough, short, little	0.42	0.93
rough, long, little	0.80	0.96
rough, short, accumulated	0.55	0.94
rough, long, accumulated	0.22	0.90

Table A.42: Bartlett test of homogeneity of variances. Variances were tested between short and long contact times. All variances are homogeneous.

surface, secretion	P	Bartletts K^2
smooth, little	0.52	0.41
smooth, accumulated	0.65	0.20
rough, little	0.72	0.13
rough, accumulated	0.25	1.32

A.2.3 *Scaling of whole body forces*

Table A.43: Descriptive statistics of stick insect's whole body force measurements (centrifuge technique). Shapiro-Wilks normality test applied to logarithmic data. Force (the dependent variable) was normally distributed ($P > 0.05$). All descriptive variables (length, contact area and weight) were not normally distributed ($P < 0.05$).

	P	*W*
log force ($N = 26$)	0.25840	0.95
log length ($N = 26$)	0.00064	0.83
log weight ($N = 26$)	0.01275	0.89
log force ($N = 24$)	0.22642	0.94
log area ($N = 24$)	0.00171	0.83

BIBLIOGRAPHY

Abbott, S. J. and Gaskell, P. H. (2007). Mass production of bio-inspired structured surfaces. *Proceedings of the Institution of Mechanical Engineers Part C-Journal of Mechanical Engineering Science*, 221(10):1181–1191. (Cited on page 1.)

Aiken, R. B. and Khan, A. (1992). The adhesive strength of the palettes of males of a boreal water beetle, *Dytiscus alaskanus* J. Balfour Browne (Coleoptera: Dytiscidae). *Canadian Journal of Zoology*, 70(7):1321–1324. (Cited on page 17.)

Arzt, E., Gorb, S. N., and Spolenak, R. (2003). From micro to nano contacts in biological attachment devices. *Proceedings of the National Academy of Sciences of the United States of America*, 100(19):10603–10606. (Cited on pages 14 and 25.)

Autumn, K., Liang, Y., Hsieh, S., Zesch, W., Chan, W., Kenny, T., Fearing, R., and Full, R. (2000). Adhesive force of a single gecko foot-hair. *Nature*, 405(6787):681–685. (Cited on page 21.)

Barnes, H. (1994). Rheology of emulsions – a review. *Colloids and Surfaces A-Physicochemical and Engineering Aspects*, 91(3):89–95. (Cited on page 93.)

Barnes, W. J. P. (1999). Tree frogs and tire technology. *Tire Technology International*, March 99:42–47. (Cited on page 18.)

Barnes, W. J. P. (2007). Functional morphology and design constraints of smooth adhesive pads. *MRS Bulletin*, 32:479–485. (Cited on pages 78 and 97.)

Barnes, W. J. P., Oines, C., and Smith, J. M. (2006). Whole animal measurements of shear and adhesive forces in adult tree frogs: insights into underlying mechanisms of adhesion obtained from studying the effects of size and scale. *Journal of Comparative Physiology A Sensory Neural and Behavioral Physiology*, 192(11):1179–1191. (Cited on pages 4, 18, and 97.)

Barnes, W. J. P., Smith, J., Oines, C., and Mundl, R. (2002). Bionics and wet grip. *Tire Technology International*, Dec 2002:56–60. (Cited on pages 18, 19, and 89.)

Barquins, M. and Ciccotti, M. (1997). On the kinetics of peeling of an adhesive tape under a constant imposed load. *International Journal of Adhesion and Adhesives*, 17(1):65–68. (Cited on page 9.)

Barquins, M., Khandani, B., and Maugis, D. (1986). Stick-slip motion during peeling of a viscoelastic solid. *Comptes Rendus de l'Académie des Sciences Serie II*, 303(17):1517–1519. (Cited on page 7.)

Barquins, M. and Roberts, A. (1986). Rubber-friction variation with rate and temperature – some new observations. *Journal of Physics D-Applied Physics*, 19(4):547–563. (Cited on page 91.)

Betz, O. (2002). Performance and adaptive value of tarsal morphology in rove beetles of the genus *Stenus* (Coleoptera, Staphylinidae). *Journal of Experimental Biology*, 205(8):1097–1113. (Cited on pages 13 and 90.)

Betz, O. and Kölsch, G. (2004). The role of adhesion in prey capture and predator defence in arthropods. *Arthropod Structure & Development*, 33(1):3–30. (Cited on page 12.)

Beutel, R. G. and Gorb, S. N. (2001). Ultrastructure of attachment specializations of hexapods, (Arthropoda): evolutionary patterns inferred from a revised ordinal phylogeny. *Journal of Zoological Systematics and Evolutionary Research*, 39(4):177–207. (Cited on pages 13, 16, and 97.)

Bhushan, B. (2003). Adhesion and stiction: Mechanisms, measurement techniques, and methods for reduction. *Journal of Vaccum Science & Technology B*, 21(6):2262–2296. (Cited on pages 1, 23, 24, 89, and 95.)

Bhushan, B., Israelachvili, J., and Landman, U. (1995). Nanotribology: friction, wear and lubrication at the atomic scale. *Nature*, 374(6523):607–616. (Cited on page 8.)

Blackwall, J. (1830). Remarks on the pulvilli of insects. *Transactions of the Linnean Society*, 16:487–492. (Cited on page 17.)

Bowden, F. and Tabor, D. (1939). The area of contact between stationary and between moving surfaces. *Proceedings of the Royal Society of London Series A Mathematical, Physical and Engineering Sciences*, 169(938):391–413. (Cited on page 7.)

Bowden, F. and Tabor, D. (1950). *The friction and lubrication of solids*. Oxford University Press, Oxford. (Cited on pages 7 and 91.)

Braun, O. M. and Naumovets, A. G. (2006). Nanotribology: Microscopic mechanisms of friction. *Surface Science Reports*, 60(6-7):79–158. (Cited on page 8.)

Brochard-Wyart, F. and de Gennes, P. G. (1994). Dewetting of a water film between a solid and a rubber. *Journal of Physics: Condensed Matter*, 6(S23):A9–A12. (Cited on pages 8 and 92.)

Bruening, T. (2006). *Biomechanik des Wachslaufens bei* Crematogaster *(*Decacrema*)-Partnerameisen von* Macaranga*-Bäumen*. PhD thesis, Universität Würzburg, Fakultät für Biologie, Germany. (Cited on page 13.)

Chambers, J. M., Cleveland, W. S., Kleiner, B., and Tukey, P. A. (1983). *Graphical methods for data analysis.* Wadsworth & Brooks/Cole., Pacific Grove, CA. (Cited on page 44.)

Crawley, M. J. (2005). *Statistics. An Introduction using R*. John Wiley & Sons, Ltd, 1 edition. (Cited on page 44.)

Creton, C. and Gorb, S. N. (2007). Sticky feet: From animals to materials. *MRS Bulletin*, 32:466–472. (Cited on page 1.)

Dai, Z., Gorb, S. N., and Schwarz, U. (2002). Roughness-dependent friction force of the tarsal claw system in the beetle Pachnoda marginata (Coleoptera, Scarabaeidae). *Journal of Experimental Biology*, 205(16):2479–2488. (Cited on page 13.)

del Campo, A., Greiner, C., Alvarez, I., and Arzt, E. (2007). Patterned surfaces with pillars with controlled 3d tip geometry mimicking bioattachment devices. *Advanced Materials*, 19(15):1973–1977. (Cited on page 1.)

Dettner, K. (1993). Defensive secretions and exocrine glands in free-living Staphylinid beetles - their bearing on phylogeny

(Coleoptera, Staphylinidae). *Biochemical Systematics And Ecology*, 21(1):143–162. (Cited on page 12.)

Dewitz, H. (1884). Über die Fortbewegung der Thiere an senkrechten, glatten Flächen vermittelst eines Secretes. *Pflügers Archiv European Journal of Physiology*, 33(1):440–481. (Cited on pages 17 and 18.)

Dixon, A. F. G., Croghan, P. C., and Gowing, R. P. (1990). The mechanism by which aphids adhere to smooth surfaces. *Journal of Experimental Biology*, 152(1):243–253. (Cited on pages 18 and 88.)

Dowson, D. (1998). *History of Tribology*. Professional Engineering Publishing. (Cited on page 7.)

Edwards, J. and Tarkanian, M. (1970). The adhesive pads of heteroptera: a re-examination. *Proceedings of the Royal Entomological Society of London Series A*, 45:1–5. (Cited on pages 13, 14, 18, and 88.)

Emerson, S. and Diehl, D. (1980). Toe pad morphology and mechanisms of sticking in frogs. *Biological Journal of the Linnean Society*, 13(3):199–216. (Cited on pages 5, 18, and 19.)

Ernst, V. (1973a). The digital pads of the tree frog, *Hyla cinerea*, I. The Epidermis. *Tissue and Cell*, 5(1):83–96. (Cited on page 17.)

Ernst, V. (1973b). The digital pads of the tree frog *Hyla cinerea*. II. The mucous glands. *Tissue and Cell*, 5(1):97–104. (Cited on page 17.)

Federle, W. (2006). Why are so many adhesive pads hairy? *Journal of Experimental Biology*, 209(14):2611–2621. (Cited on pages 9 and 14.)

Federle, W., Baumgartner, W., and Hölldobler, B. (2004). Biomechanics of ant adhesive pads: frictional forces are rate- and temperature-dependent. *Journal of Experimental Biology*, 207(1):67–74. (Cited on pages 18, 20, 90, 92, and 93.)

Federle, W., Brainerd, E., McMahon, T., and Hölldobler, B. (2001). Biomechanics of the movable pretarsal adhesive organ

in ants and bees. *Proceedings of the National Academy of Sciences of the United States of America*, 98(11):6215–6220. (Cited on pages 11, 12, 32, 91, and 97.)

Federle, W. and Bruening, T. (2006). Ecology and biomechanics of slippery wax barriers and wax running to *Macaranga*-ant mutualisms. In Herrel, A., Speck, T., and Rowe, N. P., editors, *Ecology and biomechanics*, chapter 8, pages 163–184. CRC Taylor & Francis. (Cited on page 13.)

Federle, W. and Endlein, T. (2004). Locomotion and adhesion: dynamic control of adhesive surface contact in ants. *Arthropod Structure & Development*, 33(1):67–75. (Cited on pages 12, 18, 25, 32, 35, 87, 88, 91, and 97.)

Federle, W., Maschwitz, U., Fiala, B., Riederer, M., and Hölldobler, B. (1997). Slippery ant-plants and skilful climbers: Selection and protection of specific ant partners by epicuticular wax blooms in macaranga (euphorbiaceae). *Oecologia*, 112(2):217–224. (Cited on page 13.)

Federle, W., Riehle, M., Curtis, A., and Full, R. (2002). An integrative study of insect adhesion: mechanics and wet adhesion of pretarsal pads in ants. *Integrative and Comparative Biology*, 42(6):1100–1106. (Cited on pages 4, 12, 13, 18, 25, 29, 33, 34, 87, 88, 92, 93, and 97.)

Federle, W., Rohrseitz, K., and Hölldobler, B. (2000). Attachment forces of ants measured with a centrifuge: better "wax-runners" have a poorer attachment to a smooth surface. *Journal of Experimental Biology*, 203(3):505–512. (Cited on pages 16, 26, and 42.)

Fogden, A. and White, L. R. (1990). Contact elasticity in the presence of capillary condensation: 1. The nonadhesive Hertz problem. *Journal of Colloid and Interface Science*, 138(2):414–430. (Cited on page 3.)

Francis, B. and Horn, R. (2001). Apparatus-specific analysis of fluid adhesion measurements. *Journal of Applied Physics*, 89(7):4167–4174. (Cited on pages 6, 24, and 89.)

Fuller, K. N. G. and Tabor, D. (1975). The effect of surface roughness on the adhesion of elastic solids. *Proceedings of the Royal*

Society of London Series A Mathematical, Physical and Engineering Sciences, 345(1642):327–342. (Cited on pages 89 and 90.)

Gao, C. and Kuhlmannwilsdorf, D. (1990). On stick-slip and the velocity dependence of friction at low speeds. *Journal of Tribology-Transactions of the ASME*, 112(2):354–360. (Cited on page 7.)

Gao, J., Luedtke, W., Gourdon, D., Ruths, M., Israelachvili, J., and Landman, U. (2004). Frictional forces and Amontons' law: From the molecular to the macroscopic scale. *Journal of Physical Chemistry B*, 108(11):3410–3425. (Cited on page 8.)

Geim, A., Dubonos, S., Grigorieva, I., Novoselov, K., Zhukov, A., and Shapoval, S. (2003). Microfabricated adhesive mimicking gecko foot-hair. *Nature Materials*, 2(7):461–463. (Cited on page 1.)

Gent, A. N. and Petrich, R. P. (1969). Adhesion of viscoelastic materials to rigid substrates. *Proceedings of the Royal Society of London Series A Mathematical, Physical and Engineering Sciences*, 310(1502):433–448. (Cited on page 9.)

Glassmaker, N. J., Jagota, A., Hui, C.-Y., Noderer, W. L., and Chaudhury, M. K. (2007). Biologically inspired crack trapping for enhanced adhesion. *Proceedings of the National Academy of Sciences of the United States of America*, 104(26):10786–10791. (Cited on page 97.)

Goodwyn, P. P., Peressadko, A., Schwarz, H., Kastner, V., and Gorb, S. N. (2006). Material structure, stiffness, and adhesion: why attachment pads of the grasshopper (*Tettigonia viridissima*) adhere more strongly than those of the locust (*Locusta migratoria*) (Insecta: Orthoptera). *Journal of Comparative Physiology A Sensory Neural and Behavioral Physiology*, 192(11):1233–1243. (Cited on page 97.)

Gorb, S. N. (1998). The design of the fly adhesive pad: distal tenent setae are adapted to the delivery of an adhesive secretion. *Proceedings of the Royal Society of London Series B Biological Sciences*, 265(1398):747–752. (Cited on page 13.)

Gorb, S. N. (2001). *Attachment devices of insect cuticle*. Kluwer Academic Publishers, Dordrecht, Boston. (Cited on pages 12, 13, 14, 15, 16, and 97.)

Gorb, S. N., Beutel, R., Gorb, E., Jiao, Y., Kastner, V., Niederegger, S., Popov, V., Scherge, M., Schwarz, U., and Vötsch, W. (2002). Structural design and biomechanics of friction-based releasable attachment devices in insects. *Integrative and Comparative Biology*, 42(6):1127–1139. (Cited on page 91.)

Gorb, S. N. and Beutel, R. G. (2001). Evolution of locomotory attachment pads of hexapods. *Naturwissenschaften*, 88(12):530–534. (Cited on pages 13 and 14.)

Gorb, S. N., Gorb, E., and Kastner, V. (2001). Scale effects on the attachment pads and friction forces in syrphid flies. *Journal of Experimental Biology*, 204(8):1421–1431. (Cited on page 90.)

Gorb, S. N. and Gorb, E. V. (2004). Ontogenesis of the attachment ability in the bug *Coreus marginatus* (Heteroptera, Insecta). *Journal of Experimental Biology*, 207(17):2917–2924. (Cited on page 90.)

Gorb, S. N., Jiao, Y., and Scherge, M. (2000). Ultrastructural architecture and mechanical properties of attachment pads in *Tettigonia viridissima* (Orthoptera Tettigoniidae). *Journal of Comparative Physiology A Sensory Neural and Behavioral Physiology*, 186(9):821–831. (Cited on pages 13, 16, 25, 33, and 89.)

Gorb, S. N. and Scherge, M. (2000). Biological microtribology: anisotropy in frictional forces of orthopteran attachment pads reflects the ultrastructure of a highly deformable material. *Proceedings of the Royal Society of London Series B Biological Sciences*, 267(1449):1239–1244. (Cited on pages 20, 21, 32, 87, 90, 91, and 97.)

Gorb, S. N., Varenberg, M., Peressadko, A., and Tuma, J. (2007). Biomimetic mushroom-shaped fibrillar adhesive microstructure. *Journal of the Royal Society Interface*, 4(13):271–275. (Cited on page 25.)

Granick, S. (1991). Motions and relaxations of confined liquids. *Science*, 253(5026):1374–1379. (Cited on pages 93 and 94.)

Green, D. M. (1979). Tree frog toe pads: comparative surface morphology using scanning electron microscopy. *Canadian Journal of Zoology*, 57:2033–2046. (Cited on page 17.)

Green, D. M. (1981). Adhesion and the toe pads of tree frogs. *Copeia*, 1981(4):790–796. (Cited on page 18.)

Grenon, J.-F. and Walker, G. (1981). The tenacity of the limpet, *Patella vulgata* L.: an experimental approach. *Journal of Experimental Marine Biology and Ecology*, 54(3):277–308. (Cited on page 11.)

Griffith, A. A. (1921). The phenomenon of rupture and flow in solids. *Philosophical Transactions of the Royal Society*, 221:163–198. (Cited on page 8.)

Grosch, K. (1963). The relation between the friction and viscoelastic properties of rubber. *Proceedings of the Royal Society of London Series A Mathematical, Physical and Engineering Sciences*, 274:21–39. (Cited on page 7.)

Hanna, G. and Barnes, W. J. P. (1991). Adhesion and detachment of the toe pads of tree frogs. *Journal of Experimental Biology*, 155(1):103–125. (Cited on pages 5, 18, and 24.)

Harrell, F. E. (2001). *Regression Modeling Strategies, with Applications to Linear Models, Survival Analysis and Logistic Regression*. Springer. (Cited on page 44.)

Heiberger, R. M. and Holland, B. (2004). *Statistical Analysis and Data Display: An Intermediate Course with Examples in S-Plus, R, and SAS*. Springer Texts in Statistics. Springer. (Cited on page 44.)

Herrel, A., Meyers, J. J., Aerts, P., and Nishikawa, K. C. (2000). The mechanics of prey prehension in chameleons. *Journal of Experimental Biology*, 203(21):3255–3263. (Cited on page 12.)

Hertz, H. (1881). Über die Berührung fester elastischer Körper. *Journal für Reine und Angewandte Mathematik*, 92:156–171. (Cited on page 3.)

Hill, D. E. (1977). The pretarsus of salticid spiders. *Zoological Journal of the Linnean Society, London*, 60:319–338. (Cited on page 22.)

Homola, A. M., Israelachvili, J. N., McGuiggan, P. M., and Gee, M. L. (1990). Fundamental experimental studies in tribology:

The transition from 'interfacial' friction of undamaged molecularly smooth surfaces to 'normal' friction with wear. *Wear*, 136(1):65–83. (Cited on pages 8 and 91.)

Hooke, R. (1665). *Micrographia*. Oxford Press, London. (Cited on page 17.)

Hui, C.-Y., Glassmaker, N. J., and Jagota, A. (2005). How compliance compensates for surface roughness in fibrillar adhesion. *The Journal of Adhesion*, 81(7-8):699–721. (Cited on page 97.)

Hui, C.-Y., Glassmaker, N. J., Tang, T., and Jagota, A. (2004). Design of biomimetic fibrillar interfaces: 2. Mechanics of enhanced adhesion. *Journal of the Royal Society Interface*, 1(1):35–48. (Cited on page 97.)

Ishii, S. (1987). Adhesion of a leaf-feeding ladybird *Epilachna vigintioctomaculata* (Coleoptera, Coccinellidae) on a vertically smooth surface. *Applied Entomology and Zoology*, 22(2):222–228. (Cited on pages 13 and 14.)

Israelachvili, J. (1992a). Interfacial forces. *Journal of Vacuum Science & Technology A*, 10(5):2961–2971. (Cited on pages 2, 3, 5, and 8.)

Israelachvili, J. (1992b). *Intermolecular and surface forces*. Academic Press, London. (Cited on pages 8 and 89.)

Israelachvili, J. and Berman, A. (1995). Irreversibility, energy dissipation and time effects in intermolecular and surface interactions. *Israel Journal of Chemistry*, 35(1):85–91. (Cited on page 8.)

Jiao, Y., Gorb, S. N., and Scherge, M. (2000). Adhesion measured on the attachment pads of *Tettigonia viridissima* (Orthoptera, Insecta). *Journal of Experimental Biology*, 203(12):1887–1895. (Cited on pages 17, 18, 25, and 95.)

Johnson, K., Kendall, K., and Roberts, A. (1971). Surface energy and the contact of elastic solids. *Proceedings of the Royal Society of London Series A Mathematical, Physical and Engineering Sciences*, 324(1558):301–313. (Cited on pages 3, 24, 25, and 95.)

Kendall, K. (1971). The adhesion and surface energy of elastic solids. *Journal of Physics D-Applied Physics*, 4(8):1186–1195. (Cited on pages 9, 24, and 88.)

Kendall, K. (2001). *Molecular adhesion and its applications: The sticky universe*. Kluwer Academic/Plenum Publishers, New York, USA. (Cited on pages 2 and 8.)

Langer, M. G., Ruppersberg, J. P., and Gorb, S. N. (2004). Adhesion forces measured at the level of a terminal plate of the fly's seta. *Proceedings of the Royal Society of London Series B Biological Sciences*, 271(1554):2209–15. (Cited on page 18.)

Leckband, D. and Israelachvili, J. (2001). Intermolecular forces in biology. *Quartely Review of Biophysics*, 34(2):105–267. (Cited on page 23.)

Lees, A. D. and Hardie, J. (1988). The organs of adhesion in the aphid *Megoura viciae*. *Journal of Experimental Biology*, 136(1):209–228. (Cited on pages 13, 18, and 25.)

Martin, A., Buguin, A., and Brochard-Wyart, F. (2001). Dewetting nucleation centers at soft interfaces. *Langmuir*, 17(21):6553–6559. (Cited on page 93.)

Martin, A., Buguin, A., and Brochard-Wyart, F. (2002). 'Cerenkov' dewetting at soft interfaces. *Europhysics Letters*, 57(4):604–610. (Cited on page 92.)

Martin, A., Rossier, O., Buguin, A., Auroy, P., and Brochard-Wyart, F. (2000). Spinodal dewetting of thin liquid films at soft interfaces. *European Physical Journal E*, 3(4):337–341. (Cited on page 8.)

Martin, P. and Brochard-Wyart, F. (1998). Dewetting at soft interfaces. *Physical Review Letters*, 80(15):3296–3299. (Cited on pages 20, 92, and 93.)

McFarlane, J. S. and Tabor, D. (1950). Adhesion of solids and the effect of surface films. *Proceedings of the Royal Society of London Series A Mathematical, Physical and Engineering Sciences*, 202:224–243. (Cited on page 89.)

Mizuhira, V. (2004). The digital pads of rhacophorid tree-frogs. *Journal of Electron Microscopy*, 53(1):63–78. (Cited on pages 17 and 97.)

Nachtigall, W. (1974). *Biological mechanisms of attachment*. Springer, Berlin, Heidelberg, New York. (Cited on pages 12 and 18.)

Niederegger, S. and Gorb, S. N. (2003). Tarsal movements in flies during leg attachment and detachment on a smooth substrate. *Journal of Insect Physiology*, 49(6):611–620. (Cited on pages 12, 18, 25, 87, 88, and 97.)

Niederegger, S. and Gorb, S. N. (2006). Friction and adhesion in the tarsal and metatarsal scopulae of spiders. *Journal of Comparative Physiology A Sensory Neural and Behavioral Physiology*, 192(11):1223–1232. (Cited on pages 18, 21, and 32.)

Niederegger, S., Gorb, S. N., and Jiao, Y. (2002). Contact behaviour of tenent setae in attachment pads of the blowfly *Calliphora vicina* (Diptera, Calliphoridae). *Journal of Comparative Physiology A Sensory Neural and Behavioral Physiology*, 187(12):961–970. (Cited on pages 17, 21, 32, and 91.)

Page, E. B. (1963). Ordered hypotheses for multiple treatments: A significance test for linear ranks. *Journal of the American Statistical Association*, 58:216–230. (Cited on page 44.)

Persson, B. N. J. (1998). *Sliding friction: physical principles and applications*. Springer, Berlin, Heidelberg, New York. (Cited on page 83.)

Persson, B. N. J. (1999). Sliding friction. *Surface Science Reports*, 33(3):85–119. (Cited on page 7.)

Persson, B. N. J. (2002). Adhesion between an elastic body and a randomly rough hard surface. *European Physical Journal E*, 8(4):385–401. (Cited on pages 8 and 90.)

Persson, B. N. J. (2007a). Biological adhesion for locomotion: basic principles. *Journal of Adhesion Science and Technology*, 21(12):1145–1173. (Cited on page 94.)

Persson, B. N. J. (2007b). Wet adhesion with application to tree frog adhesive toe pads and tires. *Journal of Physics: Condensed Matter*, 19(37):376110 (16pp). (Cited on pages 94, 96, and 97.)

Persson, B. N. J., Albohr, O., U, T., Volokitin, A. I., and Tosatti, E. (2005). On the nature of surface roughness with application to contact mechanics, sealing, rubber friction and adhesion. *Journal of Physics: Condensed Matter*, 17(1):R1–R62. (Cited on pages 7 and 89.)

Pesika, N. S., Tian, Y., Zhao, B., Rosenberg, K., Zeng, H., McGuiggan, P., Autumn, K., and Israelachvili, J. N. (2007). Peel-zone model of tape peeling based on the gecko adhesive system. *The Journal of Adhesion*, 83(4):383–401. (Cited on page 9.)

Piau, J.-M., Ravilly, G., and Verdier, C. (2005). Peeling of polydimethylsiloxane adhesives at low velocities: Cohesive failure. *Journal of Polymer Science Part B: Polymer Physics*, 43(2):145–157. (Cited on pages 9 and 89.)

R Development Core Team (2007). *R: A Language and Environment for Statistical Computing*. R Foundation for Statistical Computing, Vienna, Austria. (Cited on page 45.)

Radhakrishnan, V. (1998). Locomotion: Dealing with friction. *Proceedings of the National Academy of Sciences of the United States of America*, 95(10):5448–5455. (Cited on page 19.)

Riskin, D. K. and Fenton, M. B. (2001). Sticking ability in spix's disk-winged bat, thyroptera tricolor (microchiroptera : Thyropteridae). *Canadian Journal of Zoology*, 79(12):2261–2267. (Cited on page 17.)

Rivlin, R. S. (1944). The effective work of adhesion. *Paint Technology*, 9:215–216. (Cited on page 9.)

Roberts, A. D. (1971a). The shear of thin liquid films. *Journal of Physics D-Applied Physics*, 4(3):433–440. (Cited on pages 19 and 92.)

Roberts, A. D. (1971b). Squeeze films between rubber and glass. *Journal of Physics D-Applied Physics*, 4(3):423–432. (Cited on page 94.)

Schargott, M., Popov, V. L., and Gorb, S. N. (2006). Spring model of biological attachment pads. *Journal of Theoretical Biology*, 243(1):48–53. (Cited on pages 23 and 95.)

Scholz, I., Baumgartner, W., and Federle, W. (2007). Micromechanics of smooth adhesive organs in stick insects: pads are mechanically anisotropic and softer towards the adhesive surface. submitted. (Cited on page 97.)

Sitti, M. and Fearing, R. S. (2003). Synthetic gecko foot-hair micro/nano-structures as dry adhesives. *Journal of Adhesion Science and Technology*, 17(8):1055–1073. (Cited on page 1.)

Smith, J., Barnes, W., Downie, J., and Ruxton, G. (2006a). Structural correlates of increased adhesive efficiency with adult size in the toe pads of hylid tree frogs. *Journal of Comparative Physiology A Sensory Neural and Behavioral Physiology*, 192(11):1193–1204. (Cited on page 97.)

Smith, J. M., Barnes, W. J. P., Downie, J. R., and Ruxton, G. D. (2006b). Adhesion and allometry from metamorphosis to maturation in hylid tree frogs: a sticky problem. *Journal of Zoology*, 270(2):372–383. (Cited on pages 79 and 97.)

Snodgrass, R. (1956). *Anatomy and physiology of the honey-bee*. McGraw-Hill Book Company, New York. (Cited on page 16.)

Spolenak, R., Gorb, S. N., Gao, H., and Arzt, E. (2004). Effects of contact shape on the scaling of biological attachments. *Proceedings of the Royal Society of London Series A Mathematical, Physical and Engineering Sciences*, 461(2054):305–319. (Cited on page 23.)

Stefan, J. (1874). Versuche über die scheinbare Adhäsion. *Sitzb. Akad. Wiss. Wien (Mathem-naturwiss. Kl)*, 69:713–735. (Cited on pages 6 and 24.)

Stork, N. E. (1980). Experimental analysis of adhesion of *Chrysolina polita* (Chrysomelidae: Coleoptera) on a variety of surfaces. *Journal of Experimental Biology*, 88(1):91–107. (Cited on pages 18, 25, and 90.)

Stork, N. E. (1983). A comparison of the adhesive setae on the feet of lizards and arthropods. *Journal of Natural History*, 17(6):829–835. (Cited on page 89.)

Tadros, T. (1994). Fundamental principles of emulsion rheology and their applications. *Colloids and Surfaces A-Physicochemical and Engineering Aspects*, 91(3):39–55. (Cited on pages 20 and 93.)

Vincent, J. (1990). *Structural Biomaterials*. Princeton University Press, Princeton, NJ, revised edition. (Cited on page 10.)

Vogel, S. (2003). *Comparative Biomechanics: Life's Physical World*. Princeton University Press. (Cited on page 10.)

Vötsch, W., Nicholson, G., Müller, R., Stierhof, Y., Gorb, S. N., and Schwarz, U. (2002). Chemical composition of the attachment pad secretion of the locust *Locusta migratoria*. *Insect Biochemistry and Molecular Biology*, 32(12):1605–1613. (Cited on pages 13 and 93.)

Waite, J. H., Andersen, N. H., Jewhurst, S., and Sun, C. (2005). Mussel adhesion: Finding the tricks worth mimicking. *The Journal of Adhesion*, 81(3–4):297–317. (Cited on pages 11 and 12.)

Walker, G., Yue, A., and Ratcliffe, J. (1985). The adhesive organ of the blowfly, *Calliphora vomitoria*: a functional approach (Diptera: Calliphoridae). *Journal of Zoology London (A)*, 205:297–307. (Cited on pages 12, 13, 14, 18, and 25.)

Warton, D. I. and Weber, N. C. (2002). Common slope tests for bivariate errors-in-variables models. *Biometrical Journal*, 44(2):161–174. (Cited on pages 44 and 81.)

Warton, D. I., Wright, I. J., Falster, D. S., and Westoby, M. (2006). Bivariate line-fitting methods for allometry. *Biological Reviews*, 81(2):259–291. (Cited on page 44.)

Welsch, U., Storch, V., and Fuchs, W. (1974). The fine structure of the digital pads of rhacophorid tree frogs. *Cell and Tissue Research*, 148(3):407–416. (Cited on page 17.)

West, G. (1911). On the resistance to the motion of a thread of mercury in a glass tube. *Proceedings of the Royal Society of London Series A Mathematical, Physical and Engineering Sciences*, 86(583):20–25. (Cited on page 84.)

West, T. (1862). The foot of the fly, its structure and action elucidated by comparison with the feet of other insects. *Transactions of the Linnean Society*, 23:393–421. (Cited on pages 1 and 17.)

Yule, A. and Walker, G. (1984). The adhesion of the barnacle, *balanus balanoides*, to slate surfaces. *Journal of the marine biological Association of the United Kingdom*, 64(1):147–156. (Cited on page 11.)

Zhang, G. (2005). Evaluating the viscoelastic properties of biological tissues in a new way. *Journal of Musculoskeletal Neuronal Interaction*, 5(1):85–90. (Cited on page 10.)

Zhang, X., Zhu, Y., and Granick, S. (2002). Hydrophobicity at a Janus Interface. *Science*, 295(5555):663–666. (Cited on pages 93 and 94.)

ACKNOWLEDGMENTS

I would like to express my gratitude to my supervisor, Dr. Walter Federle, who has not only introduced me to a fascinating research topic, but whose expertise, understanding, and patience, added considerably to my graduate experience. I appreciate his vast knowledge and skill in many areas, which have on occasion made me green with envy. Without his motivation and encouragement life would have been a lot more difficult.

I would like to thank Dr. Jon Barnes for broadening my horizon by introducing my to the fascinating field of frog adhesion. Furthermore Jon showed me that modern day science does not always have to competitive: Collaborations are fun!

Many thanks go to all the past and present members of Walter's workgroup in Würzburg and Cambridge: Holger Bohn, Tanja Brüning, Thomas Endlein, Jan-Henning Dirks, Ulrike Bauer, Nanna Evers, Karin Moll and Kerstin Tüchert. Besides valuable research discussions they also confirmed that there is a life beyond university work.

Thanks also to the underpaid student helpers Sandra Ulmann, Sebastian Schumann and Karoline Winkel for going through millions of high speed video frames of insect and frog feet.

I am thankful to the members of the Departments of Zoology in Würzburg and Cambridge. Although research on animal adhesion is far away from subjects like sociobiology, bee brains, mussel ecology and dinosaur flight, these interdisciplinary discussions were always very rewarding.

I would also like to thank my friends for their support and putting up with me during this time: Paul Reck (for believing in me), Frank and Iris, Lasse and Anna, Tanja, Stefan, Ray, Chris, Judith, Danie, Steffi, André, Olaf, Oli, Marko, and most of all Thomas Heinzerling and Judith Albrecht (without their help I would have never been able to finish).

And, most importantly, I am deeply indebted to Kerstin Klein for the love and support she has provided me with over the past years.

COLOPHON

This thesis was typeset with LaTeX 2ε using Hermann Zapf's *Palatino* and *Euler* type faces (Type 1 PostScript fonts *URW Palladio L* and *FPL* were used). The listings are typeset in *Bera Mono*, originally developed by Bitstream, Inc. as "Bitstream Vera".

The typographic style was inspired by Robert Bringhurst's genius as presented in *The Elements of Typographic Style* (Version 2.5, Hartley & Marks, 2002).

CURRICULUM VITAE

Personal information:

Name:	Patrick Drechsler
Date of birth:	25.01.1974
Place of birth:	Böblingen, Germany

Education

1995	Abitur, Peter-Vischer-Schule, Nürnberg, Germany
11/1995 – 10/1998	Friedrich-Alexander-Universität, Erlangen, Germany
11/1995 – 06/1997	Undergraduate studies biology
1997	Vordiplom (pre-diploma) in biology
11/1997 – 10/1998	Graduate studies biology
10/1998 – 06/2002	Universität des Saarlandes, Saarbrücken, Germany, graduate studies "Technical biology and bionics"
2002	Diploma in biology
	Diploma thesis: "Effects of different active regeneration times after a training camp on selected immunological parameters of triathletes.". Supervisor: Dr. med. J. Scharhag
10/2002 – 11/2005	Universität Würzburg, Germany, Doctoral work
11/2005 – 08/2006	University of Cambridge, UK, Doctoral work

ERKLÄRUNG

Hiermit erkläre ich ehrenwörtlich, dass ich die vorliegende Arbeit selbständig angefertigt und keine anderen als die von mir angegebenen Quellen und Hilfsmittel benutzt habe.

Ich habe diese Dissertation weder in gleicher noch in ähnlicher Form in einem anderen Prüfungsverfahren vorgelegt.

Ich erkläre ferner, dass ich bisher noch keine weiteren akademischen Grade erworben oder zu erwerben versucht habe.

Würzburg, Januar 2008

Patrick Drechsler